NIST Recommended Practice Guide

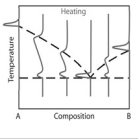

Special Publication 960-15

DTA and Heat-flux DSC Measurements of Alloy Melting and Freezing

W. J. Boettinger, U. R. Kattner
K.-W. Moon

Metallurgy Division
Materials Science and Engineering Laboratory,
National Institute of Standards and Technology

J. H. Perepezko

Department of Materials Science and Engineering,
University of Wisconsin - Madison

Special Publications

November 2006

U.S. Department of Commerce
Carlos M. Gutierrez, Secretary

Technology Administration
Robert C. Cresanti , Under Secretary of
Commerce for Technology

National Institute of Standards and Technology
Dr. William Jeffrey, Director

Certain commercial entities, equipment, or materials may be identified in this document in order to describe an experimental procedure or concept adequately. Such identification is not intended to imply recommendation or endorsement by the National Institute of Standards and Technology, nor is it intended to imply that the entities, materials, or equipment are necessarily the best available for the purpose.

National Institute of Standards and Technology
Special Publication 960-15
Natl. Inst. Stand. Technol.
Spec. Publ. 960-15
90 pages (November 2006)
CODEN: NSPUE2
U.S. GOVERNMENT PRINTING OFFICE
WASHINGTON: 2001
For sale by the Superintendent of Documents
U.S. Government Printing Office
Internet: bookstore.gpo.gov Phone: (202) 512-1800 Fax: (202) 512-2250
Mail: Stop SSOP, Washington, DC 20402-0001

Part 1: Introduction

1.1. Focus of this guide

This document is focused on differential thermal analysis (DTA)* and heat-flux differential scanning calorimetry (HF-DSC)† of metals and alloys. A thermal analysis guide focused only on metals and alloys is appropriate because they behave quite differently from molecular materials such as polymers and organics. First, metals are good conductors of heat so that temperature differences at any instant can often be ignored within the small (200 mg) samples typical of differential thermal analysis. Secondly, liquid metals and alloys are typically monatomic. Freezing and melting occur rapidly in response to changes in temperature compared to other materials. Melting and freezing transformations, once initiated, take place within, at most, a degree of local thermodynamic equilibrium‡. Therefore the guide also focuses on melting and solidification behavior because special methods can be employed that are not necessarily useful for a broader class of materials and processes. The metallurgist should expect a high level of precision when proper attention is paid to technique and interpretation of data.

Thermal analysis is a widely used experimental measurement technique with a long history, [49Vol], [65Gar], [66Tsa], [68Gra], [70Cun], [75McN], [78Bar], [86Hey], [88Fly], [94Spe] and [00Opf]. In contemporary application, most work is performed with instruments that are commercially available and under computer control. Under these conditions even the novice user can obtain data and software generated analysis of measurements in a relatively short time. However the expert may want to consider specific sample characteristics in order to judge whether the traditional measurement protocols are satisfactory or if modifications are necessary. The specific sample characteristics also impact the interpretation and analysis of the thermal analysis measurements and the manner in which the software might be used. Best practice may also require a departure from standard practice to include, for example, thermal cycling schedules and holding treatments in order to address specific sample characteristics. Similarly, the proper interpretation of the thermal analysis signals should include consideration of the multicomponent phase equilibrium as well as analysis of the phase evolution during solidification and melting that again is specific to a given sample. It is the intention of this guide to provide the thermal analysis user with the considerations that are necessary for proper

* Items in blue are defined in the glossary, Appendix A.

† The Guide does not treat power-compensating scanning calorimetry (PC-DSC).

‡ However, supercooling of a liquid is often required to initiate freezing (nucleation supercooling).

sample preparation and to illustrate how the sample characteristics influence the proper interpretation and analysis of measurements. Since the specific characteristics of a given sample determine the best practice in measurement and analysis, it is not possible to include all possible advice. Instead, the cornerstone of best practice should be the flexibility to alter procedures in response to specific sample characteristics and types of information sought.

In the remainder of the introduction, we describe the different types of information usually sought from DTA/HF-DSC during the melting and freezing of alloys. In Part 2, the details of instruments, operation and calibration are described. The goal is to describe the thermal lags between the sample and sample thermocouple that must be understood to enable good analysis of data. In Parts 3 and 4, the response of the DTA to binary and ternary alloys, respectively, is detailed. Here a strong use is made of the enthalpy vs. temperature relation for melting and freezing of alloys with different phase diagram features when one assumes full diffusional equilibrium and when diffusion in the solid is so slow as to be ignored. Part 5 makes some concluding remarks. The appendices include a glossary of terms that are printed blue in the text, recommended reading, a heat flow model for the DTA and a description of DTA response for alloys with more than 3 components.

1.2. Information sought from DTA and heat-flux DSC measurements

DTA and HF-DSC thermal measurement instruments attempt to measure the difference in temperature between a sample and an inert standard during programmed heating or cooling. As such, the measurements are sensitive to the difference between the enthalpy vs. temperature relation of a sample and the enthalpy vs. temperature relation of a standard. The enthalpy vs. temperature relations of pure metals are well-known and output information from such pure metals from a DTA/HF-DSC is used primarily for calibration.

Figure 1.1 shows the general shape of the DTA output for the melting and freezing of a pure metal under ideal conditions. On heating, melting requires an input of heat and the downward peak is endothermic. On cooling, freezing releases heat and the upward peak is exothermic. Peak shapes have a linear portion up to the maximum deflection from the horizontal followed by an exponential return to the horizontal. The initial detection of melting or freezing is indicated by the beginning of the linear portion of the peak and is used for temperature calibration. The area of the peak is used for calibration of the heat flow. The details of the ideal DTA shape shown in Figure 1.1 as well as

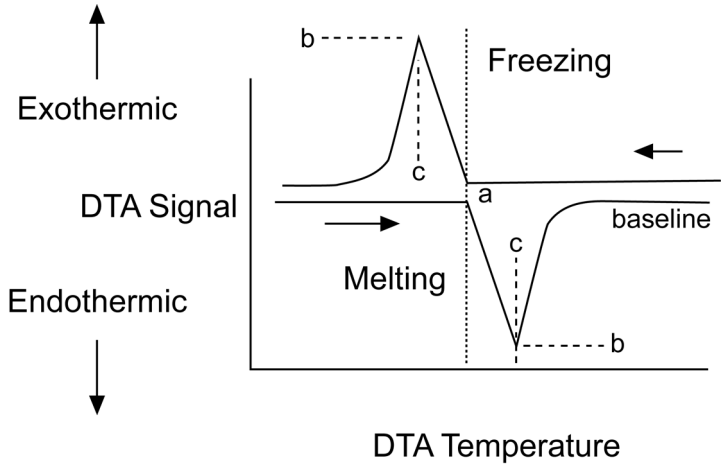

Figure. 1.1 *DTA responses to melting and freeezing of a pure material under ideal conditions. a-onset temperatures (taken here as equal to the melting point, T_M), b-peak signals, c-peak temperatures.*

offsets from the true melting temperature and rounding of various curve features are described in section 2.4.

Once the instrument is calibrated, various types of information for melting and solidification of alloys using a DTA/HF-DSC are sought. The most common measurement involves liquidus and solidus temperature determination. These terms will be used here to refer to thermodynamic quantities that depend only on the alloy composition (at fixed pressure). For phase diagram research one might also want to determine other thermodynamic temperatures associated with melting and freezing; e.g., in binary alloys, invariant reaction temperatures and their character; viz., eutectic and peritectic. In ternary and higher order systems, information is sought regarding additional thermodynamic transitions with one or more degrees of freedom.

Related measurements of interest can include the amount of supercooling possible prior to solidification and the microstructurally and solid diffusion rate sensitive final freezing temperature/incipient melting point. One might want to know the supercooling tendency of a particular alloy in contact with a certain type of crucible or in the presence of a grain refiner. These temperatures are not purely thermodynamic in origin, but are needed for the modeling of castings, for the determination of maximum heat treatment temperature, etc. DTA/HF-DSC may at times be used for the identification of alloys from within a small class of alloys as a quality control method; i.e., the DTA plot could be used as a "finger print" of the alloy.

A more difficult measurement is the determination of the enthalpy vs. temperature relation for the sample. One may want the thermodynamic (equilibrium) enthalpy-temperature relation, or for practical considerations, one may want the enthalpy vs. temperature relation as it would apply under certain casting conditions where freezing would end at a final temperature generally lower than the solidus.

DTA and DSC are sometimes used in a non-scanning mode where the temperature is held constant and evidence for isothermal transformation is detected. Such an approach is sometimes used for solidification studies involving measurement of nucleation kinetics and diffusion bonding.

1.3. Relevant standards

ASTM Subcommittee E37.01 is responsible for thermal analysis test methods. A summary of relevant ASTM Standards is given below. Many of the methods suggested in these documents have been developed with a broad array of materials in mind. With a focus on metal and alloy melting and freezing, variations of these methods are sometimes more appropriate as we will describe in this document. Various other international standards are available. In particular we note many relevant standards of the Deutsche Institut für Normung (DIN), Association Française de Normalisation (AFNOR) and the British Standard Institution (BSI). Many of these are available from the ANSI web store (http://webstore.ansi.org).

1.3.1 Terms and definitions

ASTM E473, "Standard Terminology Relating to Thermal Analysis," is a compilation of definitions of terms used in other ASTM documents on all thermal analysis methods including techniques besides DTA and HF-DSC.

ASTM E1142, "Terminology Relating to Thermophysical Properties," is a compilation of definitions of terms used in other ASTM documents that involve the measurement of thermophysical properties in general.

1.3.2 Calibration and sensitivity

ASTM E967, "Practice for Temperature Calibration of DSC and DTA," presents simple recipes for calibration for fixed mass and heating rate using two pure materials to obtain a linear correction for conversion of measured temperature to actual temperature. The onset temperature extracted from the melting peak is determined by the extrapolation method, see section 2.4.3. For some

materials the standard suggests using the peak for calibration, a method not recommended for metals.

ASTM E968, "Standard Practice for Heat Flow Calibration of DSC," uses sapphire as heat capacity standard. The method is described in section 2.4.4.

ASTM E2253, "Standard Method for Enthalpy Measurement Validation of Differential Scanning Calorimeters," presents a method using three small masses to determine the detection limit of DTA/DSC.

1.3.3 Analysis of data

ASTM E928, "Standard Test Method for Determining Purity by DSC," employs comparison of the shape of the melting peak of an impure sample to the shape for a high purity sample to determine the concentration of the impurity. The method uses the "1/F plot" which examines the down slope of the melting peak.

ASTM E794, "Standard Test Method for Melting and Crystallization Temperatures by Thermal Analysis," employs the extrapolated onset determination method.

ASTM E793, "Standard Test Method for Enthalpies of Fusion and Crystallization by DSC," uses area on signal vs. time plot for comparison to known heats of fusion of pure materials.

ASTM E1269, "Standard Test Method for Determining Specific Heat Capacity by DSC," uses sapphire or aluminum as a standard.

1.4 Major points

- This guide focuses on melting and solidification of metals and alloys.
- Different types of information are sought by different users.
- Some deviation from standard practice may be useful for specific measurements.

Part 2: Instruments and Operation

2.1. Variations among instruments

For precision work, it is important for users to understand the operation of their particular DTA/HF-DSC, as different instruments employ different designs and control features and employ different data analysis and presentation methods.

2.1.1 Heat transfer between system components

A DTA/HF-DSC instrument consists of a single furnace and two crucibles with thermocouples (Figure 2.1). One crucible is for the sample being tested and the other is for a reference material, often alumina powder. The sample or reference thermocouple temperatures are given by the voltage difference between thermocouple legs A and B for either cup with suitable cold junction compensation. In the DTA, the difference signal is obtained by shorting the B legs and measuring the voltage between the A legs. In the heat flux DSC, the connecting metal strip is often used as an active sensing element to obtain the difference signal by measuring the voltage between legs B and B.

Depending on the geometrical arrangement of these parts, the atmosphere, and the temperature range of operation, heat flow will have different contributions from radiation, convection and conduction processes. The relative contributions will change the size and heating rate dependence of the temperature

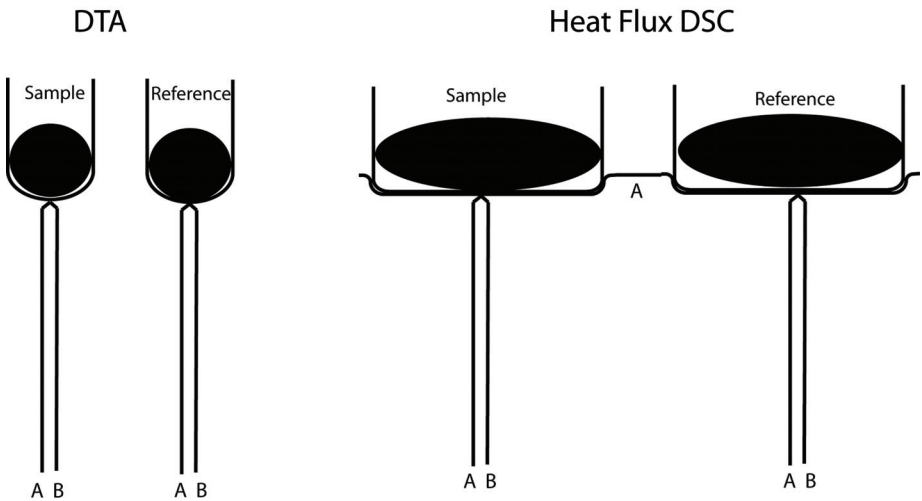

Figure 2.1. *Schematic of DTA and HF-DSC geometries (not to scale). A and B denote the different legs of themocouples.*

differences and thermal lags during heating and cooling between the sample, the reference and the thermocouples. The manner in which these lags influence the interpretation of DTA data will be a central focus of this document.

Appendix C presents a model for the heat transfer within a DTA instrument and an experimental method to determine three time constants for the instrument. With these time constants, the sample mass and an enthalpy vs. temperature relationship for the sample, one can calculate DTA curves. This procedure permits one to understand an important difficulty of DTA analysis as demonstrated by the fact that the sample thermocouple in a DTA does not remain isothermal during the melting of a pure metal. This is not due to the kinetics of the melting process, but is due to the difference between the sample temperature and the sample thermocouple temperature‡. The model will be used to clarify calibration procedures in section 2.4.1 and aid in the interpretation of DTA signals from alloys in Parts 3 and 4 and Appendix G.

2.1.2 DTA / heat flux DSC vs. power compensating (true) DSC

This document is limited to a description of devices with one heater. The term differential scanning calorimeter was originally applied to instruments with separate heaters for the reference and the sample. The differential signal of a true DSC is the power difference required to keep the temperatures of the reference and sample identical during a defined temperature ramp. Thus, the signal is in units of watts per unit sample mass. This type of instrument is today called a power compensating DSC. Many instruments with a single heater are called a DSC, but are more properly called a heat flux DSC. The basic measurement, just as for a DTA, is a difference in voltage between the output of the sample thermocouple and the reference thermocouple. Although quantitative measurements of heats of transformation can be evaluated by either DTA or heat flux DSC, there are differences in sensitivity and accuracy. In a heat flux DSC, the heat flow path between the sample and the reference is provided by a metal strip whose thermal conductivity is high and well defined. This minimizes the temperature difference between the sample and reference and also makes the temperature difference directly proportional to the heat flux between the two. For both, a calibration procedure can be used to relate the difference signal integrated over time to an enthalpy (see 2.4.4). Such instru-

‡ It is to be noted that cooling and heating curves obtained with direct immersion of a thinly protected thermocouple in the melt are often superior to conventional DTA methods because of greatly reduced thermal lags. Such experiments require custom equipment designed for the specific alloy of interest to provide suitable atmosphere and refractory coatings; see e.g., [79Fre], [88Fre] and [03Don]. Because the DTA is a common desktop instrument available in many laboratories, its capabilities and limitations are nevertheless worth consideration.

ments are not capable of the same accuracy as a power compensating DSC, but are usually built to operate at the higher temperatures (>1000°C) necessary for metallurgical work.

2.1.3 How does the instrument control the heating rate?

In its simplest configuration, the control thermocouple for a DTA* is in the furnace. The controller applies power to maintain a linear heating or cooling rate for this thermocouple. In this case, there is usually a thermal transient between the furnace thermocouple and the reference and sample thermocouples, which is particularly noticeable at the beginning and end of a DTA scan.

A second method uses the reference thermocouple to control the application of power. This has the advantage of preventing the initial (and final) transients. Finally some instruments use the sample thermocouple for control in an attempt to maintain a constant heating rate in the sample itself. However while control of a sample thermocouple to a constant heating rate may be possible for phase changes with sluggish kinetics or very small enthalpy of transformation, it is practically impossible to maintain a constant heating rate during the melting or freezing of metals and alloys. This method is not recommended. Some instruments provide user selectable choices of control method. Modulated DTA/DSC is an instrument that adds a small sinusiodally varying temperature oscillation on the usual temperature program. This last subject, as well as power compensating DSC, are beyond the scope of the present document.

2.1.4 What is the signal, millivolts or Kelvin?

As the name implies, the signal for a DTA is a difference. This is the y - axis of standard DTA plots (See Figure 1.1). It is the difference in either the voltage or the derived temperature difference between the sample thermocouple and the reference thermocouple. When the signal is given as temperature difference, a reference table or equation has been used by the instrument to obtain temperature difference from a voltage difference. The choice of one or the other by individual manufacturers is mostly historical or an attempt to provide numbers with which the user is comfortable. Unfortunately, both types of output are not usually available on a single instrument. In some cases the millivolt signal is divided by the sample mass for presentation. The signal can either be endothermic or exothermic; i.e., indicating heat into or out of the

* In the remainder of the document, we will usually drop the distinction between DTA and HF-DSC for brevity.

sample. For transformations of materials that remain close to equilibrium, heating scans lead to endothermic signals and cooling scans lead to exothermic signals. Unfortunately, there is no common practice for whether a positive y - axis is endothermic or exothermic. In this guide we will always assume that an endothermic signal is negative on the y-axis. Some instruments use a thermopile between the sample and the reference. A thermopile is a number of thermocouples connected in series. Connecting many thermocouples in series produces a higher differential voltage signal.

2.1.5 Plotting signal vs. temperature or time

Figure 2.2a shows experimental data for the sample and reference thermocouple temperatures plotted vs. time for the melting of pure Ag. The derived difference between these temperatures can be plotted vs. time, vs. reference thermocouple temperature or vs. sample thermocouple temperature as shown in Figure 2.2b. The output table or graphics display of a particular instrument may provide some or all of these choices as the x-axis of DTA plots. Significant differences in the shapes of the curves are evident depending on the x-axis choice. A display vs. temperature is useful for directly reading temperatures of thermal events. A display vs. time is required when peak area (Kelvin second or millivolt second) is calculated from the data for quantitative measures of total enthalpy change associated with a thermal event. For display or numerical output, some instruments choose the temperature as the reference thermocouple temperature, while others choose the sample thermocouple temperature. For precision work the latter is preferable because the changes in sample thermocouple temperature are more closely related to events in the material of interest. Most importantly, it is necessary for the user to know which temperature is being used by the instrument software. Then replotting of data can be performed using external manipulations if desired.

Parts 3 and 4 of this document will delve in considerable detail into the expected shape and interpretation of DTA curves for alloys. For the melting and solidification of a pure metal, DTA curves are simple and one can define several features of the curve as seen in Figure 1.1. The baseline is the graphical feature corresponding to the ΔT signal over temperature ranges where no transformation of the sample takes place. The baseline is horizontal if the signal is a constant. The onset temperature is the beginning of the deviation from the baseline measured by some quantitative measure as described in 2.4.3. The peak signal is the maximum deviation of the signal (Δy-value) from the baseline and the peak temperature is the temperature (x-value) corresponding to the peak signal. The term peak will be used regardless of whether it is negative or positive. The temperature at which the signal returns to the

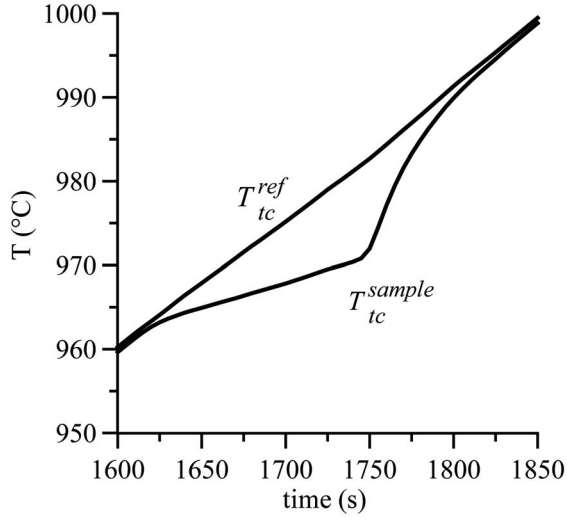

(a)

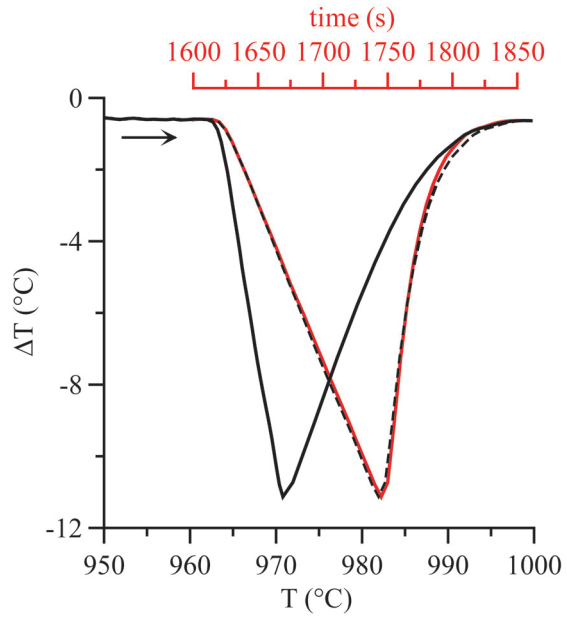

(b)

Figure 2.2. *DTA melting of a 211.6 mg of pure Ag at 10 K/min. (a) Reference thermocouple temperature* T_{tc}^{ref} *and sample thermocouple temperature* T_{tc}^{sample} *vs. time. (b) Differential signal* $\Delta T = T_{tc}^{sample} - T_{tc}^{ref}$ *vs. time (red), vs. sample temperature (solid black), and vs. reference temperature (dashed black). For this data, the reference temperature remains quite linear in time as the sample melts, so that a linear scaling of the time axis makes the plots with x-axes of time and reference temperature practically identical.*

baseline has no significance with respect to thermal events in the sample and reflects heat transfer characteristics within the instrument. See Appendix C.

2.2. Samples

2.2.1 Mass

Figure 2.3 compares the signal during melting of different masses of pure Ag with a fixed mass of the reference. A large sample produces a larger peak signal (deflection from the baseline). However, the larger signal delays the temperature at which the signal returns to the baseline, making detection of closely spaced thermal events more difficult. On the other hand, large masses decrease the response time between the sample and sample cup. For careful work, sample mass vs. signal output should be examined for optimal performance. These items are discussed further in Appendix D.

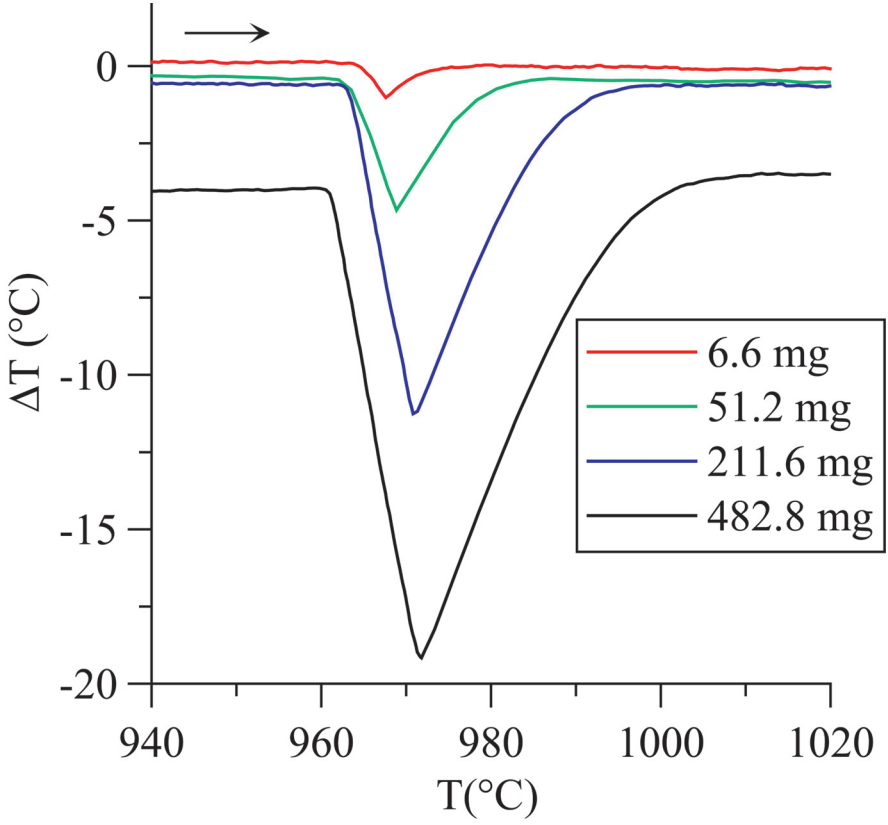

Figure 2.3. *Effect of sample mass on DTA signal for pure Ag. The reference mass was held constant. Heating rate is 10 K/min.*

2.2.2 Shape

Sample shape is a significant factor if the user wants to extract information on the first melting cycle. The shape will typically not conform to the shape of the sample cup. The thermal contact area between the sample and the cup will change during the melting process. This change can lead to a DTA peak shape that is difficult or impossible to interpret. Sometimes the effect of changing sample shape on first melt is more subtle. For the melting of pure Ag and for Ag-Cu eutectic, Figure 2.4 shows a shift of the baseline in the y-direction after the first melting that is not evident for the second melt. A more rounded onset and absence of linearity of the down-slope is also evident for the first melt (the expected linearity is described in section 2.4.2). If data from a first melt is desired, success may be achieved by careful grinding of the sample to conform to the crucible shape. In general, it is preferable to discard data obtained from the first melting run of a sample.

2.2.3 Powder samples

In general, the use of powder sample of metals and alloys can increase chances of contamination from atmosphere (oxidation), reduce heat flow

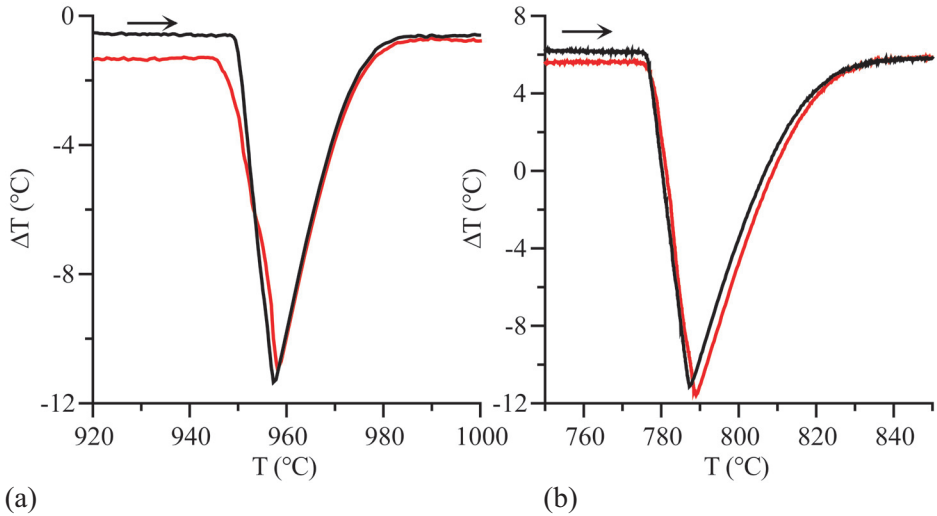

Figure 2.4. *DTA signal for melting of (a) pure Ag (211.6 mg; 10 K/min) and (b) Ag-Cu eutectic (231.3 mg; 15 K/min) comparing first melt (red) and second melt (blue). Note the offset of the baselines, the more rounded onsets and the lack of linearity of the down-slopes for the first melt compared to the second.*

within the entire sample mass and reduce the area of contact with the sample cup. However supercooling studies are enhanced by the use of powdered samples due to isolation of the most active heterogeneous nucleation sites into a small fraction of the powder population [84Per].

2.2.4 Inert powder cover

Some standard practice suggests mixing Al_2O_3 powder with powder samples or covering samples with a layer of Al_2O_3. This is done in an attempt to match the heat capacity and thermal conductivity of the sample and the (alumina) reference and produce a flatter baseline. Such practice must be weighed against the possibility of reaction between the sample and powder cover. If the wetting angle between the cup and sample is close to 180°, some authors suggest that use of an inert powder cover increases the thermal conduction to the sample cup.

2.2.5 Lid

A lid is useful for high vapor pressure materials to reduce material loss and contamination of the other parts of the instrument. A lid will also prevent sample radiation loss and help maintain an isothermal sample.

2.2.6 Atmosphere

For precision work, the use of commercial purity inert gas is not adequate. High purity inert gas coupled to a Ti getter furnace is usually adequate for most metals. Helium has a higher thermal conductivity than Ar; the choice can alter the thermal transport rates in the DTA instrument [03Rab]. Calibration should be performed with the same atmosphere as will be used for samples.

2.2.7 Crucible selection/reaction

High purity alumina is a standard DTA cup material. Zirconia and yttria cups can be made/purchased for highly reactive metals. The inside of alumina cups can also be coated with zirconia or yttria washes. Coatings of boron nitride may be useful for some materials. Graphite is usually an excellent crucible material for some non-reactive metals, like Au and Ag. For the selection of oxide crucibles, Table 1 gives the negative of the enthalpy of formation from the elements per mole of O (not O_2) for various oxides of the elements. Use of this table is shown by the following example that examines the suitability of using Al_2O_3 or Y_2O_3 as a crucible for Ti. The numbers taken from the table

Table 1 - Enthalpies of Formation of Solid Oxides ({ } Liquid, ( ) Gas)

$-\Delta H_f$ in kJ/mol for ½ O_2

$2/n\ M_mO_n(s) \leftrightarrow 2m/n\ M(s) + O_2(g)$ $\quad \Delta S = 184 \pm 10$ J/K
$M(s) + O_2(g) \leftrightarrow MO_2(g)$ $\quad \Delta S = 15 \pm 5$ J/K
$O_2 \leftrightarrow 2\ O$ $\quad \Delta H \approx 498$ kJ

{H_2O} 286 {H_2O_2} 94								
Li_2O 595 Li_2O_2 318	BeO 610							
Na_2O 415 NaO_2 261 NaO_2* 130 Na_2O_2* 256	MgO 601							
K_2O 361 KO_2 142 K_2O_2* 142	CaO 635	Sc_2O_3 623	Ti_2O_5 490 TiO_2 472 Ti_2O_3 507 TiO* 543	V_2O 456 VO 431 V_2O_3* 406 VO_2* 357 V_2O_5* 310	Cr_2O_3 376 CrO_2 293 CrO_3* 196	MnO 385 Mn_3O_4 346 Mn_2O_3* 319 MnO_3* 270	$Fe_{0.95}O$ 264 Fe_3O_4 280 Fe_2O_3* 274	CoO 239 Co_3O_4 226
Rb_2O 330 Rb_2O_3 176	SrO 604 SrO_2 326	Y_2O_3 627	ZrO_2 547	NbO 410 NbO_2 399 Nb_2O_5* 380	MoO_2 294 MoO_3 248	TcO_2 216 TcO_3 180	RuO_2 150 RuO_4 46	RhO 92 Rh_2O_3* 119 RhO_4 96
Cs_2O 318 Cs_2O_3 188	BaO 581 BaO_2 318	La_2O_3 597	HfO_2 556	Ta_2O_5 408	WO_2 295 W_3O_8 284 WO_3* 281	ReO_2 213 ReO_3 205 Re_2O_7* 178	OsO_2* 147 OsO_4 97	IrO_2 111
Fr	Ra	Ac						

Ce_2O_3 599 CeO_2 594	Pr_2O_3 603 PrO_2 475	Nd_2O_3 602	Pm	Sm_2O_3 609
ThO_2 613	Pa	UO_2 541 U_4O_9 502 U_2O_8* 447 UO_3* 408	NpO_2 514	PuO_2 527

Reference: A.W. Searcy, "Enthalpy and Predictions of Solid-State Reaction Equilibria" in "Chemical and Mechanical Behavior of Inorganic Materials," Eds. A.W. Searcy, A.V. Ragone and U. Colombo, Wiley-Interscience, New York, NY, 1970, pp. 33-55

* O. Kubaschewski, C.B. Alcock and P.J. Spencer, "Materials Thermochemistry," 6th Ed., Pergamon Press, Oxford, UK, 1993

								He
			B_2O_3 426	(CO_2) 197 (CO) 111	(N_2O_4) -10 (N_2O_5) -15	O	(OF_2) 18	Ne
			Al_2O_3 558	SiO_2 455	P_2O_3 273 P_2O_5 61 P_2O_5* 300	SO_3 151	(OCl_2) -81	Ar
NiO 240	Cu_2O 171 CuO 155	ZnO 348	Ga_2O 355 Ga_2O_3 363	GeO 212 GeO_2 363 GeO_2* 290	As_2O_4 198 As_2O_5 185	SeO_2 112 Se_2O_5 82	Br	Kr
PdO 96 PdO* 115	Ag_2O 30	CdO 258	In_2O_3 308	SnO 285 SnO_2 290	Sb_2O_3 240 SbO_2 290 SbO_2* 227	TeO_2 161	I	Xe
PtO_2 -85	Au_2O_3 1	HgO 91	Tl_2O 166 Tl_2O_3 129	PbO 217 Pb_3O_4 179 PbO_2* 137	Bi_2O_3 191	Po	At	Rn

EuO* 590 Eu_2O_3 554	Gd_2O_3 607	Tb_2O_3 622 TbO_2 486	Dy_2O_3 621	Ho_2O_3 627	Er_2O_3 632	Tm_2O_3 629	Yb_2O_3 604	Lu_2O_3 625
Am_2O_3 585	Cm	Bk	Cf	Es	Fm	Md	No	Lw

are: Al_2O_3 (ΔH_f = -558 kJ/mol), Y_2O_3 (ΔH_f = -627 kJ/mol), TiO ΔH_f = -543 kJ/mol). For the possible reaction of Al_2O_3 with Ti,

$$\tfrac{1}{3}(Al_2O_3) + Ti \rightarrow TiO + \tfrac{2}{3}Al$$

$$\Delta H_{reaction} = \Delta H_f^{products} - \Delta H_f^{reactants}$$

$$= (-543 + \tfrac{2}{3}\cdot 0)\text{kJ/mol} - (-558 + 0)\text{kJ/mol} = 15\ \text{kJ/mol}$$

whereas for the possible reaction of Y_2O_3 with Ti

$$\tfrac{1}{3}(Y_2O_3) + Ti \rightarrow TiO + \tfrac{2}{3}Y$$

$$\Delta H_{reaction} = \Delta H_f^{products} - \Delta H_f^{reactants}$$

$$= (-543 + \tfrac{2}{3}\cdot 0)\text{kJ/mol} - (-627 + 0)\text{kJ/mol} = 74\ \text{kJ/mol}$$

The equilibrium constant, *K*, is given by

$$\ln K = -\frac{\Delta H_{reaction}}{RT}.$$

At the melting point of Ti, *RT*=16.2 kJ/mol, so the equilibrium constant is of order unity, exp(–1), for the reduction of Al_2O_3, whereas the equilibrium constant is of order exp(–4) for the reduction of Y_2O_3. Thus a significant amount of Al_2O_3 can be reduced by Ti, whereas negligible amount of Y_20_3 is reduced by Ti. Yittria is a better crucible for Ti than alumina.

The observed absence of a distinct reaction product between a crucible and a sample can be misleading. Reaction products can sometimes go into liquid or solid solution in the sample, affect the thermal measurement, and not be easily observable; e.g., Al and O from Al_2O_3 into Ti alloys.

2.2.8 Evaporation

Excessive evaporation can reduce the sample mass and lead to incorrect measurement of enthalpy. Preferential loss of one or more components of an alloy can also lead to composition change. Mass loss is one of the reasons to employ simultaneous DSC/TGA (thermal gravimetric analysis). In addition, metals and alloys with high vapor pressure will lead to contamination of the furnace interior and thermocouple support assemblies. A good rule of thumb is to avoid materials with vapor pressures higher than approximately 100 Pa at the melting point, e.g., Zn and Cd.

2.2.9 Initial metallurgical state of alloy samples

At heating rates typical of a DTA, one cannot be certain that the microstructure of an alloy sample is in global equilibrium prior to or during analysis. A characteristic time required to eliminate spatial concentration gradients within phases is $\lambda^2/4D_S$ where D_S is the solid diffusion coefficient and λ is a distance that characterizes the modulation of the concentration. Near the solidus, D_S is typically 10^{-13} m^2/s for substitutional solutes or 10^{-10} m^2/s for interstitial solutes. For solidified samples cooled at between 5 K/min and 15 K/min, typical spacings of dendritic structures are approx. 100 µm to 200 µm. Hence, hold times of the order of 10^5 s or 10^2 s may be required for substitutional or interstitial alloys, respectively, to become homogenized. For interstitial alloys, normal thermal equilibration of the instrument prior to scans is usually sufficient to eliminate concerns about the prior homogeneity state of the sample and global equilibrium is likely to be maintained at slow scan rates in the DTA. However, the microstructural state of the substitutional materials must always be considered. If the user wants to determine the thermodynamic solidus, a series of melting runs following isothermal holds at successively higher temperatures below the proposed solidus value should be conducted to ensure that the sample has been annealed into an equilibrium structure. See section 3.2.2.

2.3. Reference materials

The ideal reference material is a substance with the same thermal mass as the sample, but with no thermal events over the temperature range of interest. The thermal mass is the product of the mass and the heat capacity. This provides the optimum condition to obtain a horizontal baseline. When the baseline is not horizontal, various methods (see for example [00Opf]) are used to fit and subtract a non-constant baseline from the signal. For some instruments, such a subtraction is done by the software. A horizontal baseline is not essential for the measurement of transition temperatures, but is important for quantitative enthalpy measurement. Alumina powder obtained from the instrument maker is often used as a convenient reference material for DTA and DSC of metals and alloys, even though the heat capacity differs significantly from that of most metals.

2.4. Calibration and DTA signal from pure metals

2.4.1 Fixed point (pure metal) enthalpy vs. temperature curves and DTA response

Calibration is performed by melting a pure metal because a pure metal exhibits a particularly simple enthalpy vs. temperature relation $H_S(T_S)$ as shown in Figure 2.5a. The subscript S is used to denote sample enthalpy and sample temperature as distinguished from, e.g., reference material enthalpy, sample thermocouple temperature. Below the melting point, T_M, the slope, $dH_S(T_S)/dT_S$, of the curve is the solid heat capacity. At the melting point, the curve experiences a jump in enthalpy, L, equal to the latent heat of fusion. Above the melting point the slope is the liquid heat capacity. Figure 2.5b shows the derivative curve, $dH_S(T_S)/dT_S$, where we employ the delta function $L\delta(T_S - T_M)$ of strength L located at $T_S = T_M$ to represent the jump of the $H_S(T_S)$ curve at T_M. Figure 2.5c shows schematic melting and cooling DTA curves. A useful way to think about the response of a DTA to melting and solidification is to consider an instrument response or transfer function that converts the delta function of Figure 2.5b into the quasi-triangular shaped peaks for melting and freezing seen in Figure 2.5c. Fourier methods are often used to represent instrument response functions. However due to the intrinsic nonlinearity of DTA response to the enthalpy curves, the heat flow model of Appendix C is preferred. The model confirms the central role that the rate of change of the sample enthalpy with respect to sample temperature, $dH_S(T_S)/dT_S$, plays in the DTA response, Eqn. C3. This derivative is usually referred to as the heat capacity; however the term is sometimes ambiguous, especially for alloys, in that it may or may not include the heat of fusion. In this document, the derivative $dH_S(T_S)/dT_S$ will be taken to include the heat of fusion. The derivative vs. temperature curve concept will be employed throughout this document as it becomes quite useful to understand and interpret alloy behavior in Parts 3 and 4 and Appendices F and G.

2.4.2 Temperature calibration: Effect of instrument thermal lags on onset determination

Temperature calibration of a DTA is typically performed using the melting of a pure metal or series of pure metals. A list of commonly used calibration substances is given in Table 2. Metals of 99.99% purity are usually adequate for metallurgical work. Research involving International Temperature Standards (ITS-90) employ higher purity metals and are available as NIST Standard Reference Materials (www.nist.gov).

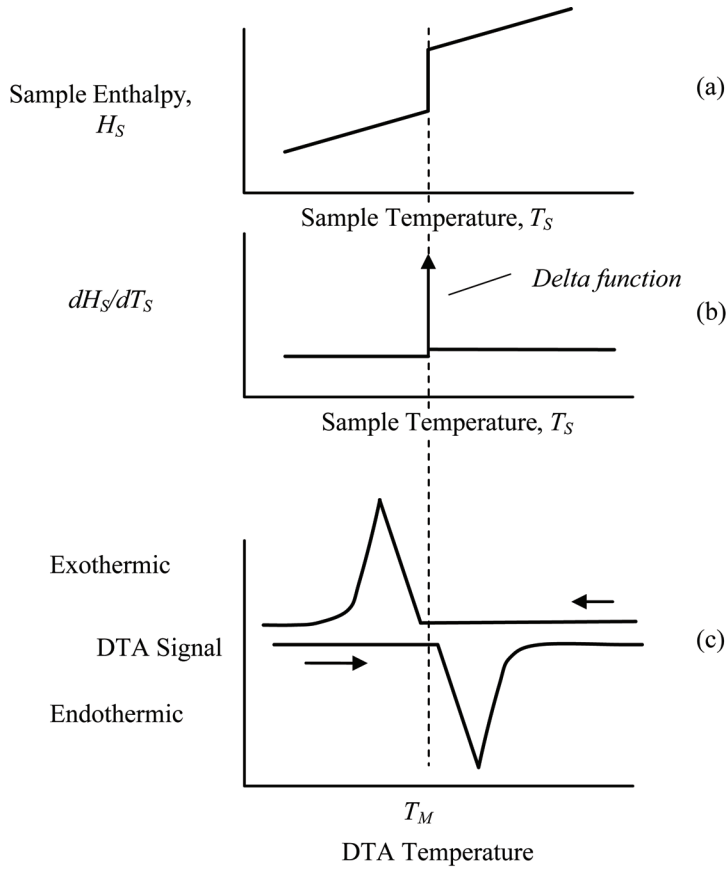

Figure 2.5. *Schematic a) enthalpy vs. temperature for a pure metal; b) corresponding derivative dH_S (T_S)/dT_S curve; c) DTA signal for melting (bottom) and freezing (top). The small difference in heat capacity of liquid and solid leads to a small offset of the baseline before and after melting. The onsets in the DTA curves are shown with a small deviation from the melting point, T_M, due to heat flow limitation in the DTA. This difference on melting is adjusted to zero by the calibration procedure, at least for one heating rate.*

In order to perform the calibration, the onset of melting must be determined from the data. For precision work, one must quantify various subtleties in the detection of melting for a pure metal and the thermal lags inherent in the instrument.

To directly observe the effects of the thermal lags, the melting and freezing of pure Sn was performed in a DTA instrument with an additional thermocouple (Type K) immersed directly into the Sn. The sheathed thermocouple was only 250 μm in diameter so that its thermal response is quite rapid. Figure 2.6a,b

Table 2 -Fixed Point Temperatures for Calibration [69Bar, 90Pre, 96Bed]

Substance	T/ºC	Ref.
In	156.5985	90Pre
Sn	231.928	90Pre
Bi	271.402	96Bed
Cd	321.069	96Bed
Pb	327.462	96Bed
Zn	419.527	90Pre
Sb	630.628	96Bed
Al	660.323	90Pre
Ag - 28.1 % Cu*	779.63	96Bed
Ag	961.78	90Pre
Au	1064.18	90Pre
Cu	1084.62	90Pre
Ni	1455	69Bar
Co	1494	69Bar
Pd	1554.8	96Bed

*Eutetic composition. In this document, the % symbol will refer to percentage by mass.

shows the temperature vs. time and associated DTA plots obtained with the immersed thermocouple and with the ordinary instrument thermocouple located beneath the sample cup. One notes the perfectly isothermal plateau at 232°C for the immersed thermocouple and the associated vertical drop in the DTA plot at the Sn melting point. The instrument sample thermocouple, on the other hand, is not isothermal during melting nor is the drop vertical on the associated DTA plot. This difference is due to the heat transfer limitations between the metal sample and the sample thermocouple and gives rise to the linear section of the DTA peak shape. In the section on supercooling effects (3.4.1), we will show the corresponding data during cooling experiments with the immersed thermocouple.

2.4.3 Temperature calibration: Choice of onset temperature

In normal DTA where the thermocouple is not immersed directly in the sample, the thermal lags cause the linear portion of the peak shape as well as a less sharp demarcation of the initiation of melting. This loss of sharpness can lead to difficulties of calibration for highly precise work as described in Appendix D. In Figure D1c, the temperature of the first detectable deviation

from baseline is labeled T_T^{onset}. The subscript T is used to denote thermocouple temperatures. Due to the inherent trouble of picking this temperature experimentally and due to the noise in the data, an alternative melting onset temperature is commonly employed. This procedure takes advantage of the fact that the thermocouple temperature vs. time, $T_T(t)$, curve quickly becomes linear after the melting onset; the onset temperature, T_T^{extrap} is taken as the intersection of a linear fit to the downward sloping linear section of the melting peak and the extrapolation of the baseline.

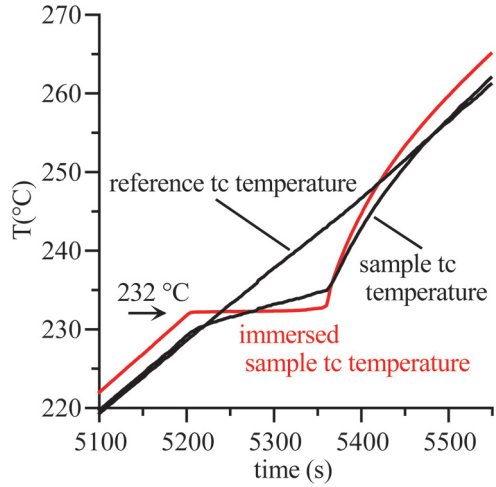

(a)

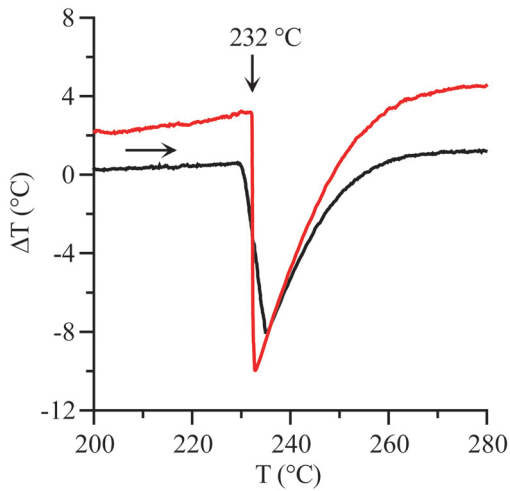

(b)

Figure 2.6. *Measured (a) temperature vs. time plots and (b) associated DTA plots for melting of pure Sn. The instrument thermocouple readings are black and the readings from a thermocouple immersed directly in the Sn in the sample cup is red. Mass = 163.2 mg; heating rate = 5 K/min.*

Following Eqns. D3 and D4, both T_T^{onset} and T_T^{extrap} deviate from T_M by an amount that depends on heating rate and on sample mass through the parameter ρ and the time constants, which depend on the area of contact between sample and cup. Thus calibration should ideally be conducted for a mass and heating rate similar to those that will be used for the test samples.

In addition to this consideration, it is best to use the first deviation from baseline method. We show in Appendix D that picking the first sign of melting actually has a smaller deviation from the true melting point and smaller heating rate dependence than the onset determined by the extrapolation procedure. This is one reason to prefer using the first detectable deviation from baseline for calibration. A second reason comes from the principle that the same method for the determination of the onset should be used for the calibration and the actual measurement on alloys. Alloys usually have a melting range and, therefore, do not melt with a linear section of the DTA curve (see e.g. Figure 3.8). Thus the onset for alloy melting is better taken using the first detectable deviation method. With these points in mind, it makes sense to use the first detectable deviation from baseline method for the calibration.

We note that ASTM E967 and articles on instrument calibration [90Höh, 91Höh] use the extrapolation onset temperature, T_T^{extrap}, to determine all onsets, even for alloys. With the use of computers for recording the thermocouple voltages, instrument manufacturers introduced software for the analysis of the DTA curves and determination of the reaction temperatures. In most cases the software uses the extrapolation method for the temperature determination T_T^{extrap} instead of T_T^{onset}.

2.4.4. Quantitative enthalpy and heat capacity calibration

In order to determine the quantitative heat flux, the difference signal (ΔT) must be converted to one of energy units by a calibration process. The method uses the heat of a specific transformation per unit mass in a standard sample, such as heat of fusion. The instrument sensitivity coefficient, S, at various temperatures is determined from the ratio

$$S = \frac{m_{standard}\Delta H_{standard}}{\int_{t_1}^{t_2} \Delta T(t)dt}$$

obtained from melting a series of standards (usually pure metals). The integral is the area of the peak deviation from the baseline determined from a plot of

ΔT vs. time. Alternately the original voltage difference from the thermocouples can be used instead of the temperature. The quantity $m_{standard}\,\Delta H_{standard}$ is the product of the mass of the standard and the heat of fusion per unit mass. For an unknown sample then,

$$m_{sample}\Delta H_{sample} = S\int_{t_1}^{t_2}\Delta T(t)dt$$

where S may be interpolated between the two standards spanning the temperature range of interest. The calibration is often performed by the instrument software and converts the DTA signal area from units of millivolt seconds or Kelvin seconds to Joules. In order to obtain accurate heat flux information, the same heating / cooling rate, gas flow rate, sample / reference cups, and temperature range should be employed for standard and unknown.

After conversion of the DTA signal to energy, some instruments provide a second calibration to directly provide heat capacity measurement. For many heat flux DSC instruments, heat capacity calibration is done by software with data obtained by performing a heating scan with a pair of empty cups, to get the baseline, and performing a second heating scan with the chosen reference material in one cup and an empty second cup. More details are given in ASTM E968.

2.5 Major points

- Important factors for proper technique:
  - Determination of what temperatures are being recorded and presented by the instrument and instrument software
  - Calibration
  - Crucible and atmosphere selection
  - Consideration of thermal gradients and associated thermal lag times within the instrument
- Determination of instrument time constants provides quantitative insight into thermal lags important in consideration of calibration procedures and general DTA response.
- For alloys, the microstructure and sample history may influence the measured response to thermal analysis.

Part 3: Analysis of DTA data for binary alloys

The general response of a DTA during cooling and heating for a series of alloys in a eutectic system where there is limited solid solubility is given schematically in Figure 3.1. In such general descriptions it is usually assumed that there is no barrier to nucleation on cooling and that solute diffusion is adequate to maintain the phases uniform in concentration at each temperature during the process. Under these assumptions, the phase fractions at each temperature follow the simple lever rule and the general shape of the DTA response is readily predicted, if the phase diagram and heats of fusion are known.

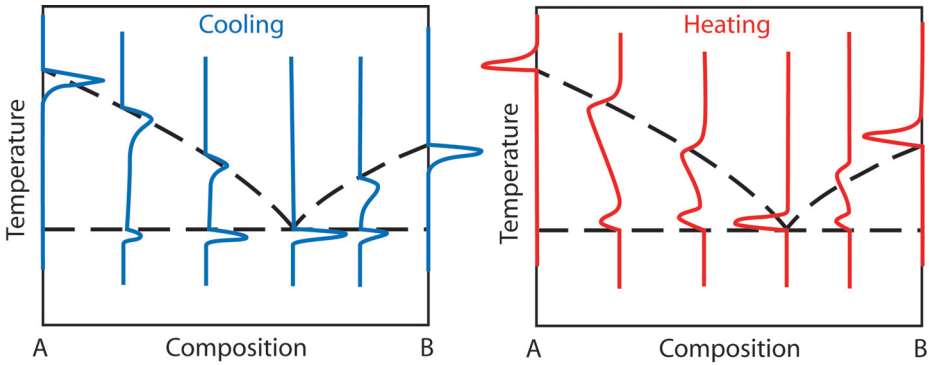

Figure 3.1. Schematic DTA response on coooling and heating of pure A and B and for other alloys superimposed on a simple eutectic phase diagram.

For other binary phase diagram features, such as peritectic reactions, the DTA response is not so easily understood. Thus the model of Appendix C is used to simulate how various phase diagram features are reflected in the DTA signals. It is our belief that such simulations can provide the DTA user with the understanding to enable more accurate interpretation of DTA results from samples with unknown phase diagrams.

For the simulations, we not only use the full equilibrium (lever rule) to obtain enthalpy vs. temperature curves but also another limiting case that is important in solidification. If an alloy has been solidified (even in the DTA), it may contain spatial gradients of composition within the phases. A limiting case of this kind of solidification is given by the Scheil (Scheil-Gulliver) approach. This approach, well-known in the solidification and casting field, assumes that no diffusion occurs in the solid during freezing, but that the liquid composition is uniform [74Fle]. DTA melting simulations using the lever enthalpy-temperature relation apply to an alloy equilibrated prior to melting and where diffusion was adequate to guarantee spatial concentration uniformity of all

(a)

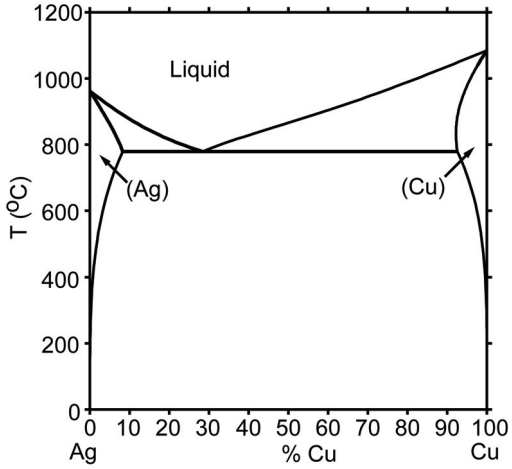

(b)

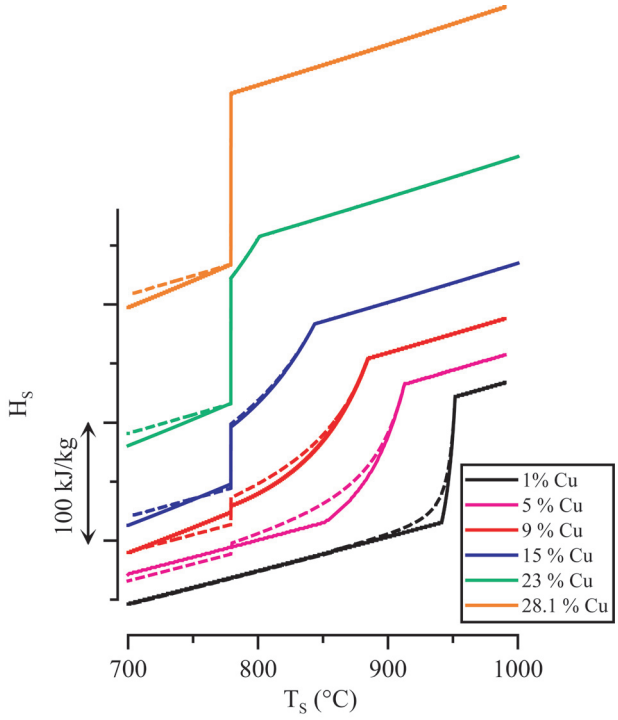

Figure 3.2. *(a) Ag-Cu phase diagram; (b) Enthalpy vs. temperature curves for five Ag-Cu alloys (solid, equilibrium; dashed, Scheil); the curves have been shifted vertically for clarity, only differences of enthalpy are relevent; (c) dH_S / dT_S vs. T_S curves for equilibrium conditions for various Ag-Cu alloys derived from the equilibrium enthalpy curves (overleaf). The vertical arrows at the eutectic temperature (779°C) represent delta functions of the indicated strength in kJ/kg.*

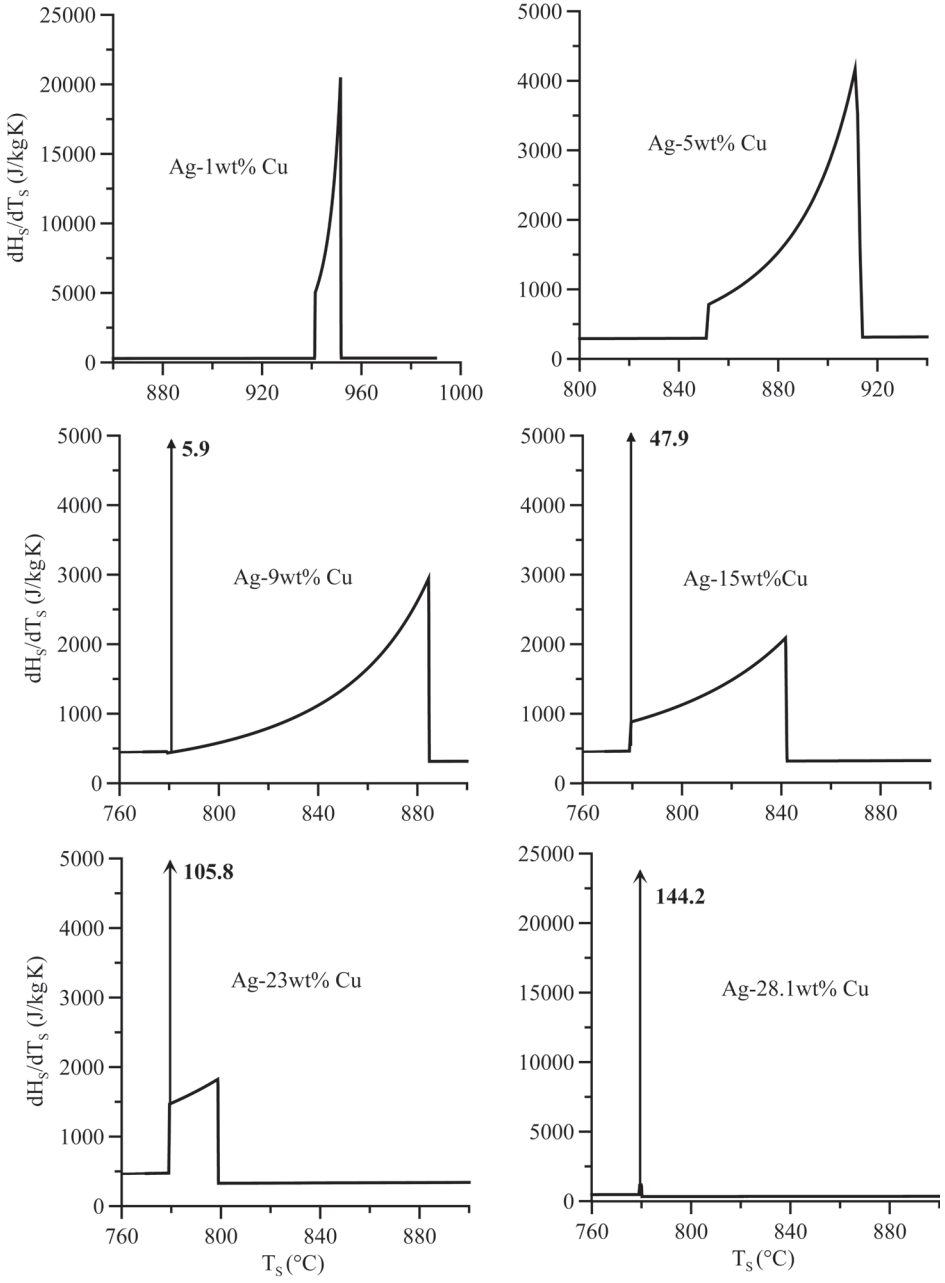

(c)

Figure 3.2. *(continued)*

phases during melting. DTA melting simulations using the Scheil enthalpy relations apply to a microstructure that was previously solidified and remelted where there was no solid diffusion during *both* processes. Clearly these are extreme cases; interpreting DTA data from the melting of an equilibrated sample as well as an as-cast sample requires an analysis of solid diffusion for both the freezing process and the melting process that is beyond the scope of this document ([02Boe] treat diffusion during melting). Enthalpy vs. temperature relations can be computed more simply for the extreme cases without the requirement of any kinetic information or geometry of the microstructure. The enthalpy vs. temperature relations are obtained from two different methods in this document: analytical expressions applicable to straight line phase diagrams (Appendix E) and numerical data applicable to real alloy systems obtained from a Calphad assessment of the thermodynamic functions.

3.1 General behavior for a binary eutectic system; example Ag-Cu alloy melting

The Ag-Cu alloy system is used to illustrate various features of DTA analysis.

3.1.1 Enthalpy vs. Temperature curves

Figure 3.2a shows the Ag-Cu phase diagram, and Figure 3.2b shows the enthalpy vs. temperature curves for six Ag-rich Ag-Cu alloys, under equilibrium and Scheil conditions. The thermodynamic data of [86Hay] were employed to construct the phase diagram and to produce the enthalpy vs. temperature information using code developed by [96Kat]. Other code, such as Thermo-Calc or Pandat, could have also been used. The 1% Cu alloy exists as a single phase solid solution alloy with liquidus and solidus temperatures defining the temperature range where liquid phase and the Ag-rich face centered cubic (FCC) phase coexist. (In this document, the % symbol will refer to percentage by mass.) With increasing temperature, the enthalpy curve has a sharp increase of slope at the solidus for the equilibrium curve but a smooth increase in slope for the Scheil curve[§]. For the 5% Cu alloy, the enthalpy curve has a sharp increase of slope at the solidus for the equilibrium curve but an isothermal jump for the Scheil curve corresponding to the eutectic. The enthalpy curve is concave up between the solidus and the liquidus, combining the effects of changing heat capacity of the solid and liquid phases as well as the heat of fusion associated with the changing fractions of liquid and solid phases. The 9% Cu and 15% Cu compositions are two phase alloys when

[§] Technically, the Scheil approach predicts some eutectic for all alloys. In this case, the mass fraction of eutectic is very small. 0.003 and would not be detected.

solid; the solidus is the eutectic temperature. The enthalpy curves for both Scheil and equilibrium conditions have isothermal (vertical) rises in enthalpy corresponding to the eutectic melting of a mixture of Ag-rich phase and Cu-rich phase. The height of the isothermal rise is larger for Scheil than for equilibrium conditions and is larger for the 15% alloy than for the 9% alloy. Upon completion of eutectic melting, all of the Cu-rich phase has melted and the enthalpy curve rises with heating corresponding to the continued melting of the Ag-rich phase. For the Ag-28.1% Cu alloy, the enthalpy curves has only an isothermal rise in enthalpy corresponding the eutectic melting.

For the Ag-15% Cu and 23% Cu alloys there is little difference between the Scheil and equilibrium calculations**. This is because there is so little non-eutectic Ag-rich FCC phase that any microsegregation within this phase has little effect on the heat evolution and fraction of eutectic that forms. For the other alloys, significant differences arise between equilibrium and Scheil enthalpies that are important to the interpretation of DTA curves. Most striking is the presence of an isothermal rise in the enthalpy corresponding to the eutectic in the 5% Cu alloy for the Scheil enthalpy whereas no rise is present for the equilibrium enthalpy. The microsegregation within the Ag-rich FCC phase predicted by the Scheil calculation leads to the formation of eutectic, whereas when solid diffusion is adequate to keep the Ag-rich FCC phase uniform in composition, no eutectic forms.

3.1.2 Derivative of enthalpy vs. temperature curve and their relation to DTA curves

As developed in section 2.4.1, the temperature derivative (slope) of the enthalpy vs. temperature curve determines the DTA response. Figure 3.2c shows these derivatives for the Ag-Cu alloys for the equilibrium enthalpy. The delta functions corresponding to the isothermal jumps in enthalpy are labeled with the size of the jump. Just as the DTA response to a delta function for a pure metal is altered by the instrument, so is the response to the alloy dH_S / dT_S curve. This alteration can be quantitatively viewed through the following sequence of operations. First flip a dH_S / dT_S vs. T_S curve (from Figure 3.2c) so that the positive y-axis become negative. Second, broaden this

** We note the difference in solid heat capacity predicted by the equilibrium and Scheil models. This difference is due to the fact that the equilibrium computations permit the solid state adjustment of the phase fraction and compositions of the Ag-rich and Cu-rich phases as temperature changes, whereas the Scheil calculation assumes that these phases have fixed composition and phase fractions as the temperature changes.

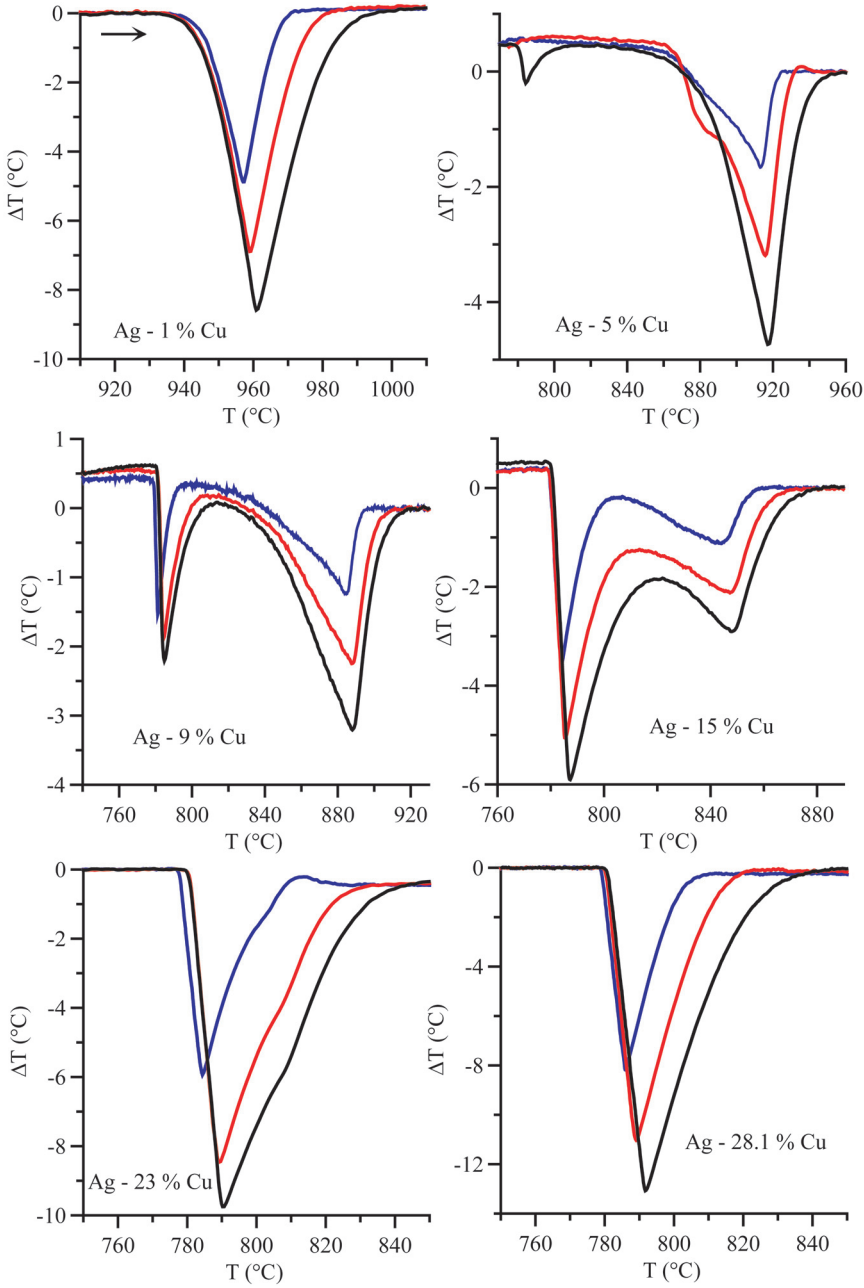

Figure 3.3. *Experimental DTA melting scans for a series of Ag-Cu alloys at three different heating rates, 5 K/min (blue), 10 K/min (red) and 15 K/min (black). Note that the small signal for the eutectic melting is absent in the Ag-5 % Cu alloy at the slower heating rates. Note also the absence of a distinct second peak in Ag-23 % Cu. Percentage is by mass.*

curve in the direction of the x-axis (temperature axis). This shape is a rough approximation to the DTA curve for melting.

The experimentally determined DTA melting responses of a series of Ag-Cu alloys at three heating rates are shown in Figure 3.3. It can be seen that the general shapes of the DTA curves are indeed modified versions of the derivative curves, dH_S / dT_S vs. T_S. For Ag-1% Cu and Ag-28% Cu only a single peak is observed. For Ag-9% Cu and Ag-15% Cu two peaks are clearly shown. The first peak begins near the eutectic temperature and the maximum signal of the second peak occurs near the liquidus. The reason the maximum signal of the second peak is associated with the liquidus temperature will be discussed in section 3.3. For Ag-5 % Cu at the fastest heating rate, a small signal is evident at the eutectic temperature. At the slowest heating rate, the small signal for the eutectic melting is absent. The two peaks for Ag-9% Cu and Ag-15% Cu are for the completion of eutectic melting and the final melting of the Ag-rich FCC phase. For Ag-23% Cu, while there are not two distinct peaks, there is a slight bulge or shoulder for the final melting of the Ag-rich FCC phase before the return to the baseline that corresponds to the liquidus. Clearly, the peak temperature corresponding to the end of melting of the Ag-rich phase is too close in temperature to the strong signal from the end of melting of the eutectic for the response times of the instrument. Thus no distinct peak is observed for the liquidus.

3.1.3 Comparison to Experiment

Figure 3.4 shows how the measured DTA scans at 5 K/min compared to the calculated DTA scans using the equilibrium and Scheil enthalpies. The general agreement between the calculated and measured results validates the use of the model to simulate and assist in the data interpretation of more complex alloys. For the 15% Cu, 23% Cu and 28.1% Cu, the model predicts all observed features as well as trends of amplitude and observed temperatures with alloy composition. The general shapes of the experimental curve for the 1% Cu and 5% Cu alloys generally lie between the shapes of the lever calculation and Scheil simulation in the lack of sharpness of the onset. This intermediate behavior indicates that solid diffusion is not sufficient to permit full equilibration to be reached at each temperature during heating.

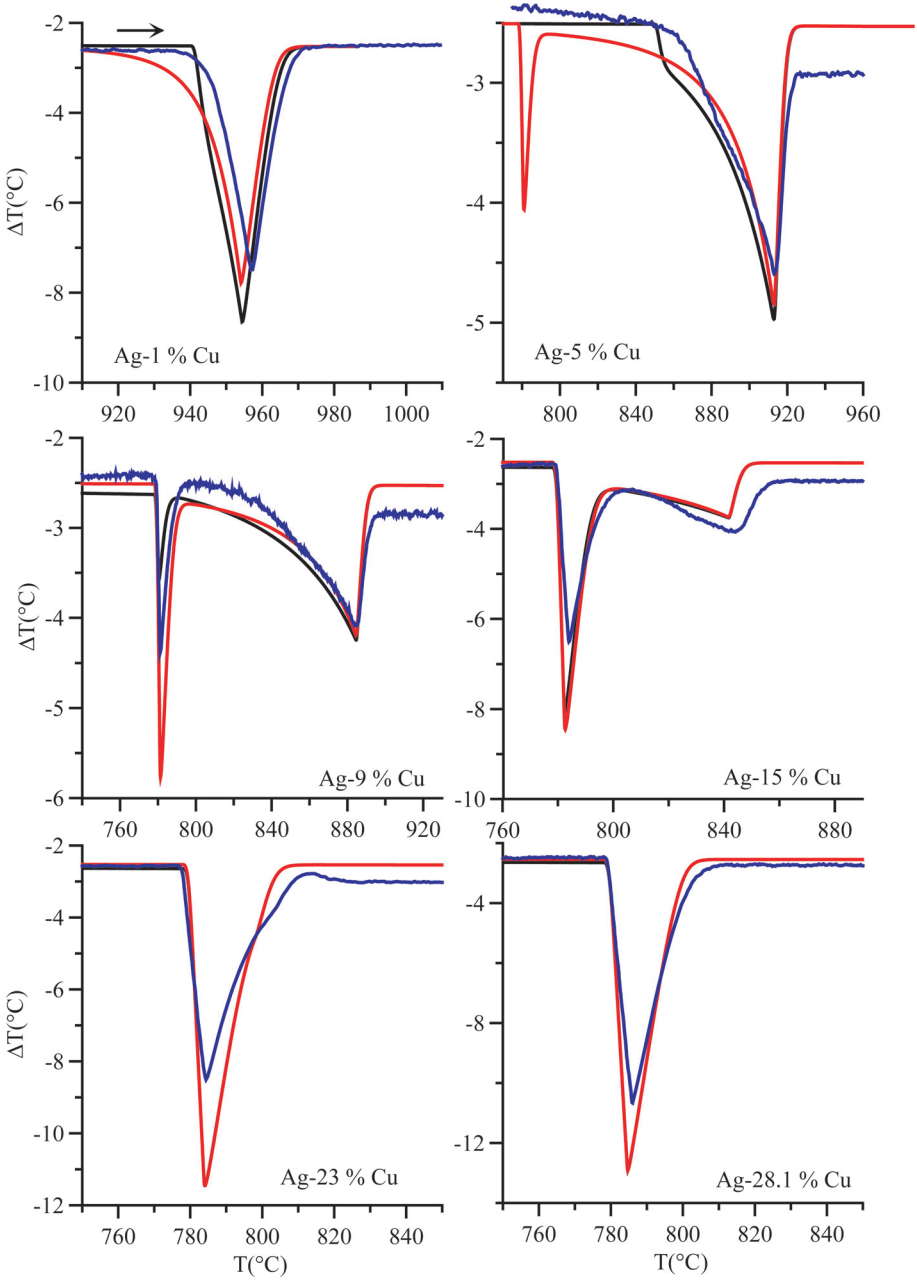

Figure 3.4. *Computed DTA curves for Lever (black) and Scheil (red) at 5 K/min. The experimental DTA curves are shown blue. Lever and Scheil curves for two alloys are essentially identical and only the Scheil curve is shown for Ag-23 % Cu, and 28.1 % Cu.*

3.2 Problems with solidus determination on heating

3.2.1 Incipient melting point vs. solidus

The temperature at which a solid alloy begins to melt depends on the history of the material. The terms *solidus, nonequilibrium solidus* and *incipient melting point*, are variously used in the literature to describe the minimum temperature where some liquid forms. As mentioned earlier, this Guide only uses the term solidus to refer to the thermodynamic quantity. Cast alloys often begin melting at temperatures below the solidus of the average composition, the incipient melting point, which stems from the existence of composition gradients within individual phases or the presence of extra phases in the alloy microstructure. Whether a DTA sample is taken directly from a casting or if it has been frozen in the DTA, it is uncertain if the solid microstructure is in global equilibrium at heating rates typical of a DTA. Hence, the microstructural state of the material must always be considered when performing an alloy melting experiment. This point was previously discussed in section 2.2.9.

3.2.2 Effect of hold time prior to melting

If the user wants to determine the thermodynamic solidus rather than the incipient melting point, a series of melting runs following isothermal holds at successively higher temperatures below the proposed solidus value should be conducted to ensure that the sample has been annealed into an equilibrium structure. An example of this situation is shown in Figure 3.5 for a Ag - 5 % Cu alloy. After a first melting scan to obtain good thermal contact with the alumina crucible, the sample was cooled at 15 K/min to 760°C and then immediately remelted at 15 K/min. This cycle was repeated with successively increasing hold times at 760°C. The temperature of the large peak remains relatively fixed, but the onset varies considerably. For the sample with zero hold time, the onset of melting occurs at the eutectic temperature, 779°C. This onset disappears with the 5 min hold, the onset increasing to 862°C, where it remains with further increase of the hold time. The lower onset occurs without hold time because of the metallurgical state of the alloy after freezing. Such a sample contains dendritic coring of the Ag-rich phase (microsegregation) and eutectic consisting of Ag- and Cu-rich phases. The amount of time needed to homogenize the phases and dissolve the eutectic depends on the hold temperature, which affects the solid diffusion coefficient, and on the distance between dendrite arms. The required hold time increases as the square of the length scale. The finer the length scale, the shorter the hold time. Therefore, as a corollary, more rapid preceding freezing results in a finer spacing and a shorter hold time. Significantly, this is contrary to normally

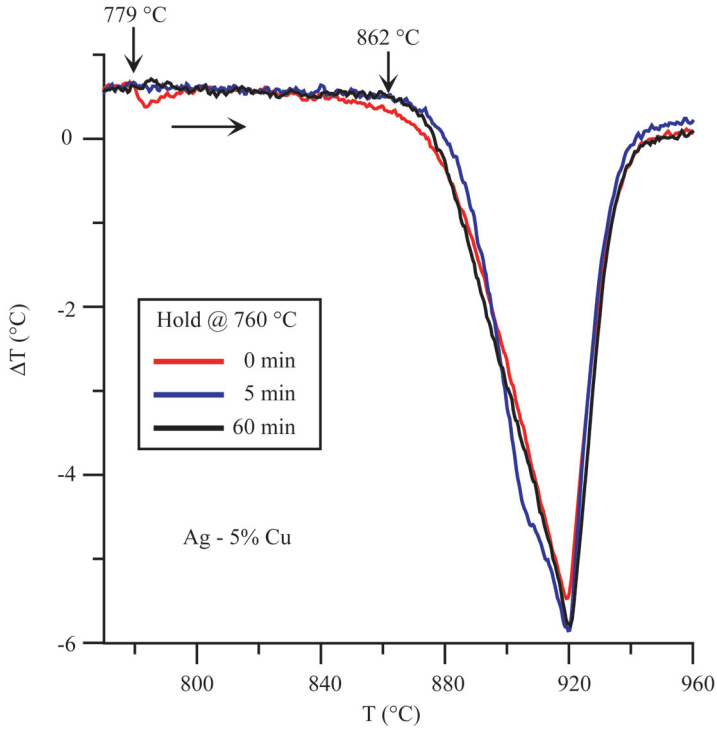

Figure 3.5. *DTA signal for melting of Ag- 5 % Cu showing the effect of hold time at 760°C and subsequent heating at 15 K/min.*

accepted DTA practice where slower cooling is usually thought to be better, an idea based on the assumption that the slow rates in a DTA are sufficient to guarantee freezing following the lever rule.

Figure 3.6 shows the computed DTA curve for an enthalpy vs. temperature relation when diffusion can occur in the solid as derived from a *back diffusion* model of solidification, Eqn. E11, at 5 K/min for a Ag 5 % Cu alloy. The predicted strength of the eutectic signal is less than that for the Scheil case, but is not as small as the measured eutectic signal with no annealing in Figure 3.5. This might indicate that the fraction of eutectic in the DTA cast alloy has undergone further reduction during the short equilibration time required before the heating scan was begun.

Figure 3.7 shows another example of how annealing time prior to melting changes the DTA signal for Inconel 718 alloy [91Cao]. With annealing, the $(Fe,Cr)_2Nb$ Laves phase present in the industrially cast sample dissolves

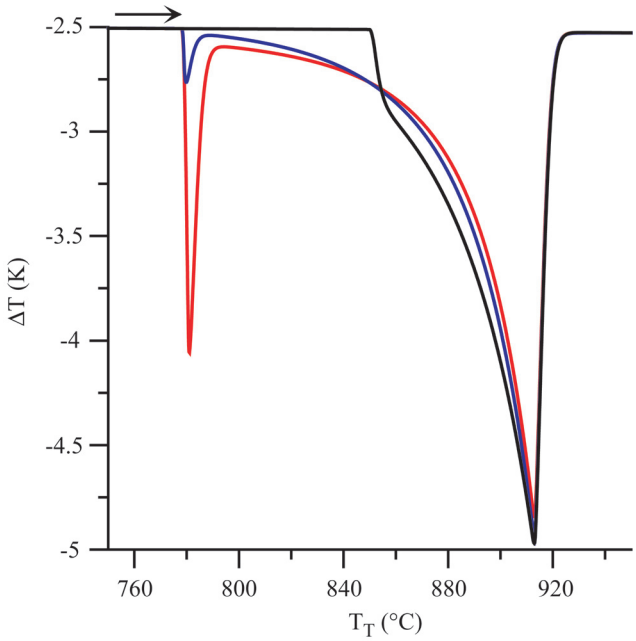

Figure 3.6. *Computed DTA curve for an enthalpy vs. temperature relation derived from a back diffusion model of solidification at 5 K/min of Ag 5 % Cu is shown blue.* $D_S = 1 \times 10^{-14}$ m^2 / s, $\lambda_2 = 3.8 \times 10^{-5}$ *m. The equilibrium curve is black and the Scheil is red. The peak eutectic signal at approx. 780°C is intermediate between that for the Scheil and equilibrium cases but is not as small as the measured eutectic signal with no annealing in Figure 3.5.*

and the onset of melting increases from 1163°C to 1247°C to reveal the true solidus temperature. The lower temperature is the incipient melting point of the casting and is important for constructing heat treatment schedules for the casting.

3.2.3 Errors caused by using extrapolated melting onset (tangent construction)

It has already been noted (2.4.3) that the temperature of the first visible onset of melting is generally preferable over linear extrapolation methods for solidus determination (in spite of the prevalent use of the latter). This is especially true for solid solution alloys. Unlike a pure metal or an alloy containing eutectic, there is no physical basis for a linear section of the DTA curve. There is thus no theoretical basis for using the intersection of the baseline with the linear extrapolation of any portion of the DTA curve to determine the

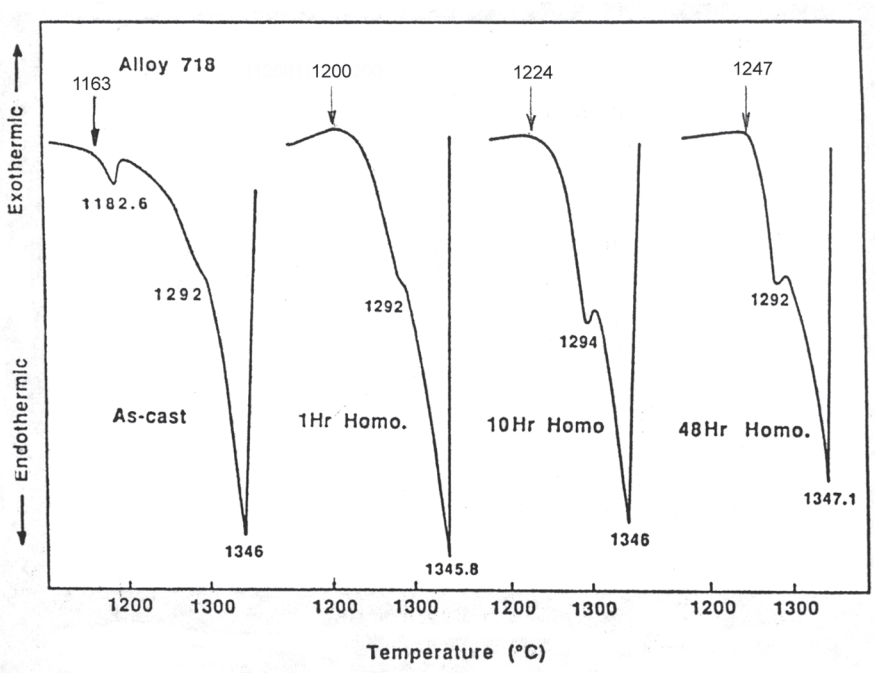

Figure 3.7. *DTA signal for Inconel 718 showing the effect of annealing time [91Cao]. With annealing, the* $(Fe,Cr)_2Nb$ *Laves phase dissolves and the onset of melting increases from 1163°C to 1247°C.*

solidus temperature. As soon as a deflection from the baseline occurs, melting is surely taking place. Compare the DTA curves for the melting behavior of pure Ag and eutectic (Figure 2.4, second melts) to the curves for Ag-1% Cu and Ag-5% Cu (Figure 3.3); see also Figure 3.10 b,c below. For the pure metal and the eutectic, the onset is quite sharp and the DTA curve is linear after the onset; the DTA curves for the alloys with no eutectic have no linear portion near the onset of melting from which to construct an extrapolated onset. Examples of errors introduced using the extrapolation method of determining onset compared to the first detectable departure from baseline are shown schematically in Figure 3.8.

3.3 Problems with liquidus determination on heating

It is customary to select the peak temperature of the last thermal event on heating as the liquidus temperature. However in the results for Ag - 23% Cu (mass), Figure 3.3, it was seen that a distinct peak did not exist for the end of melting because the liquidus temperature was too close to the eutectic temperature. Other subtleties of liquidus determination on melting require exposition.

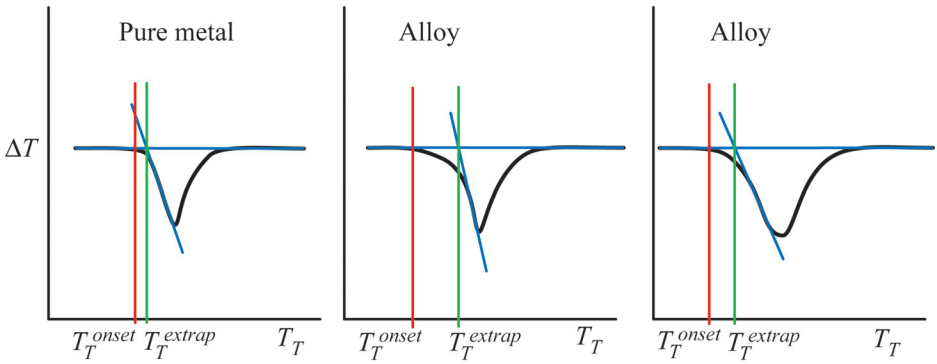

Figure 3.8. *Schematic DTA plots showing error introduced by using the extrapolation method for onset determination rather than the first detectable departure from baseline.*

3.3.1 General DTA curve analysis

The alloy, Ag - 15 % Cu, is examined in more detail to indicate which features of its DTA curves are important and which features are unimportant during melting and freezing. This discussion may appear obvious to some but examples abound in the literature of incorrect conclusions drawn from DTA curves. Figure 3.9 repeats the dH_S / dT_S vs. T_S using the equilibrium enthalpy for Ag - 15 % Cu from Figure 3.2c and also shows the computed DTA melting and freezing scans at 5 K/min. As the dH_S / dT_S plot shows, there are only two temperatures that have significance: the vertical jump at 842°C (liquidus temperature) and the delta function at 779°C (eutectic temperature). Features on the DTA scans are labeled with: **i** = important or **n** = not important depending on how well they approximate these two temperatures. The significant temperatures **i** are close to the liquidus and the eutectic temperature. In contrast, the heat transfer details produce other features **n** on the DTA scans which bear no direct relation to the above two temperatures. Furthermore, note the asymmetry of the interpretation of the melting and freezing scans. For example, the peak on melting near the liquidus temperature is important but the peak just below the liquidus on cooling is unimportant. Similarly the temperature of minimum deflection from baseline between the eutectic and liquidus temperatures on heating has no meaning yet the minimum deflection between the liquidus and eutectic temperatures on cooling is important; it is the onset of eutectic freezing.

We also note that after the completion of melting or the completion of freezing, no extra heat beyond the liquid heat capacity is required for contin-

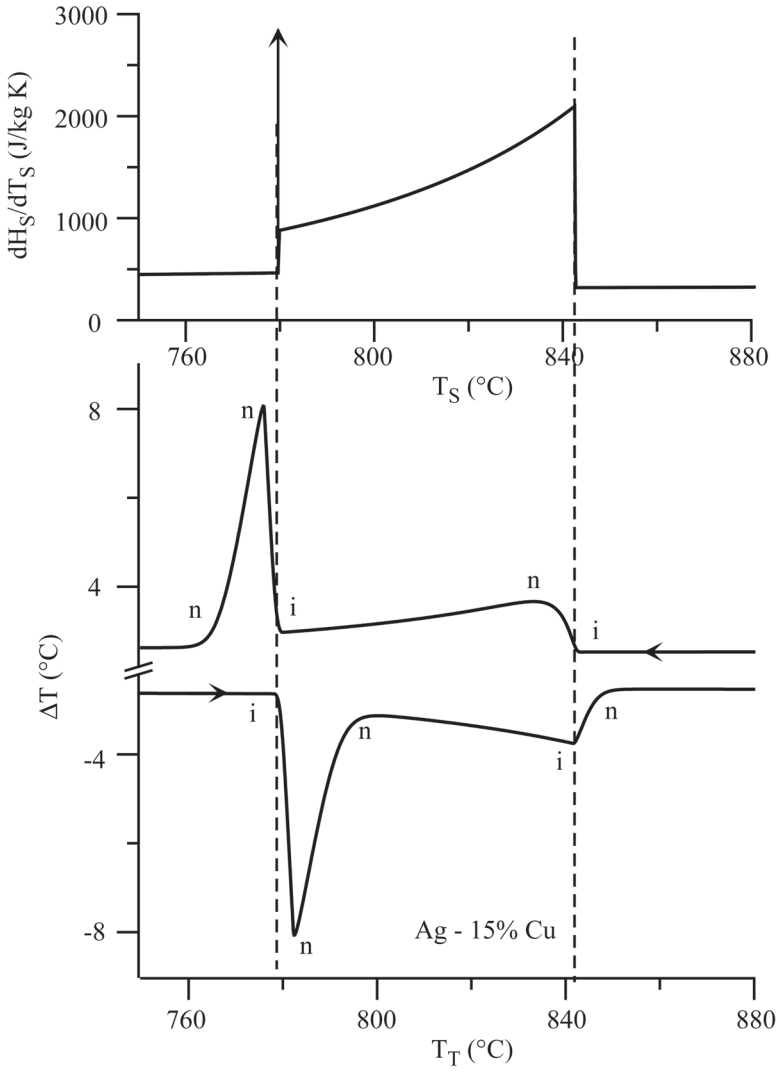

Figure 3.9. *dH_S / dT_S* vs. *T_S (top) and computed DTA scans for melting and freezing at 5 K/min (bottom) for Ag- 15 % Cu using equilibrium enthalpy. Features on the DTA scans are labeled with: **i** = important or **n** = not important.*

ued sample heating or cooling. The sample temperature increases/decreases rapidly after the completion of melting/freezing to catch up with the reference and furnace temperatures; the shape of the return and the temperature of the return of the DTA signal to the baseline are only measures of the efficacy of heat transfer. They have no metallurgical or thermodynamic meaning.

In solidification of binary alloys, one often employs two numbers to describe the liquidus and solidus curves for dilute allys, the liquidus slope, *m*, in units of K/% (for example) and the partition coefficient, *k*, which is the ratio of the

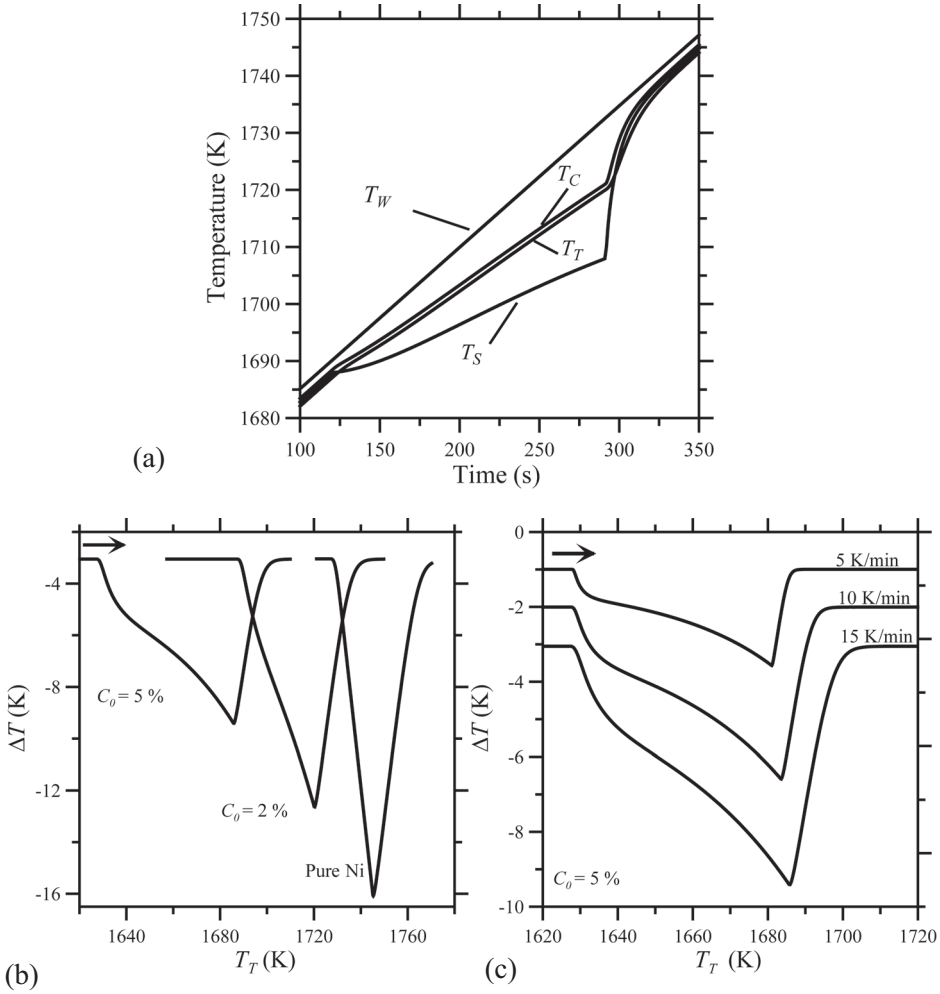

Figure 3.10. *a) Plot of calculated temperatures vs. time for sample (T_S), sample cup (T_C), sample thermocouple (T_T) and furnace wall (T_W) for melting at a heating rate of 15 K/min of a 180 mg binary alloy sample that melts following the lever rule enthalpy, with T_M = 1728 K, m = -10 K / %, k = 0.5, C_0 = 2%. The model of Appendix C and the instrument time constants from Table C1 for Ni were employed. b) Calculated DTA curves for pure Ni and alloys with C_0 = 2% and 5% following the lever rule at 15 K/min. c) Calculated DTA curves for alloy with C_0 = 5% following the lever rule at heating rates of 5 K/min, 10 K/min, and 15 K/min.*

solid composition to the liquid composition. So far, the DTA response has been described for an alloy where the liquidus slope, m, is negative and the partition coefficient, k, is less than unity. See section 3.3.5 for further complicating factors for alloys with $m>0$ and $k>1$.

3.3.2 Details of computed behavior of an alloy on melting

For a solid solution alloy with no eutectic, the equilibrium equation for enthalpy, Eqn. E11, and numerical solution of Eqn. C1 are employed to determine the temperature - time histories and the DTA signal for alloy melting. Figure 3.10 shows the time histories of the temperatures of the various parts of the DTA instrument for a hypothetical Ni - base alloy of composition of alloying addition C_0 = 2% (k=0.5, m = -10 K / %) with solidus/liquidus values of 1688 K/1708 K. It is important to note that the value of the thermocouple temperature at the instant when the sample completes melting at the liquidus temperature (Figure 3.10a at ≈ 290 s) is ≈ 1720 K, 12 K higher than the liquidus temperature. Figure 3.10b shows that the peak temperature is near 1720 K. The figure also shows the DTA plots of a 5% alloy and also pure Ni for comparison. Figure 3.10c shows how heating rate affects the computed DTA scan.

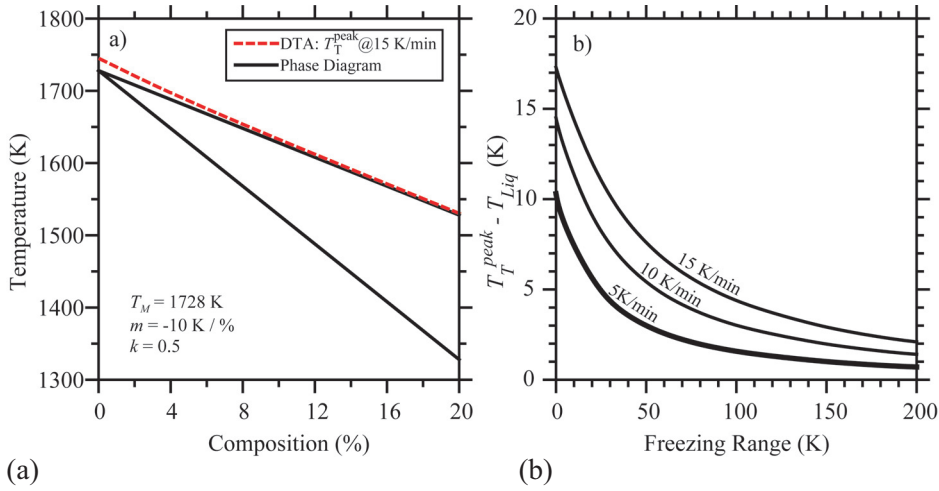

Figure 3.11. *a) DTA peak temperature calculated at a heating rate of 15 K/min for different alloy compositions using a lever assumption. Peak temperature is superimposed on the phase diagram (T_M = 1728 K, m = -10 K /%, k = 0.5). b) The difference between the peak temperature and the liquidus temperature as a function of freezing range at three heating rates. The freezing range is given by mC_0 [(k - 1)/k)].*

3.3.3 Small liquidus solidus separation

Figure 3.11a shows calculated DTA peak temperatures superimposed on the phase diagram for $0\% < C_0 < 20\%$. Figure 3.11b shows the difference between the peak temperature and the liquidus temperature. One notes that the peak temperature lies above the liquidus temperature with an error increasing as the concentration of the alloying element decreases. In other words, if the freezing range of the alloy is small (of the order of the temperature difference between the onset and peak temperature of a pure metal melting DTA scan), the peak temperature of the DTA can only serve as an upper bound on the liquidus temperature.

3.3.4 Resolution of difficulties using temperature cycling near the liquidus

Cycling experiments can be used to determine the liquidus for small freezing range alloys or for alloys where the fraction of the final phase on melting is small. This approach was demonstrated by [00Wu] for complex superalloys and is shown in Figure 3.12. First an upper bound on the liquidus is determined from the peak temperature of an ordinary DTA scan, 1399°C in (a). Then a lower bound is determined by the cooling curve, 1358°C in (b) as the nucleation temperature. Clearly significant supercooling has occurred. Next the sample is cooled, reheated and held at a temperature below the upper bound temperature, 1380°C in (c) for 10 min, and then heating is reinitiated. Signs of an endothermic signal are sought. If absent, a fully liquid state is implied for the hold temperature and the hold temperature is above the liquidus temperature. If present, a partially solid state is implied at the hold temperature and the hold temperature is below the liquidus. In Figure 3.12c with a hold temperature of 1380°C, no endothermic signal was seen. Thus the cycle was repeated at a lower hold temperature. This process is repeated until an endothermic sign of melting is seen. With this process the liquidus temperature can be bracketed to within a few degrees, 1378°C to 1379°C in the present case.

3.3.5 Alloys with $k<1$ and $k>1$; peak temperature

A second problem with respect to liquidus temperature determination may be encountered when dealing with an alloy for which the partition coefficient $k>1$. The $k>1$ case applies whenever the liquidus/solidus separation (freezing range) decreases with decreasing temperature. The more common situation, $k<1$, applies whenever the liquidus/solidus separation increases with decreasing temperature. See Figure 3.13a. To demonstrate this effect we compare the

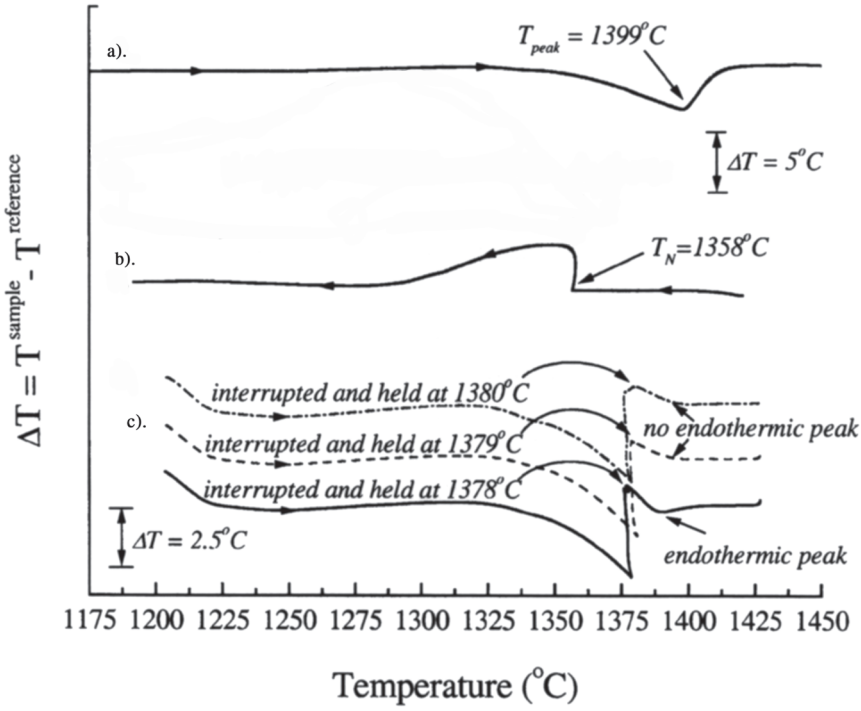

Figure 3.12. *a) Normal DTA scan on heating for a small greezing range Ni-base superally; b) Normal DTA scan on cooling. Supercooling has occurred; c) Cycling DTA to determine the liquidus temperature [00Wu].*

computed DTA response of two alloys with identical heats of fusion, and liquidus and solidus temperatures with $k = 2$ and $k = 0.5$. Again we use the straight line liquidus and solidus model, Eqn. E1, and enthalpy given by Eqn. E9, and the computation method of Appendix C. The derived dH_S / dT_S vs. T_S curves are shown in Figure 3.13b. The computed DTA scans for three heating rates are shown in Figure 3.13c,d. For $k<1$, the DTA curve exhibits a sharp peak at 1681°C (for 5 K/ min). For $k>1$, the DTA curve has a broad peak at 1639°C and a shoulder at 1679°C (for 5 K/min). The liquidus temperature for both is 1678°C. Hence it is clear that the peak temperature for the $k>1$ case bears no relationship to the liquidus. For $k<1$, more of the latent heat is released higher in the freezing range compared to the case for $k>1$ where more of the latent heat is released lower in the freezing range. In other words, for $k<1$, the value of dH_S / dT_S increases with temperature, whereas for $k>1$, the value of dH_S / dT_S decreases with temperature, Figure 3.13b. Because the $k<1$ case is much more common for alloys, there is a strong association of the peak

temperature on the DTA with the liquidus temperature. This indicates that such is not always the case. This point is reinforced by the simulation shown in Figure 3.14 using real thermodynamic data for Bi-rich and Sb-rich alloys of the Bi-Sb isomorphous system.

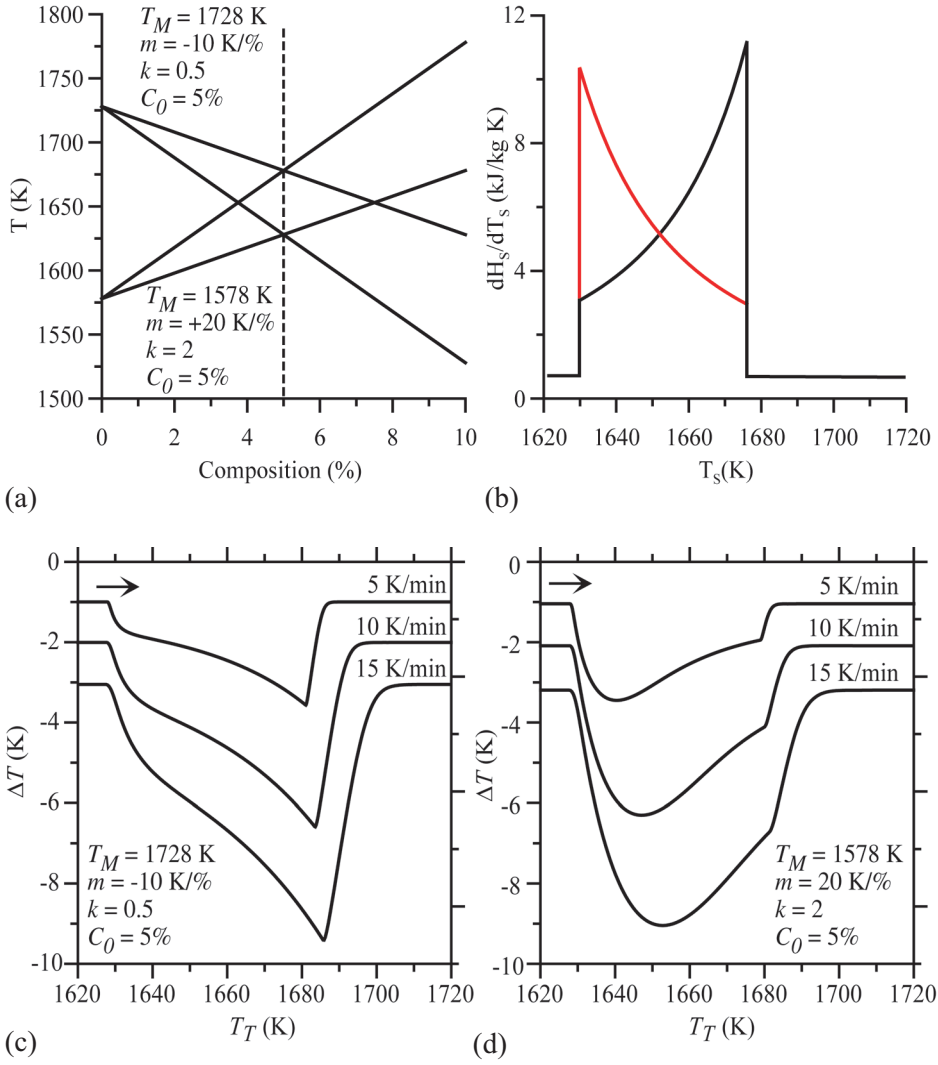

Figure 3.13. *Comparison of two hypothetical alloys with identical heat of fusion, liquidus and solidus temperatures but differing having k<1 and k>1. a) Phase diagram, b) dH_S / dT_S for k<1 (black) and k>1 (red), c) DTA for k<1 and d) DTA for k>1. For k<1, the latent heat is released higher in the freezing range compared to k>1 where the latent heat is related lower in the freezing range.*

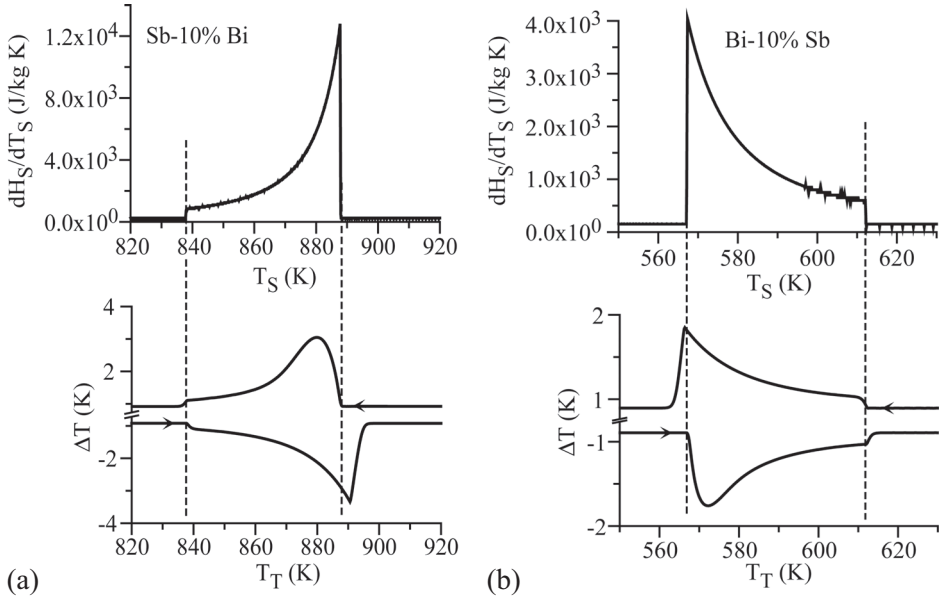

Figure 3.14. *Comparison of Bi-10% Sb with k>1 and Sb-10% Bi with k<1 alloys. The dH_S / dT_S curves computed for lever law using the thermodynamic functions of [92Feu] and the computed DTA scans for heating and cooling are shown.*

3.3.6 Failure to completely melt

Another difficulty in the determination of the liquidus temperature can occur when the alloy contains only a small fraction of the high temperature phase and the liquidus is very steep. Failure to run the DTA to a sufficient high temperature to reach the liquidus and/or failure to notice a small signal can lead to significant errors. This problem is discussed in [00Moo] for Sn-Cu-Ag alloys where the intermetallic compound Cu_6Sn_5 is the primary phase.

3.4 Supercooling problem with liquidus determination on cooling

3.4.1 Onset of freezing

Many metals and alloys are prone to supercooling prior to the initial nucleation of the solid metal from the melt. The nucleation usually occurs on foreign crystals; examples of possible nucleating sites are the ceramic grains in the crucible, oxide on the melt surfaces or fine particles dispersed throughout the liquid. Nucleation temperatures can vary from only a fraction of a degree below the liquidus to 100 or more degrees below the liquidus depending on alloy system and other factors. The failure to nucleate with small supercool-

ing complicates the measurement of a liquidus temperature during cooling.†† The events occurring during supercooling are demonstrated in Figure 3.15 showing data obtained with a fine thermocouple immersed in Sn in a DTA cup (same setup as used for Figure 2.6). Here significant supercooling has occurred. For the immersed thermocouple, the temperature reheats fully up to the melting point of 232°C as the heat of fusion is released rapidly due to the very fast dendritic freezing resulting from the large supercooling. The sample temperature does not drop again until freezing is complete. The use of the direct immersion thermocouple allows the determination of the temperature where solid first forms (nucleation temperature) in this sample as 206°C, 26°C below the melting point of 232°C. Using the instrument thermocouple, the nucleation temperature would have been measured as 203°C with a recalescence only up to 217°C. The presence of supercooling is detected quite easily in the DTA plots using either temperature (Figure 3.15b) by the positive slope of the ΔT vs. T graph. Supercooling provides the most extreme example of where the instrument thermocouple temperature and the sample temperature differ due to the limitations of heat transfer within the DTA.

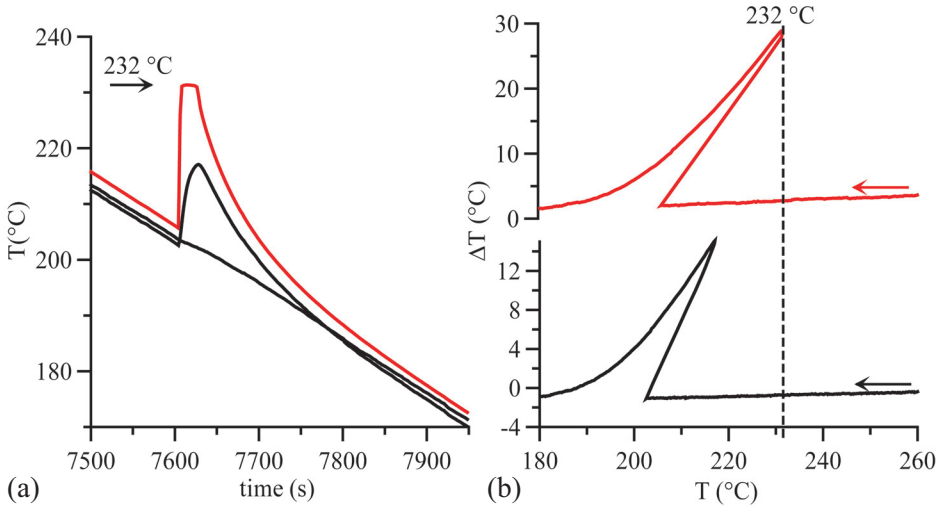

Figure 3.15. *Measured (a) temperature vs. time plots and (b) associated DTA plots for the freezing of pure Sn. The instrument thermocouple readings (sample and reference) are black and the readings from a thermocouple immersed directly into the Sn in the sample cup are red. Significant supercooling has occurred prior to freezing inducing the rapid temperature rise upon solidification in (a) and the associated positive slope in (b); mass = 163.2 mg; heating rate = 5 K/min.*

†† Nucleation of liquid on melting is not difficult due to the large number of microstructural defects (grain boundaries, defects, etc.).

3.4.2 Slope of DTA curve on initial freezing

Smaller amounts of supercooling in some samples can be harder to detect as they may not lead to a positive sloping DTA curve. In Appendix D, we have noted that the slope of the DTA on melting of a pure material is given by the ratio of two heat flow response times, $-t_{W,C} / t_{S,C}$ (wall to cup / sample to cup). This slope is easily determined experimentally by melting a pure material of similar mass. The rising linear portion of the DTA peak after the initiation of freezing (without supercooling) of a pure metal has the same slope. Thus, if the measured slope after the onset of freezing is more vertical than $-t_{W,C} / t_{S,C}$, one can be certain that supercooling has occurred and the measured onset temperature of freezing would be lower than the melting point. This simple test for the presence of initial supercooling would not necessarily be conclusive for an alloy because the slope during alloy freezing with no supercooling would also be less vertical than $-t_{W,C} / t_{S,C}$ due to slope of the liquidus curve.

3.4.3 Simulation of DTA response for alloys with supercooling

To gain insight into the DTA response when supercooling occurs for an alloy, a model of dendritic growth into a supercooled liquid for a non-dilute alloy has been coupled to the DTA response model [02Boe]. The sample, cup, thermocouple and wall temperature histories are shown for a particular set of materials parameters in Figure 3.16a for an initial supercooling of 5 K below the liquidus temperature. Several features can be noted: 1) recalescence of the sample temperature occurs as the latent heat is released during the dendritic network propagation across the sample; 2) After the recalescence temperature maximum, the sample temperature descends as the dendritic network thickens, increasing the fraction solid; 3) The cup temperature exhibits a smaller recalescence due to the heat transfer restrictions of the DTA cell and 4) the sample thermocouple actually exhibits no recalescence.

The DTA curves for initial supercoolings of 0 K, 5 K, 10 K, 15 K, 20 K and 30 K are shown along with the DTA curve for the Scheil path in Figure 3.16b. The initial rise of the DTA signal departs from the baseline at a lower temperature and rises more rapidly as the supercooling increases. The latter indicates the recalescence of the sample due to the rapid initial dendritic growth. The rise has a backward (positive) slope for supercoolings of 10 K and above. Here the sample recalescence is large enough that the thermocouple temperature also recalesces (Figure 3.16a); clearly, the absence of a backward DTA rise is not proof that supercooling is absent and that a valid liquidus temperature has been determined.

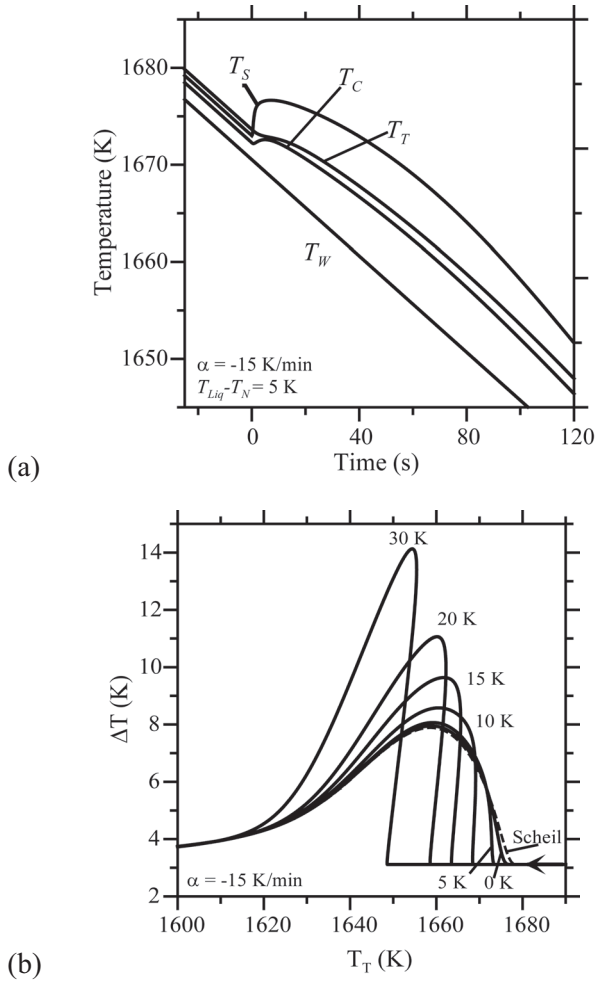

Figure 3.16. *a) Plot of calculated sample, sample cup, sample thermocouple and furnace wall temperatures vs. time curves for dendritic freezing of a 180 mg sample of alloy with C_0 = 5% at 15 K/min with an initial supercooling of 5 K/min. b) Effect of supercooling on the freezing DTA signal of the same alloy. The curves are for 0 K, 5 K, 10 K, 15 K, 20 K, 30 K supercooling. From [02Boe].*

3.5 Eutectic reactions vs. Peritectic reactions

3.5.1 Diffusion

From a purely thermodynamic point of view, eutectic reactions, $L \rightarrow \alpha+\beta$, and peritectic reactions, $L+\alpha \rightarrow \beta$, in binary alloys both take place at a fixed tem-

perature and exhibit an isothermal jump in the enthalpy vs. temperature curve at the transition temperature. However, as is well known in the solidification literature [74Fle], they are quite different in their diffusion kinetics. For eutectic solidification, $L \rightarrow \alpha+\beta$, both solid phases form directly from the liquid; i.e., locally one has $L \rightarrow \alpha$ and $L \rightarrow \beta$. Thus the necessary solute redistribution occurs in the liquid ahead of the individual interfaces, which are in close proximity. On the other hand, the peritectic reaction, $L+\alpha \rightarrow \beta$, requires the complete disappearance of the α phase, a process that involves solute diffusion in two solid phases at the peritectic temperature. The kinetics is therefore quite different for eutectic and peritectic alloys because of the extremely different rates of diffusion in liquids and substitutional solids. (If only interstitial solid diffusion is required, the peritectic reaction occurs more easily but still not as fast as the eutectic reaction.) Very little research has been performed on DTA analysis of systems containing peritectic reactions.

If one assumes as a limiting case that no diffusion occurs in the solid upon cooling, solidification merely switches from the freezing of the high temperature phase, $L \rightarrow \alpha$, to freezing of the low temperature phase, $L \rightarrow \beta$, at the peritectic temperature and below. Then the β phase usually surrounds the α phase in the microstructure resulting in a coarser two phase solid microstructure than in a eutectic microstructure. More complex arrangements of the two solid phases can occur for both eutectic and peritectic reactions especially if interface attachment kinetics are sluggish (usually encountered for crystals that grow from the liquid with crystallographic facets). Then the two solid phases grow independently from the melt with very little communication of the solute fields in the liquid. This leads to much coarser mixture of the two solid phases.

When the eutectic portion of a microstructure melts, both solid phases melt very close to a common temperature. This is because the phases usually exist as a fine two-phase intermingled microstructure. The melting DTA signal looks like that of a pure material (Figure 2.4b). For melting of an alloy with a phase diagram containing a peritectic reaction, the two solid phases are not intermingled as closely as they would be in a eutectic alloy. The melting response of the two-phase microstructure can occur over a range of temperatures due to the requirements of solid diffusion. The DTA response, as in freezing, again depends of the rate of solid diffusion with lever and Scheil enthalpies representing the extremes of behavior.

3.5.2 DTA Response

To illustrate these points we have chosen an alloy in the Sn-Au system that has both a peritectic reaction ($L+Sn_2Au \rightarrow Sn_4Au$) at 252°C and a eutectic

reaction ($L \rightarrow Sn_4Au+Sn$) at 217°C as shown in Figure 3.17a. Figure 3.17b shows the enthalpy vs. temperature and dH_S / dT_S vs. temperature curves for Sn - 25% Au calculated for equilibrium (black) and Scheil (red) conditions using the thermodynamic description of [03Liu]. For the equilibrium curves, note the presence of two isothermal jumps in enthalpy with the corresponding delta functions in the dH_S / dT_S curves at the two invariant temperatures. For the Scheil curve the delta function is absent for the peritectic reaction. This absence occurs because the assumption of no solid diffusion in the Scheil model prevents the "peritectic reaction." When traversing the peritectic temperature during solidification, the freezing process merely switches from $L \rightarrow Sn_2Au$ to $L \rightarrow Sn_4Au$ and there is no isothermal drop in enthalpy. For melting of an alloy frozen under these conditions, again with no solid diffusion assumed, melting switches from $Sn_4Au \rightarrow L$ to $Sn_2Au \rightarrow L$ at the peritectic temperature and there is no isothermal rise in enthalpy. Real solidification and melting will be intermediate to these two cases. The corresponding computed DTA curves for melting and freezing are shown in Figure 3.17c,d. Note how the peak signal for the "peritectic" reaction near 252°C is much reduced when the Scheil enthalpy is used. The computed DTA response agrees favorably with experimental results for Sn- 25% Au alloy shown in Figure 3.17e.

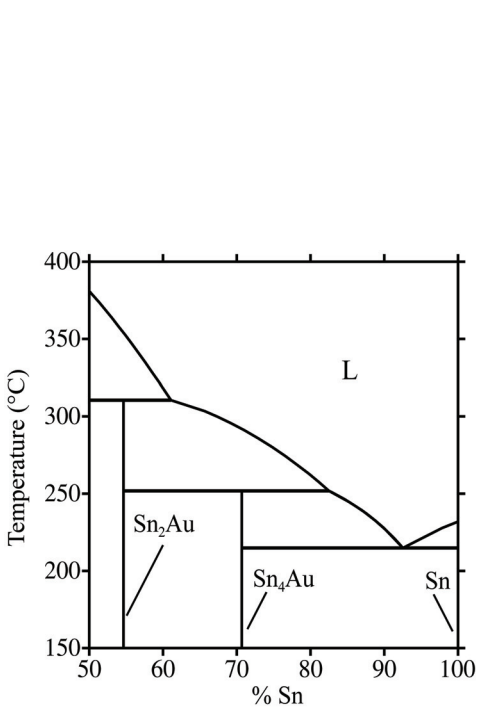

(a)

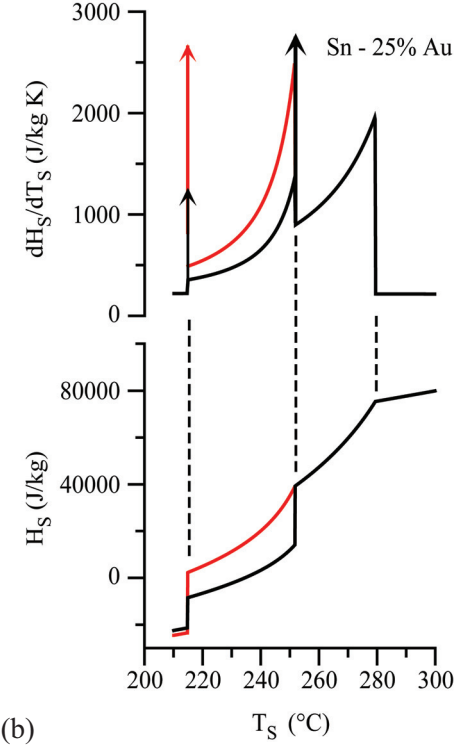

(b)

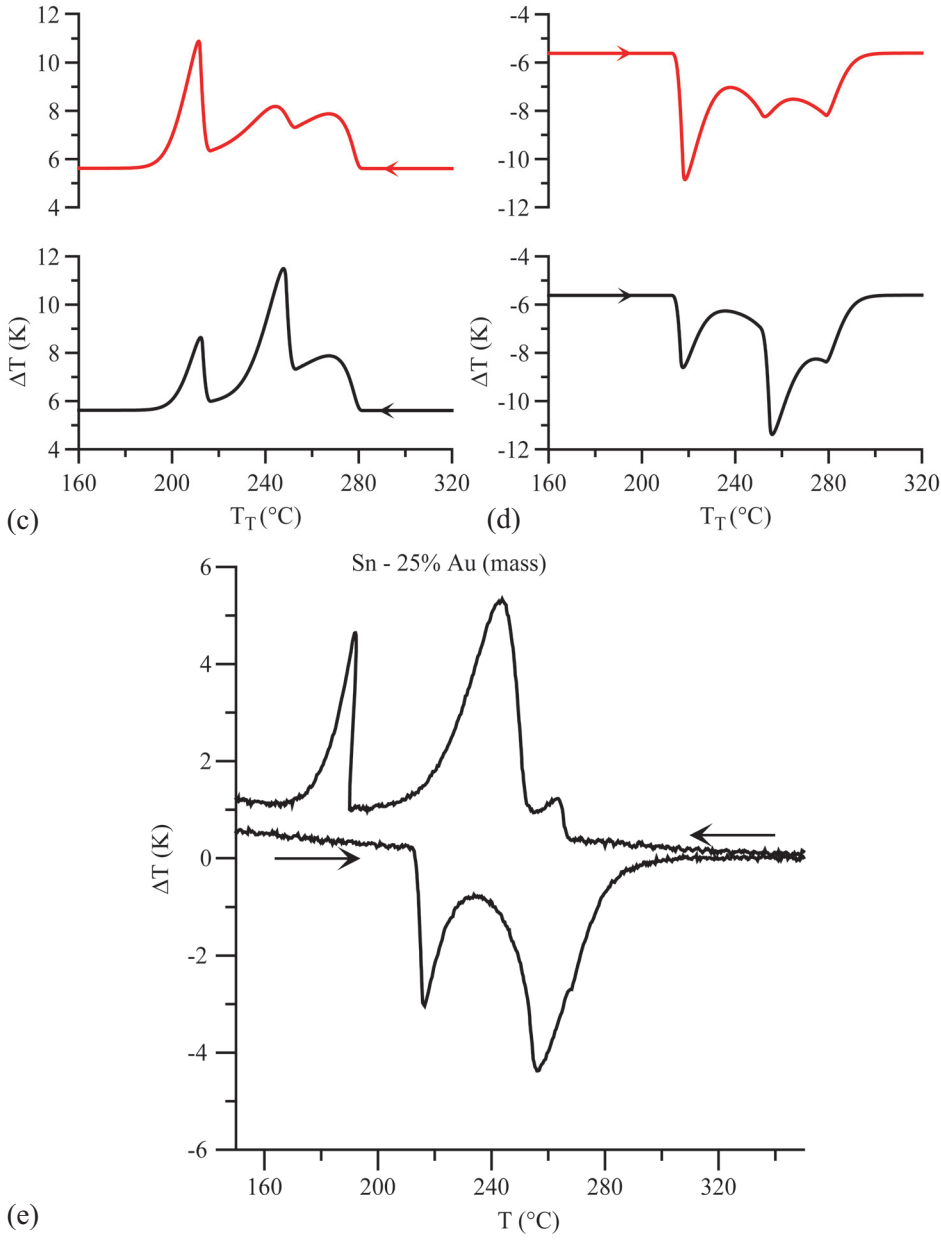

Figure 3.17. *a) Phase diagram for Sn-rich alloys, b) H_S and dH_S / dT_S curves for Sn- 25 % Au calculated for equilibrium (black) and Scheil (red) conditions using the thermodynamic description of [03Liu]. Computed DTA curves for c) freezing and d) melting. Note how the amplitude of the peak for the "peritectic" reaction near 252°C is much reduced when the Scheil enthalpy is used. e) Experimental melting and freezing curves at 5 K/min.*

DTA responses for the basic cases in binary eutectic and peritectic systems are summarized in Appendix F.

3.6 Major points

- Melting onset depends on metallurgical state of sample prior to analysis.
- Slow cooling and heating rates do not necessarily guarantee an equilibrated sample at each instant.
- The melting onset during heating should be determined by the first deviation from baseline method. The common practice of using the intersection temperature of a tangent to the DTA curve and the extrapolated baseline can lead to significant error because alloy DTA scans do not in general posses a linear section.
- Annealing of samples in the instrument prior to melting is sometimes required to obtain the thermodynamic solidus.
- Peak temperature on heating for alloys with small freezing ranges may overestimate the liquidus temperature. Cycling experiments can be used to obtain a true liquidus.
- Liquidus temperature determination on heating for alloys with partition coefficient $k > 1$ is more difficult than alloys with $k < 1$.
- Peritectics do not produce as sharp a melting peak as do eutectics.
- Not all temperatures that can be extracted from alloy DTA scans have meaning with regard to the alloy. Some temperatures are merely an indication of thermal lags within the instrument.

Part 4 - Analysis of DTA data for ternary alloys

The analysis of DTA curves for ternary and higher order systems is best accomplished with knowledge of the general thermodynamic aspects of multicomponent phase equilibrium. See Appendix B for selected readings. An excellent discussion of the DTA signals obtained during the melting and solidification of ternary alloys is given by [01Göd]. In this work, Gödecke treats the situation when complete equilibrium is maintained during melting and freezing; i.e., that all phases nucleate without superheating or supercooling and that the compositions of all phases are uniform at every temperature and thus follow the predictions of the lever rule. While this is an excellent starting point for understanding alloys, we highlight here some of the different responses obtained when interfacial equilibrium is maintained, but diffusion is not adequate to maintain uniformity of the phases during melting and solidification. We do this by comparing the DTA response to enthalpy temperature relations obtained from a thermodynamic calculation for two ternary aluminum alloys using, as in previous sections, full equilibrium and Scheil conditions.

Appendix G gives examples of similar DTA response for alloys with more than three components.

4.1 Al-rich corner of Al-Cu-Fe phase diagram

First we discuss solidification. Figure 4.1 shows the liquidus surface (projection) of the Al-rich corner of the Al-Cu-Fe ternary system. The diagram is like a topographic map where the temperature takes the place of elevation. The various surfaces represent the range of liquid alloy composition and the temperatures where various phases are first to solidify. The phase is labeled on the surface. In the aluminum-rich corner, the FCC aluminum solid solution forms. At higher Fe content and with no Cu, the Al_3Fe phase is first to form. At high Cu content with no Fe, the θ phase, Al_2Cu, is the first phase to form. Other regions where the α phase, $Al_6(Fe,Cu)$, and the β phase, Al_7Cu_2Fe, form first are indicated. Intersections of these surfaces occur in this diagram along lines (e.g.; ab, bd, cd, de) that descend in temperature. Many of these lines correspond to valleys‡‡. They represent the monovariant eutectic solidification

‡‡ We have not discussed the situation where the liquidus surfaces intersect to form a monovariant peritectic reaction as for the intersection of Al_3Fe and $Al_6(Fe, Cu)$ liquidus surfaces on "bc" in Figure 4.1. Such an intersection is not a "valley" but a change in slope of the liquidus. Lever solidification follows this line but Scheil solidification crosses it, switching from Al_3Fe to $Al_6(Fe, Cu)$.

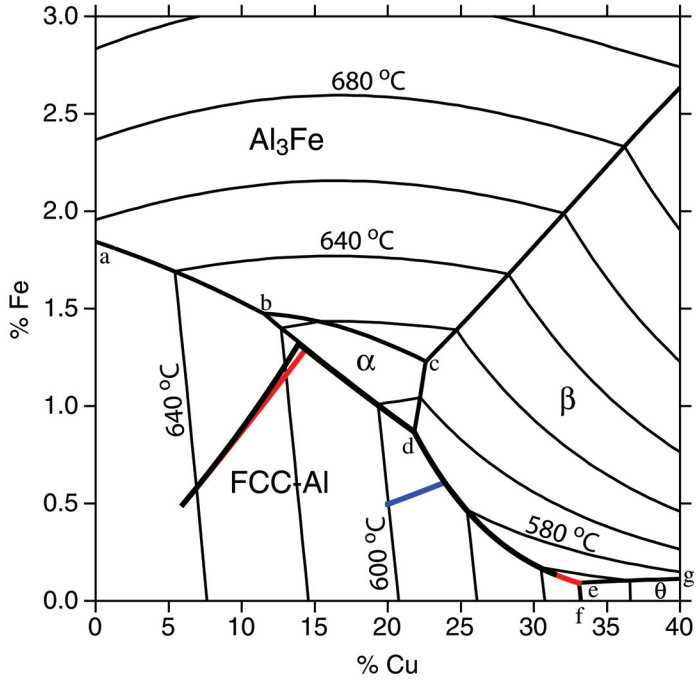

Figure 4.1. *Liquidus surface of Al-rich corner of Al-Cu-Fe alloy with lines of constant temperature (labeled), monovariant lines (ab, bc, bd, cd, de, ef and eg) and invariant points (a, b, c, d, e) at 654°C, 623°C, 608°C, 592°C, and 548°C, respectively. Diagram is computed from thermodynamic data of [96Sau1]. The calculated paths of the liquid concentration for the two alloys discussed in Figures 4.2, 4.3, 4.4 are indicated: Al - 6% Cu - 0.5% Fe equilibrium is black (ends along line de), Scheil is red (ends at point e) and Al-20 wt% Cu- 0.5% Fe equilibrium and Scheil are blue (both end at point e and are essentially identical).*

of two solid phases whose liquidus surfaces have intersected. Where two monovariant eutectic valleys join to form a third monovariant valley that continues to descend, such as at (d), an invariant occurs, variously termed a transition reaction, Class II four-phase invariant reaction [56Rhi], quasi-peritectic [66Pri] or ternary peritectic [60Mas]. When three descending monovariant valleys intersect, such as at (e), a different type of invariant occurs, termed a ternary eutectic reaction or Class I four-phase invariant reaction.

The solidification path is the entire history of how the liquid composition, whose concentration is assumed uniform at each temperature, changes as the various solids form from the melt. During primary (or first) solidification, the

path moves away from the composition of the primary phase, until it intersects one of the valleys. Solidification proceeds down in temperature following the valley and traversing whatever invariant reaction is encountered. The paths of liquid concentration superimposed on the liquidus surface for the two alloys discussed below, Al - 20% Cu - 0. 5% Fe and Al - 6% Cu - 0.5% Fe for the equilibrium calculation are shown in Figure 4.1.

For illustrations of the DTA responses, we employ the model of Appendix C, using an alloy mass of 200 mg, heating and cooling rates of 5 K/min and instrument time constants obtained by linear interpolation to 600°C between the results obtained experimentally for Sn and Ag in Appendix D; i.e., $t_{S,C} = 9.8$ s, $t_{W,C} = 23.6$, $t_{T,C} = 20.9$ s.

4.2 Al - 20% Cu - 0.5% Fe

With the brief preceding description of the phase diagram, we proceed to describe the DTA response. The alloy Al - 20% Cu - 0.5 % Fe has been chosen for exposition because it exhibits the most common behavior for a ternary alloy; i.e., a three stage process on cooling that progresses from freezing of one, then two and finally three solid phases from the melt. Figure 4.2 shows the DTA and dH_S / dT_S plots under equilibrium conditions. The solidification sequence is:

$L \rightarrow FCC$,
$L \rightarrow FCC + Al_7Cu_2Fe$,
$L \rightarrow FCC + Al_7Cu_2Fe + Al_2Cu$.

With decreasing temperature, the dH_S / dT_S plot first encounters a jump in value at the liquidus temperature, ≈ 598°C. The derivative value then slowly decays until another jump occurs when the monovariant valley (de) is encountered at ≈ 584°C. The value of dH_S / dT_S then slowly decays again until the delta function associated with the ternary eutectic temperature (e) is encountered at ≈ 548°C. The corresponding DTA plot on cooling shows an onset associated with the liquidus, a second onset associated with encountering the monovariant valley and a third onset associated with the ternary eutectic. Supercooling may be required to enable the nucleation of each new solid phase. Thus, problems can occur in identification of onsets during cooling not only for the first phase to form from the melt but also for each new phase in the various later stages of solidification.

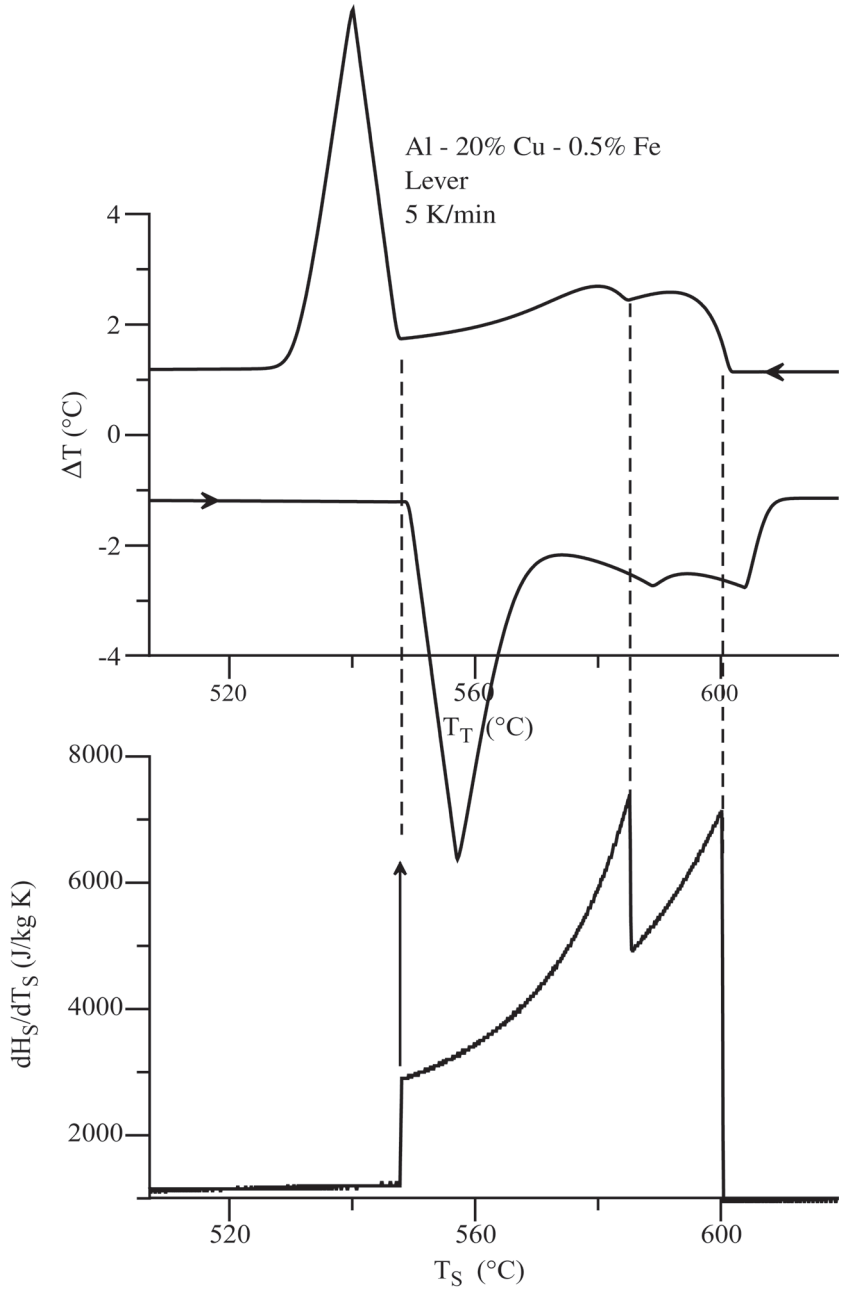

Figure 4.2. *DTA and dH_S / dT_S plots for Al - 20 % Cu - 0.5 % Fe under equilibrium conditions. The aluminum alloy thermodynamic database [96Sau1] was employed. The solidification sequence is: $L \rightarrow FCC$, $L \rightarrow FCC+Al_7Cu_2Fe$, $L \rightarrow FCC+Al_7Cu_2Fe+Al_2Cu$.*

On heating, an onset is encountered that is associated with the ternary eutectic melting. All three solid phases are melting, but only one, Al_2Cu, is completely consumed by this process. The other solid phases, FCC and Al_7Cu_2Fe, although reduced in amount, still remain. The temperature associated with the maximum deflection does correspond to the *time* when Al_2Cu is gone, but the temperature of the sample thermocouple at this time has no significance due to the thermal lags of the instrument; this case is analogous to the peak shape during melting of a pure metal in that the peak temperature after an invariant reaction has no thermodynamic meaning.

On continued heating, according to the dH_S / dT_S plot, the rate at which the remaining FCC and Al_7Cu_2Fe melt increases with increasing temperature until a sudden drop in the dH_S / dT_S value occurs. This drop indicates that all of the Al_7Cu_2Fe has melted. This drop in the dH_S / dT_S value produces the maximum deflection in the DTA plot associated with the temperature where all of the Al_7Cu_2Fe has melted. According to the dH_S / dT_S plot, the rate at which the remaining FCC melts increases with increasing temperature until a sudden drop in the dH_S / dT_S value occurs. This drop indicates that all of the FCC has melted. The final peak temperature in the DTA scan is thus associated with the temperature when all of the FCC has melted. We have used the term "associated with" to indicate that the measured onset and peak temperatures suffer from same thermal lags from the temperatures where the events are truly taking place in the instrument; this deviation appears in Figure 4.2 as the offset of the DTA peaks from the dashed vertical lines indicating the thermodynamic temperatures. We note finally that, for this alloy, there is little difference between the lever and Scheil enthalpies because the fraction of the FCC phase (in which dendritic coring can exist) occupies a relatively small amount of the total alloy.

4.3 Al - 6% Cu - 0.5% Fe

This alloy has been chosen for exposition because it exhibits the second most common behavior for a ternary alloy, i.e., a four (five for Scheil) stage process on cooling that progresses from the freezing of one solid phase, then two solid phases, interrupted by an invariant reaction, continued freezing of two solid phases and finally three solid phases. The solidification sequence is:

$L \rightarrow FCC$,
$L \rightarrow FCC + Al_6(Fe,Cu)$,
$L + Al_6(Fe,Cu) \rightarrow Al_7Cu_2Fe + FCC$ (invariant); Lever path only.

$L \rightarrow FCC + Al_7Cu_2Fe$,
$L \rightarrow FCC + Al_7Cu_2Fe + Al_2Cu$ (invariant); Scheil path only.

Solidification first involves the formation of the FCC phase from the melt. The liquid is enriched in Cu and Fe as the temperature drops until the concentration reaches the monovariant valley (bd), $L \rightarrow FCC + Al_6(Fe,Cu)$, at 616°C. Then simultaneous liquid freezing to FCC and $Al_6(Fe,Cu)$ phases occurs with decreasing temperature until the valley encounters a second valley that is between the FCC and Al_7Cu_2Fe liquidus surfaces (de). Under the equilibrium assumption, all of the $Al_6(Fe,Cu)$ dissolves at the invariant temperature (d) at 592°C, in the process forming more FCC and the new phase, Al_7Cu_2Fe. Subsequently, solidification continues with decreasing temperature (along de) forming more FCC and Al_7Cu_2Fe. Solidification is completed at 556°C on (de) between (d) and (e) at 556°C). In contrast, under Scheil assumptions, the invariant temperature (d) is merely the temperature (592°C) where solidification switches from $L \rightarrow FCC + Al_6(Fe,Cu)$ to $L \rightarrow FCC + Al_7Cu_2Fe$ as the temperature drops. For Scheil conditions, the curve (de) is followed as FCC and Al_7Cu_2Fe solids form, the temperature descending and the liquid concentrations increasing to the end of (de) until the ternary eutectic temperature at (548°C) and liquid concentration are reached at (e). Here all liquid disappears via the ternary invariant eutectic, $L \rightarrow FCC + Al_7Cu_2Fe + Al_2Cu$.

Figure 4.3 shows dH_S / dT_S and melting and freezing DTA plots under equilibrium conditions for this alloy. Figure 4.4 shows dH_S / dT_S and melting and freezing DTA plots under Scheil conditions. Note the presence of the delta function at ≈ 592°C in the dH_S / dT_S plot corresponding to the invariant reaction, $L + Al_6(Fe,Cu) \rightarrow FCC + Al_7Cu_2Fe$, in the equilibrium case but not for the Scheil case. Also note the presence of the delta function corresponding to the ternary eutectic at 547°C in the Scheil case and its absence in the equilibrium case (Figure 4.4). These differences are due to the assumptions of complete diffusional equilibrium in the first case and no solid diffusion in the second case, again representing extremes of behavior. Just like a peritectic reaction in a binary alloy (section 3.5), the reaction $L + Al_6(Fe,Cu) \rightarrow FCC + Al_7Cu_2Fe$ requires solid state diffusion and thus does not occur under the Scheil assumption. On solidification, one merely switches at 592°C from the formation of $FCC + Al_6(Fe,Cu)$ to the formation of $FCC + Al_7Cu_2Fe$. $Al_6(Fe,Cu)$ is not consumed on continued cooling but remains in the alloy's microstructure. These differences in the dH_S / dT_S curves are then reflected in the DTA scans.

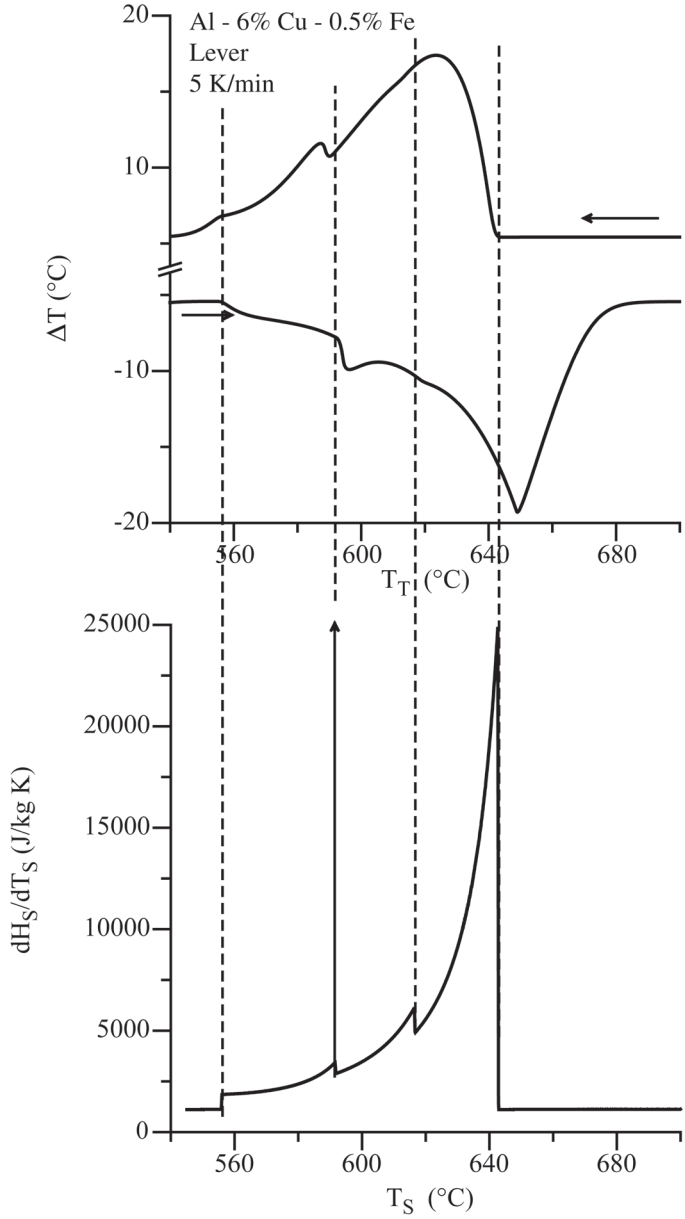

Figure 4.3. *DTA and dH_S / dT_S plots for Al-6 % Cu-0.5 % Fe under equilibrium conditions. The aluminum alloy thermodynamic database [96Sau1] was employed. The solidification sequence is:$L \rightarrow FCC$, $L \rightarrow FCC+Al_6(Fe,Cu)$, $L+Al_6(Fe,Cu) \rightarrow FCC+Al_7Cu_2Fe$, $L \rightarrow FCC+Al_7Cu_2Fe$. Note the delta function at ≈ 592°C corresponding to the invariant reaction, $L+Al_6(Fe,Cu) \rightarrow FCC+Al_7Cu_2Fe$.*

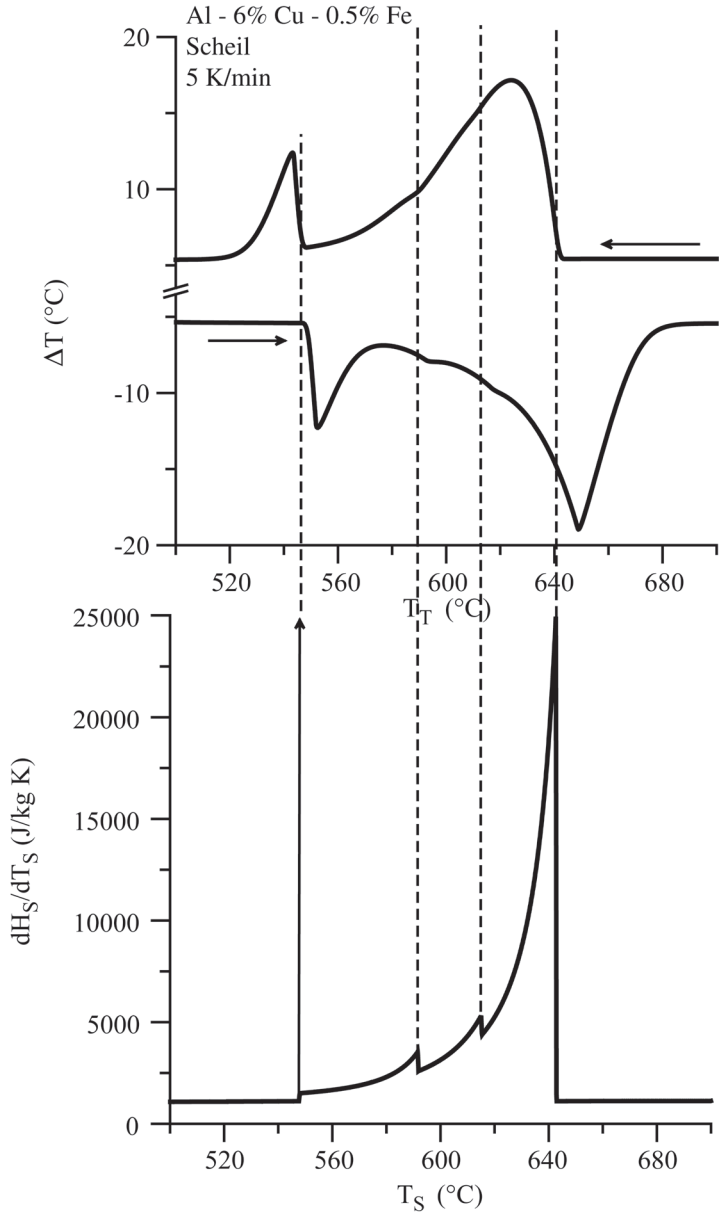

Figure 4.4. *DTA and dH_S / dT_S plots for Al-6 % Cu-0.5 % Fe under Scheil conditions. The aluminum alloy thermodynamic database [96Sau1] was employed. The solidification sequence is: L→FCC, L→FCC+Al_6(Fe,Cu), L→FCC+Al_7Cu_2Fe, L→FCC+Al_7Cu_2Fe+Al_2Cu. Note the delta function in the dH_S / dT_S plot at ≈ 592°C in Figure 4.3 corresponding to the invariant reaction, L+Al_6(Fe,Cu)→FCC+Al_7Cu_2Fe is gone.*

4.4 - Major points

- Knowledge of ternary alloy phase equilibrium is necessary to interpret data for ternary and higher order systems.
- Ternary invariant transition reactions may have quite different DTA signals compared to ternary invariant eutectic reactions.
- Failure to nucleate during cooling DTA scans can occur with solid phases that form through secondary solidification processes in addition to primary solidification.

Part 5: Concluding remarks

We have attempted to highlight two important effects that must be carefully considered in the measurement of alloy melting and freezing using a DTA/HF-DSC. The first is concerned with the heat flow and the small but important temperature differences that exist within the different parts of the instrument. Thermocouple signals are the only information available and the thermocouple, not directly immersed in the metal, is not at the sample temperature. This is most easily seen in the shape of the DTA curves for the melting of a pure material, where one might naively think that the sample temperature ranges from the onset temperature to the peak temperature during melting due to an erroneous concept of kinetics. This is clearly not the case. Thus the heat transfer between sample, through the sample container and finally to the thermocouple must be considered. A model is presented to quantify these effects and to determine heat transfer characteristic of any DTA/HF-DSC instrument.

The second important effect is that deviations from full equilibrium can and do occur during the melting and freezing of alloy samples at the rates encountered in DTA. Indeed the small sample in the DTA cup is best viewed as a small casting with all of the complications that can occur in castings. However, the loss of full equilibrium is due mostly to the slow rate of solute diffusion in alloys and is thus analyzable without recourse to complex models that involve so-called reaction kinetics. This concept is widely used in the successful modeling of castings and can be applied to DTA response. This idea has been developed in the current document in the broad usage of the comparison of full equilibrium and Scheil approaches to place bounds on expected DTA response.

The heavy use of simulations of the DTA response in this document should not be taken to imply that measurements are unnecessary. The simulations were performed using thermodynamic data that remains under constant revision by the Calphad community. Indeed these thermodynamic assessments are constructed from data sometimes obtained from incorrect interpretations of transformation temperatures using the DTA. In addition many complications of diffusion kinetics and microstructure variations can occur that are not considered here.

The emphasis of this document on problems with DTA analysis may also have led the reader to the impression that accurate temperature determination with the DTA is nearly impossible. This is not true and it is not the intention of this guide to discourage DTA measurements. The intention is to increase user

awareness of the factors that influence the DTA signal by providing physical explanations that enable thorough and meaningful analysis of the results and temperature determinations.

Appendices

Appendix A: Glossary

Back (solid) diffusion: Diffusion in the solid phase(s) to attain equilibrium composition throughout the solid phase during solidification.

Baseline: The signal recorded without a thermal event such as melting taking place.

Calphad: **Cal**culation of **pha**se **d**iagrams. The Gibbs energy of each phase is represented as a function of composition, temperature and pressure. The adjustable parameters of the functions for the individual phases are derived from experimental phase equilibria and thermochemical data. The descriptions of constituent subsystems can be combined for the calculation of a multicomponent system.

Degrees of freedom: Number of variables that can be changed without changing the identity of the phases in equilibrium. The number of degrees of freedom, F, can be obtained from the phase rule, $F = N–P+2$, where N is the number of components and P is the number of phases in equilibrium. For condensed phase systems the pressure is usually dropped as a variable and the phase rule is modified to $F = N–P+1$.

Delta function: A function $\delta(x)$ that has the value of infinity for $x=0$, the value zero elsewhere. The integral from minus infinity to plus infinity is 1.

Differential scanning calorimetry (DSC): See *Heat-flux differential scanning calorimetry (HF-DSC)* or *Power-compensating differential scanning calorimetry (PC-DSC)*.

Differential thermal analysis (DTA): Thermal analysis using a reference. Sample and reference are heated in one furnace. The difference of sample temperature and reference temperature is recorded during programmed heating and cooling cycles.

Endothermic: Heat is consumed during a reaction or transformation, i.e. the enthalpy change is positive.

Enthalpy (H): Heat content of a phase.

Equilibrium: State of the lowest free energy when no further change of a system is possible. Phases in equilibrium at a given composition, temperature and pressure have no driving free energy to react or transform. See *Global equilibrium* and *Local equilibrium*.

Eutectic: Thermodynamic situation where a liquid is simultaneously saturated with respect to several solid phases and cooling decreases the amount of liquid and increases the amount of all solids. The situation may have zero or more degrees of freedom depending on the number of phases and components.

Exothermic: Heat is released during a reaction or transformation, i.e. the enthalpy change is negative.

Fraction of solid versus temperature: Amount of solid phase(s) formed during the solidification of an alloy.

Gibbs-Thomson effect: The contribution of the interface energy to the Gibbs free energy due to the effect of the shape (curvature) of the interface between phases. Phases with high curvature interfaces exhibit altered melting temperatures and solubilities.

Global equilibrium: A complete equilibrium where there are no gradients of temperature or pressure and the compositions of coexisting phases are uniform.

Heat capacity (Cp): Rate of enthalpy (heat content) change of a phase with respect to temperature at constant pressure.

Heat-flux differential scanning calorimetry (HF-DSC): Sample and reference are heated in one furnace. The difference of sample temperature and reference temperature is proportional to the heat flux between the sample and reference. Contrast with: *Power-compensating differential scanning calorimetry*.

Incipient melting: Initial melting of an alloy. This may occur below the solidus temperature of the average alloy composition due to microsegregation from prior solidification.

Interface undercooling: The departure of the interface temperature (and interface phase concentrations) from that given by the phase diagram. The interface undercooling that drives the kinetic processes involved in solidification and melting is typically quite small (< 1 K) for metals and alloys.

Interstitial solutes: Elements that occupy positions between the solvent element atoms in a crystal lattice. Diffusion of interstitial solutes is rapid because of the large number of vacant sites.

Invariant reaction: A reaction with zero degrees of freedom. Also called invariant equilibrium. Examples are *eutectic* and *peritectic* in a condensed phase system consisting of two components at constant pressure.

Latent heat: Heat change during a reaction or transformation. This quantity is only exactly defined for invariant reactions or transformations.

Lever rule: An expression of conservation of matter in which the relative phase amounts are determined from the overall alloy composition and the coexisting phase compositions assumed to be in *global equilibrium* at each temperature.

Lever rule solidification: One limiting case of solidification where complete diffusion for the liquid phase and the solid phases is assumed. The phases are in thermodynamic equilibrium and phase amounts and compositions are linked by the lever rule at each temperature during cooling.

Liquidus: Boundary in a phase diagram between phase field regions containing only the liquid phase and phase fields regions containing liquid and solid phase(s). This boundary represents the limit where the fraction of solid is zero.

Local equilibrium: Equilibrium conditions are only fulfilled at the interface between phases.

Metastable equilibrium: Equilibrium when one or more of the stable phases are absent.

Microsegregation: Concentration gradients in the solid phase formed during solidification because of insufficient diffusion in the solid phase.

Nucleation supercooling: Extent of supercooling needed for nucleation to occur. See: *Supercooling*.

Onset temperature: The temperature where the signal first departs from the baseline and which corresponds to the leading portion of a peak. Two onset temperatures are described in this document: one obtained by an extrapolation method and the other obtained as the first detectable deviation from baseline.

Peak: The entirety of the deviation and return of the DTA signal from and to the baseline.

Peak signal: The amplitude of the maximum deviation of the signal from the baseline. Can be exothermic or endothermic.

Peak temperature: The temperature corresponding to the peak signal.

Peritectic: Thermodynamic situation where a liquid is simultaneously saturated with respect to multiple solid phases and cooling decreases the amount of liquid and at least one of the solid phases while increasing the amount of the other solid phases. The situation may have zero or more degrees of freedom depending on the number of phases and components.

Phase: A portion of a material that is distinguishable by its state, composition and/or crystal structure. A phase may exhibit smooth variations in composition.

Power-compensating differential scanning calorimeter (PC-DSC): Sample and reference are heated independently in two furnaces so that their temperature difference stays zero. The difference in power used to heat the sample and reference is a measure of the enthalpy of the sample.
Contrast with: *Heat-flux differential scanning calorimetry*.

Recalescence: The rapid increase in temperature due to release of the latent heat due to the solidification from a supercooled condition.

Scheil-Gulliver solidification: One limiting case of solidification where complete diffusion for the liquid phase and no diffusion for the solid phases are assumed. This type of solidification produces the worst case of microsegregation. Also called Scheil solidification.

Solidification path: The change in liquid composition and the sequence of solid phases that form as temperature decreases.

Solidus: Boundary in a phase diagram between phase field regions containing only solid phase(s) and phase fields regions containing solid and liquid phase(s). This boundary represents the limit where the fraction of liquid is zero.

Supercooling: Failure of a solid phase to nucleate at the temperature given by the phase diagram (thermodynamic equilibrium). See: *Nucleation supercooling*

Substitutional solutes: Elements that replace the solvent element randomly in its crystal lattice. Diffusion usually occurs by a vacancy mechanism.

Thermal conductivity: The time rate of heat flow, under steady conditions, through unit area, per unit temperature gradient in the direction normal to the area.

Tie line: An isothermal, isobaric line connecting the compositions of a pair of phases in equilibrium

Transition reaction: Invariant reaction in a multicomponent system where a number of phases react to form a number of different phases. This reaction is neither a eutectic nor a peritectic reaction. However, since this reaction is somewhat similar to a peritectic reaction it is also called quasi-peritectic. Another term for this reaction is Class II reaction.

Variant eutectic reaction: A multiphase equilibrium with liquid and at least one degree of freedom with eutectic character. A monovariant (one degree of freedom) eutectic is also called a eutectic valley.

Appendix B: Recommended Reading

[56Rhi], [60Mas], [66Pri], [82Wes], [02Wes]; Monographs on ternary phase diagrams.

[65Gar]; A classic in the field, general focus on a wide range of materials, not specific to alloys.

[88Bro]; A concise summary of techniques and interpretation.

[88Met]; A general treatment of solidification.

[96Bil]; A general treatment of solidification.

[01Göd]; An excellent summary of the DTA response to the solidification of ternary alloys under equilibrium (lever law) melting and solidification (in German).

[03Fer]; A general guide to good technique for phase diagram determination

[04Sta]; Focused on Al alloys, reviews DTA techniques with a major focus on solid state reactions with some melting work. Effect of prior sample history made clear.

Appendix C: Model for simulating DTA response for melting and solidification of materials with known or assumed enthalpy vs. temperature relations. Also method for determining thermal lag time constants of DTA/DSC instruments [02Boe]

We employ an approach using ordinary differential equations (ODE) in which $T_S(t)$, $T_C(t)$, and $T_T(t)$ are the sample, sample cup and thermocouple temperatures. Thus thermal gradients within these three objects are ignored.§§ As described in section 2.1.3, different instruments control the heating rate in different ways. For this model, we will assume that the furnace wall temperature, $T_W(t)$, is controlled by the instrument to be a prescribed linear function of time. An additional triplet of variables can be used to describe the temperatures of the reference sample, cup and thermocouple. A system of ODE's that describes these six unknown temperatures is given in [02Boe] as well as the reduced set that we employ here. We consider only heat flow between: a) the sample and the sample cup; b) the sample cup and the furnace wall; and c) the sample cup and the thermocouple. We neglect heat flow between the sample and reference cups.***

We let $h_{S,C}A_{S,C}$, $h_{W,C}A_{W,C}$ and $h_{T,C}A_{T,C}$ be the products of the heat transfer coefficients $h_{X,Y}$ and areas $A_{X,Y}$ for the heat flow a), b), and c) described above, respectively. We also let m_S and H_S be the sample mass and enthalpy/unit mass, m_C and $C_p{}^C$ be the crucible mass and heat capacity/mass and m_T, and $C_p{}^T$ be the thermocouple mass and heat capacity/mass. Defining instrument time constants $t_{S,C}$, $t_{W,C}$ and $t_{T,C}$ by

$$\begin{cases} t_{S,C} = m_C C_p^C / h_{S,C} A_{S,C} \\ t_{W,C} = m_C C_p^C / h_{W,C} A_{W,C} \\ t_{T,C} = m_T C_p^T / h_{T,C} A_{T,C} \end{cases} \qquad [C1]$$

§§ A similar treatment is found in [92Shu] and one explicitly dealing with radiative heat transfer is found in [05Dom]. A finite element treatment that includes thermal gradients is given by [95Ban].

*** Examination of experimental temperature-time data for the reference thermocouple during the melting of small (180 mg) samples of pure Ni at 5 K/min in a DTA show less than 0.8 K variations from linearity. This indicates that very little heat flows beetween the reference and sample cups in these experiments and validates the use of the simple model.

a heat balance gives

$$\begin{cases} m_S \dot{H}_S = \dfrac{m_C C_p^C}{t_{S,C}}(T_C - T_S) \\ \dot{T}_C = \dfrac{1}{t_{S.C}}(T_S - T_C) + \dfrac{1}{t_{W,C}}(T_W - T_C) \\ \dot{T}_T = \dfrac{1}{t_{T,C}}(T_C - T_T) \end{cases} \qquad [C2]$$

where the dot represents time differentiation. For situations where transformation kinetics can be ignored, the enthalpy is only a function of temperature and

$$\dot{H}_S = \frac{dH_S}{dt} = \frac{dH_S}{dT_S}\frac{dT_S}{dt} = \frac{dH_S}{dT_S}\dot{T}_S \qquad . \qquad [C3]$$

Inclusion of kinetic effects produces a time dependent sample enthalpy function that is described in [02Boe].

The time parameter, $t_{S,C}$, is the characteristic response time for heat flow between the metal *sample* and the crucible *cup*; $t_{W,C}$ is the response time between the furnace *wall* and the *cup*; and $t_{T,C}$ is the response time between the *thermocouple* and the *cup*. Due to the presence of the area of contact between the sample and the cup in Eqns. C1, the response time, $t_{S,C}$ depends on the size and thus the mass of the sample. We will assume that these response times are independent of temperature over the course of melting or solidification. We will further assume that the furnace heating rate, α, is constant such that the interior furnace wall temperature is given by

$$T_w(t) = constant + \alpha\, t\,. \qquad [C4]$$

Analytic solution of these equations is possible for a pure material and is given in [02Boe], the results of which are given in Appendix D with respect to melting onset analysis. Numerical solution is necessary for alloys and is possible using standard software packages, such as Mathematica or Matlab. Simulation of DTA plots for alloys with known or assumed enthalpy vs. temperature curves are reported throughout this document.

The time constants appropriate to a particular instrument were obtained as follows. Using a least squares procedure, measured DTA data was compared to

the computed DTA response for initial guesses of the time constants. Minimization of the error using an iterative procedure led to values for the thermal lags given in Table C1 for a Perkin-Elmer DTA 1600 using the melting of ≈ 200 mg samples of Sn, Ag, and Ni. The decrease in the size of the thermal lags with increasing melting point suggests the increasing importance of radiation in the heat flow. We have also found that the parameter, $t_{S,C}$, is approximately inversely proportional to the 1/3 power of the sample mass, rather than a 2/3 power that might be expected from the increased contact area between the sample and the sample cup. This may be due to the high contact angle of the samples with the alumina cup. Parameters for a HF-DSC/DTA (Netsch DSC 404C) are given in Table C2. Note the much smaller value of $t_{T,C}$ for this instrument are probably due to the direct welding of thermocouple wires to the platinum cup support structure. Please note that the parameters given in these tables are meant only as a guide. Each user should determine a set of lag parameters for the specific instrument and operation conditions being used. We also note that a more complex heat flow model of the DTA can be employed (see for example the appendix in [02Boe]) that can include additional time parameters that characterize the heat transfer between the sample and reference cups as well as other effects that are likely more important for a HF-DSC/DTA.

Table C1 - Thermal lag time constants determined for a DTA using the model of Appendix C

	Sn (232ºC)			Ag (961ºC)			Ni (1453ºC)		
Mass (g)	0.163			0.237			0.180		
Heating rate (K/min)	5	10	15	5	10	15	5	10	15
$t_{S,C}$ (s)	13.5	15.3	15.9	6.2	6.7	6.7	6.5	6.0	5.5
$t_{W,C}$ (s)	34.5	29.2	26.3	13.0	12.7	13.1	5.1	5.0	4.7
$t_{T,C}$ (s)	27.6	18.9	17.0	14.5	12.4	11.7	7.4	6.5	6.7
$t_{W,C} / t_{S,C}$	2.56	1.91	1.65	2.10	1.90	1.96	0.78	0.83	0.85

Table C2 - Thermal lag time constants determined for a HF-DSC/DTA using the model of Appendix C

	Ag (961ºC)		
Mass (g)	0.214	0.214	0.214
Heating rate (K/min)	5	10	15
$t_{S,C}$ (s)	12.5	12.0	11.7
$t_{W,C}$ (s)	18.2	18.3	18.7
$t_{T,C}$ (s)	0.82	0.37	0.11
$t_{W,C} / t_{S,C}$	1.46	1.53	1.60

Appendix D. Expressions for the rate dependence of melting onset temperatures for a pure metal

For a pure metal, analytical solution to the differential equations in Appendix C is possible [02Boe] if one takes an enthalpy function given by

$$H_S(T_S) = \begin{cases} C_p^{S0}(T_S - T_M) & ; \quad T < T_M \\ C_p^{S0}(T_S - T_M) + L & ; \quad T > T_M \end{cases} \qquad [D1]$$

where C_p^{S0} is the (constant) heat capacity per unit mass (assumed the same for liquid and solid) and L is the heat of fusion per unit mass. For convenience we define the ratio ρ as

$$\rho = \frac{m_S C_p^{S0}}{m_C C_p^C} \qquad [D2]$$

where m_S is the sample mass and m_C and C_p^C are the crucible mass and heat capacity/mass. The solution is broken into three time regimes: before melting, during melting and after melting. For DTA instruments, the 'DTA signal' is the difference between the sample and reference thermocouple temperatures, which is the same in this simplified model as the difference between the sample temperature and the furnace wall temperature.

Figure D1 shows the calculated temperature vs. time behavior and the associated DTA curve, which is a plot of $(T_T - T_W)$ vs. T_T. Prior to melting $(t < 0)$, the temperatures are all linear in time, with the same slope α, but with different temporal or temperature offsets. These offsets are established during the initial transient of the instrument after heating is initiated. The sizes of all temperature offsets are directly proportional to the heating rate. During melting, $0 \le t < t_M$, the sample temperature is assumed constant consistent with negligible temperature differences within the metal sample and the assumption of equilibrium, $T_S(t) = T_M$. During this regime both the cup and thermocouple temperature-time curves exponentially approach linear behavior with slope $\alpha\ t_{S,C} / (t_{S,C} + t_{W,C})$, where α alpha is the heating rate as in Appendix C. The corresponding slope on the DTA plot is $-\ t_{W,C} / t_{S,C}$, which is independent of heating rate. For $t > t_M$, the sample, sample cup and thermocouple return as the sum of three exponential functions of time to the linear temperature behavior obtained during the first regime, $t < t_M$.

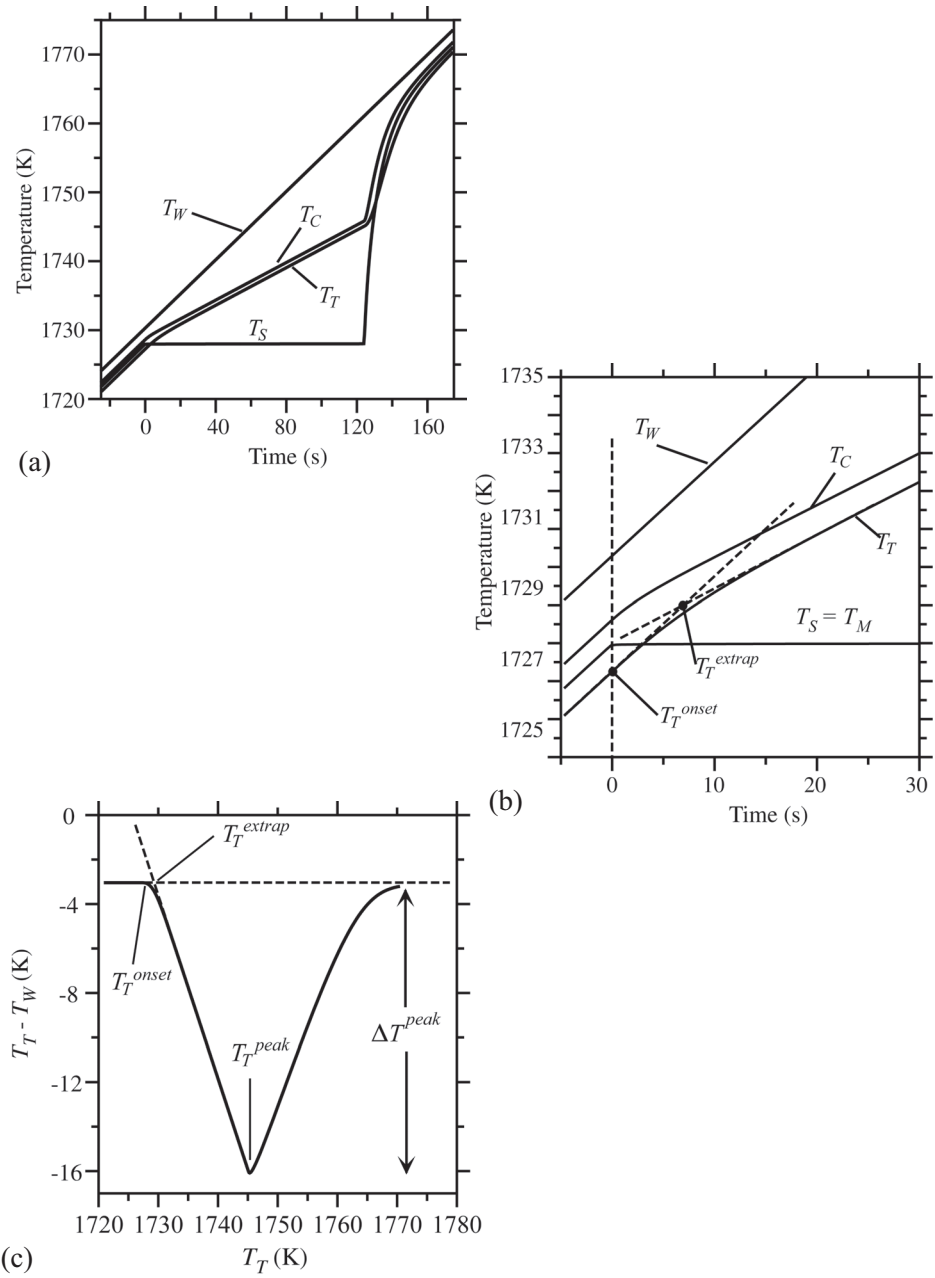

Figure D1. *a) Calculated temperatures within a DTA instrument as functions of time for pure Ni, sample (T_S), sample cup (T_C), thermocouple (T_T) and furnace wll (T_W), b) enlarged region near t = 0, c) associated DTA curve. The figures show the possible sources of error in determining the melting onset temperature for calibration purposes.*

The difficulty of picking the melting onset is shown in Figure D1b, which is an enlarged view of the temperature histories near the initiation of melting at $t = 0$. It is seen that only a gradual change in slope of the thermocouple temperature begins at $t = 0$ marked T_T^{onset}. The onset temperature of the sample thermocouple, T_T^{onset} differs from melting point of the sample T_M, the two related by

$$T_T^{onset} = T_M + \alpha\ (t_{S,C}\rho - t_{T,C})\,, \qquad [D3]$$

which can either increase or decrease from T_M with increasing heating rate depending on the values of the time constants and the ratio ρ. In principle the deviation from the melting point with heating rate might be zeroed by a proper heat flow arrangement.

An extrapolation procedure is commonly used to determine an alternate melting onset. This procedure takes advantage of the fact that the thermocouple temperature vs. time, $T_T\,(t)$, curve becomes linear quickly after the melting onset as described above. Then the onset temperature is taken from the DTA curve as the intersection of the extrapolated linear portion with the extrapolated baseline. The melting onset picked in this way is denoted T_T^{extrap}. It is always *above* T_M with a deviation from the melting point that increases with heating rate according to

$$T_T^{extrap} = T_M + \alpha \left(\frac{t_{S,C}(t_{S,C}\rho + t_{W,C}\rho + t_{W,C})}{t_{S,C} + t_{W,C}} \right) \qquad [D4]$$

For the values of the time constants given in Table C1 for Ni, and a typical value of ρ = 0.5, these two choices for onset temperature can be compared numerically. T_T^{onset} is α times 2.6 s below T_M, which equals 0.6 K for a heating rate of 15 K/min. T_T^{extrap} is α times 5.2 s above T_M, which equals 1.3 K at a heating rate of 15 K/min. Thus picking the onset (or calibrating the instrument) by the extrapolation method is more heating rate sensitive than using the first sign of deflection from the baseline. One might argue, however, that noise in the baseline makes the latter choice less preferable. In any case, using the same heating rate and method for picking the onsets for calibration and measurements on alloy samples reduces the errors.

Another important piece of information that can be obtained from the analytical solution is the characteristic time it takes for the sample

thermocouple temperature behavior to return to a slope of α; or equivalently the temperature change that occurs before the DTA plot returns to the baseline. The smaller this time is, the closer detectable thermal events can be. The return to baseline is the sum of three exponential functions in time [02Boe]. The characteristic times are:

$$t_{T,C} \text{ and } \frac{2t_{S,C}t_{W,C}}{\left(t_{W,C}+\rho t_{S,C}+\rho t_{W,C}\right)\pm\sqrt{\left(t_{W,C}+\rho t_{S,C}+\rho t_{W,C}\right)^2-4\rho t_{S,C}t_{W,C}}}, \quad \text{[D5]}$$

which, for the parameters in Table C1 for Ni and $\rho = 0.5$ are 7.4 s, 1.8 s and 9.0 s, respectively.

If we assume that the longest time above dominates and is denoted by τ, the temperature interval of a DTA scan over which the signal returns from the peak temperature to baseline is approximately $|\Delta T_{peak}| + \alpha\tau$ or $\alpha\tau$ more than the peak height. Thus detecting two events within this temperature interval is very difficult in a DTA instrument. Reduced peak signals are inherent in the heat flux DSC, and thus provide some advantage for detecting events separated by small temperature intervals.

Appendix E: Enthalpy vs. temperature relations for dilute binary solid solution alloy

For simulation and understanding of DTA response to simple alloys, it is useful to examine a hypothetical alloy with straight line liquidus and solidus curves, T_{Liq} and T_{Sol}, both terminating at a eutectic temperature T_E. The lines are given by

$$\begin{aligned} T_{Liq} &= T_M + m\,C_0 \\ T_{Sol} &= T_M + (m/k)C_0 \end{aligned} \qquad \text{[E1]}$$

where C_0 is the composition, T_M is the pure solvent melting point, k is the partition coefficient, and m is the liquidus slope taken as negative for a eutectic type diagram.‡‡‡ Equivalently, m / k is the slope of the solidus. If C_0 is such that $T_{Sol} > T_E$, the equilibrium freezing range is given by

$$T_{Liq} - T_{Sol} = \frac{m(k-1)C_0}{k} \qquad \text{[E2]}$$

First we examine different models for the liquid composition, $C_L\ (f_S)$ as a function of fraction solid, f_S, where $0<f_S<1$ and then the corresponding enthalpy curves.

For an equilibrium liquid - solid mixture (Lever law), $C_L\ (f_S)$ is given by

$$C_L(f_S) = C_0\left[1-(1-k)f_S\right]^{-1} \qquad \text{[E3]}$$

For Scheil behavior $C_L\ (f_S)$ is given by

$$C_L(f_S) = C_0\left[1-f_S\right]^{k-1} \qquad \text{[E4]}$$

‡‡‡ For a dilute alloy, m and k are related by the expression, $m = -(1-k)\frac{RT_M^2}{L_M}$, where R is the gas constant and L_M is the heat of fusion per mole of the pure solvent. This reduces to the normal melting point depression law (van't Hoff Law) if $k = 0$.

For the Ohnaka [86Ohn] model for back diffusion

$$C_L\left(f_S\right)=C_0\left[1-f_S\left(1-\frac{2ak}{1+2a}\right)\right]^{\frac{k-1}{\left(1-\frac{2ak}{1+2a}\right)}} \qquad \text{[E5]}$$

with $a=\frac{D_S\, t_f}{\lambda^2}$ and t_f and λ the local freezing time and dendrite spacing respectively. Here, the local freezing time is taken as the equilibrium freezing range divided by the cooling rate. The Ohnaka form recovers the equations for Scheil and lever as the parameter a spans the range from 0 to ∞, respectively.

It is important to determine if the liquid concentration increases to the eutectic composition when using Eqns. E3-E5; i.e., whether some value of f_S gives

$$C_L\left(f_S\right)=C_E\,. \qquad \text{[E6]}$$

The value of fraction solid f_S^P if and where this occurs is the fraction of primary phase and the fraction of eutectic will be $(1-f_S^P)$.

The enthalpy is given by

$$H\left(T\right)=C_p^{S0}T+L\left(1-f_S\left(T\right)\right) \qquad \text{[E7]}$$

where L is the heat of fusion and where $f_S\,(T)$ is obtained by solving the expression

$$T=T_M+mC_L\left(f_S\right), \qquad \text{[E8]}$$

for f_S in terms of T. Eqn. E8 is the liquidus curve combined with one of the forms for $C_L\,(f_S)$ from Eqn. E3-E5. Then the enthalpy can then be expressed as a function of temperature. For an equilibrium liquid - solid mixture (Lever law), the enthalpy is given by

$$H(T)=C_p^{S0}T+L\left[1-\left(1-k\left(\frac{T_S-T_{Sol}}{T_{Liq}-T}\right)\right)^{-1}\right] \qquad \text{[E9]}$$

For Scheil behavior, the enthalpy is given by

$$H(T) = C_p^{S0}T + L\left[1-\left(\frac{k-1}{k}\right)\left(\frac{T_{Liq}-T}{T_{Liq}-T_{Sol}}\right)\right]^{1/(k-1)} \qquad \text{[E10]}$$

For the back-diffusion form, the enthalpy is given by

$$H(T) = C_p^{S0}T + L \times\left[1-\left(\frac{1}{1-2ak/(1+2a)}\right)\right]\left[1-\left(1-\left(\frac{k-1}{k}\right)\left(\frac{T_{Liq}-T}{T_{Liq}-T_{Sol}}\right)\right)^{1-\frac{2ak}{1+2a}\over k-1}\right] \qquad \text{[E11]}$$

In these equations, T_{Sol} is strictly given by Eqn. E1 for the alloy composition of interest, C_0, even if $T_{Sol} < T_E$. These enthalpy expressions are only valid for if no eutectic forms. If the eutectic is encountered, the enthalpy suffers a jump discontinuity at T_E of height $L(1 - f_S^P)$.

Appendix F. Binary phase diagrams and DTA response

To illustrate the general shape of DTA curves for different cases in binary eutectic and peritectic systems we have chosen hypothetical systems based on Ni. The parameters used for the calculation of the DTA curves are: α = 15 K/min, $t_{S,C}$ = 5.67 s, $t_{W,C}$ = 4.65 s, $t_{T,C}$ = 5.5 s, L = 290 kJ/kg, C_p = 0.75 kJ/kg and m_S = 177 mg. Three alloy compositions were chosen for each system and the results for the eutectic system are shown in Fig. F1 and the results for the peritectic system are shown in Fig. F2.

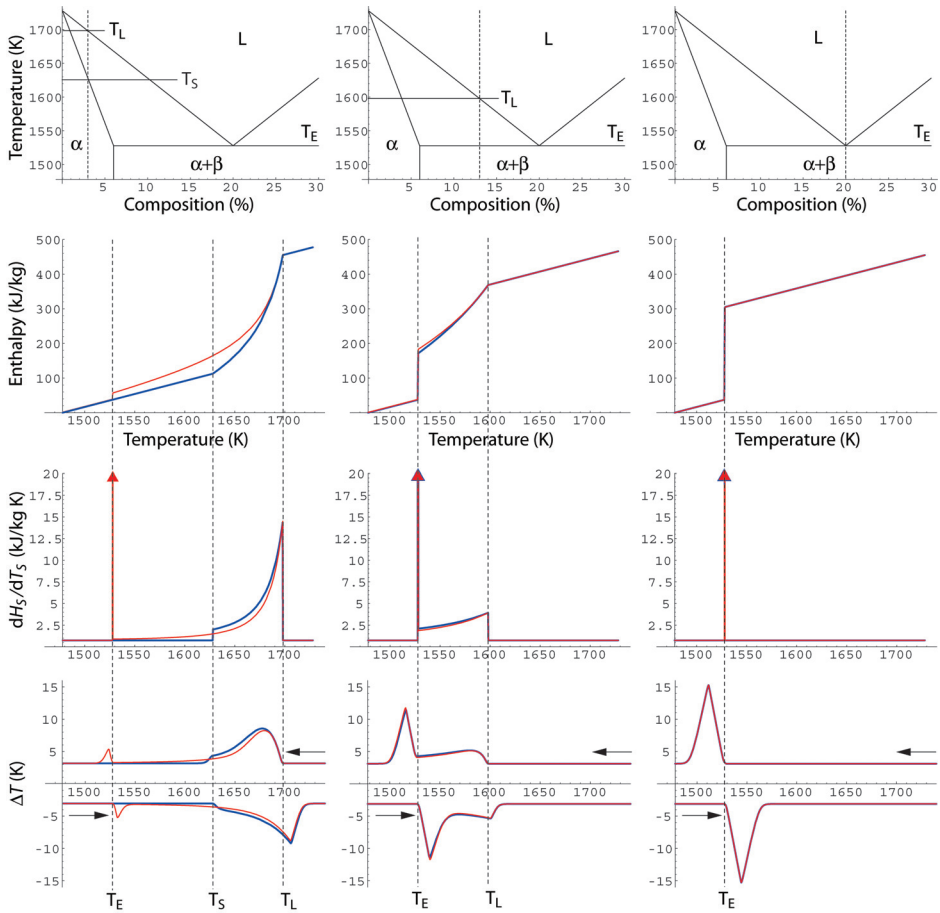

Figure F1. *Phase diagram, enthalpy, dH_S / dT_S and computed DTA curves for three different compositions in a hypothetic binary eutectic system. The blue curves are for equilibrium conditions (Lever) and the red curves are for Scheil conditions.*

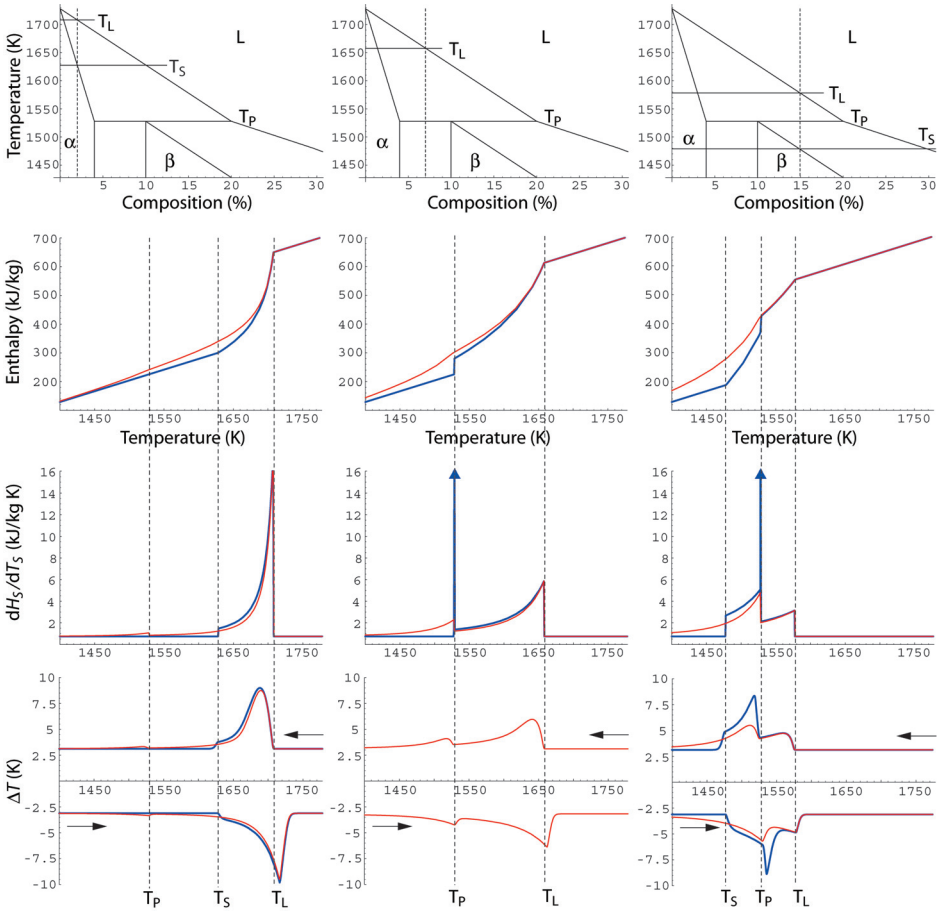

Figure F2. *Phase diagram, enthalpy, dH_S / dT_S and computed DTA curves for three different compositions in a hypothetic binary peritectic system. The blue curves are for equilibrium conditions (Lever) and the red curves are for Scheil conditions.*

Appendix G. Tutorial on melting and freezing of multicomponent alloys

We now explore the DTA melting response of a pair of complex alloys. These were first described in [02Boe]. As input to the calculation we use enthalpy vs. temperature values obtained for full equilibrium (lever law) and for Scheil freezing assumptions. DTA melting simulations, using the lever enthalpy-temperature relation, would apply to an alloy equilibrated prior to melting and where diffusion was adequate to guarantee spatial concentration uniformity of all phases during melting. DTA melting simulations, using the Scheil enthalpy calculations, would apply to a microstructure that was solidified and remelted with no solid diffusion. Clearly these are extreme cases. The melting of an equilibrated alloy as well as an as-cast sample requires an analysis of solid diffusion for both the freezing process and the melting process. The thermodynamic parameters of [96Sau1] [96Sau2] were used in conjunction with the methods of [98Boe] to give the enthalpy - temperature relations.

G.1- Aluminum Alloy 2219

Al alloy 2219 has typical mass composition of 6.63 % Cu, 0.03 % Mn, 0.2 % Fe and 0.1 % Si. Table G1 gives the sequence of phase formation 'reactions' listed in the order of decreasing temperature. More phases occur, and the final solidification temperature is lower for the Scheil assumption due to the microsegregation. Figure G1 shows the phase fractions as a function of

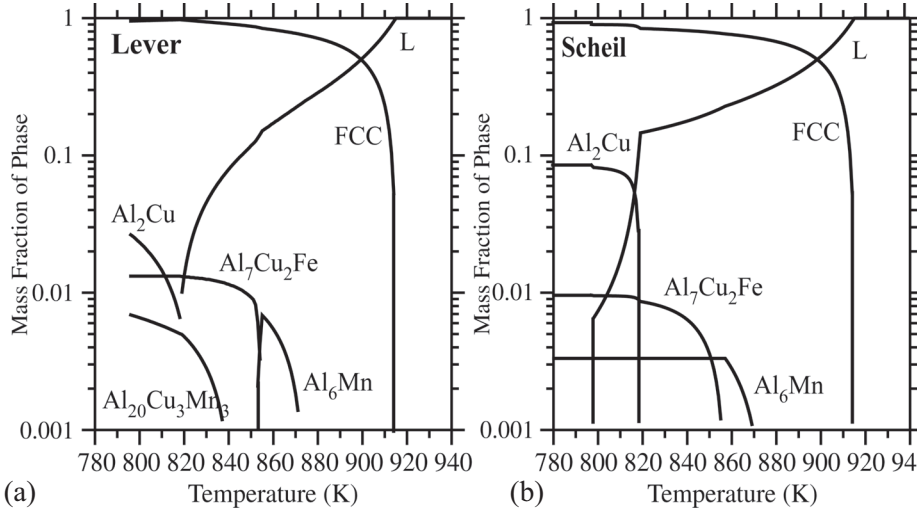

Figure G1. *Phase fraction vs. temperature computed using an aluminum alloy thermodynamic database [96Sau1] for a) lever and b) Scheil conditions for Al 2219 alloy.*

temperature. Off of the scale of Figure F1 are the α-AlSiFe and Si phases with maximum phase fractions of 8 x 10^{-4} and 3 x10^{-4} respectively. Figure G2 shows the values of dH_S / dT_S obtained from the calculated

Table G1 - Sequence of phase formation during lever and Scheil freezing of 2219 Al Alloy

Lever	Scheil
L→FCC	L→FCC
L→FCC+Al_6Mn	L→FCC+Al_6Mn
L+Al_6Mn↔FCC+Al_7Cu_2Fe	L→FCC+Al_7Cu_2Fe
L→FCC+Al_7Cu_2Fe	L→FCC+Al_7Cu_2Fe+Al_2Cu
L→FCC+Al_7Cu_2Fe+$Al_{20}Cu_2Mn_3$	L→FCC+Al_7Cu_2Fe+Al_2Cu+α-AlFeSi
L→FCC+Al_7Cu_2Fe+$Al_{20}Cu_2Mn_3$+Al_2Cu	L→FCC+Al_7Cu_2Fe+Al_2Cu+α-AlFeSi +Si (invariant reaction @797K)

enthalpy temperature - curves and the DTA simulation for 5 K/min. Comparison of Figure G1 with the dH_S / dT_S curves allows one to recognize the cause of the various peaks in the DTA signal. During melting, a peak occurs when all of a particular phase has completely melted (see however problems associated with phase diagram lines that are converging with decreasing temperature, 3.3.5). For example, for the lever melting, the first peak on heating at ≈ 820 K indicates that all of the Al_2Cu phase has melted. The second peak is barely detectable at ≈ 840 K and indicates that all $Al_{20}Cu_2Mn_3$ has melted. The third peak at ≈ 855 K indicates that all of Al_7Cu_2Fe has melted and similarly for other peaks. Note that for the Scheil DTA calculation, a peak is visible at ≈ 797 K. This is due to the melting of the invariant quinary eutectic at 797K (Table G1) where the Si phase completely disappears and reductions also occur in the phase fractions of the other phases. The alloy under consideration has five components, the reaction involves six phases, and there are zero degrees of freedom. Thus despite the small fraction of Si phase, the signal from the invariant eutectic melting is relatively large.

Simulations of alloy freezing were performed. Figure G3 compares the melting and freezing signals for the Al 2219 alloy at 5 K/min (Scheil enthalpy used for both). The vertical dashed lines are the liquidus temperature and the temperature where the Al_2Cu phase disappears, or first appears, on melting or solidification, respectively. The peak temperatures are clearly offset from these dashed lines and should not be used to characterize the melting or freezing process.

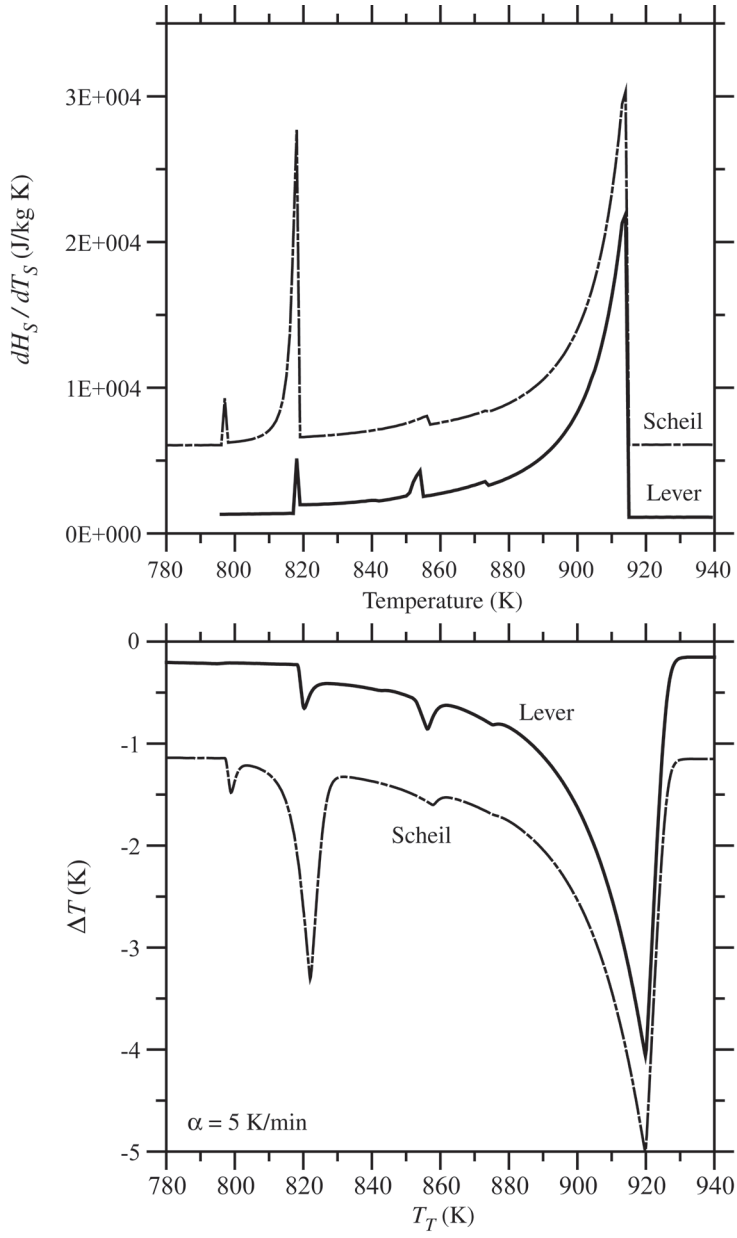

Figure G2. *Top) dH_S / dT_S obtained from the enthalpy-temperature predictions for Al 2219 alloy computed using thermodynamic database [96Sau1] for lever and Scheil conditions for Al 2219 alloy. The curve for 'Scheil' is shifted by 5×10^3 J/kg K for clarity. Bottom) Corresponding DTA plots for melting at 5 K/min. The curve for 'Lever' is shifted up 1 K for clarity.*

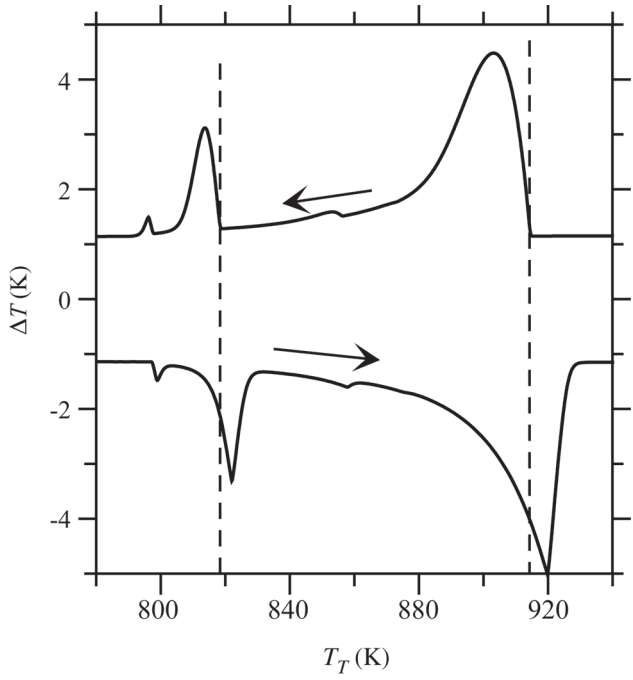

Figure G3. *Calculated DTA plots for melting and freezing at 5 K/min of Al 2219 alloy using the Scheil enthalpy-temperature relation.*

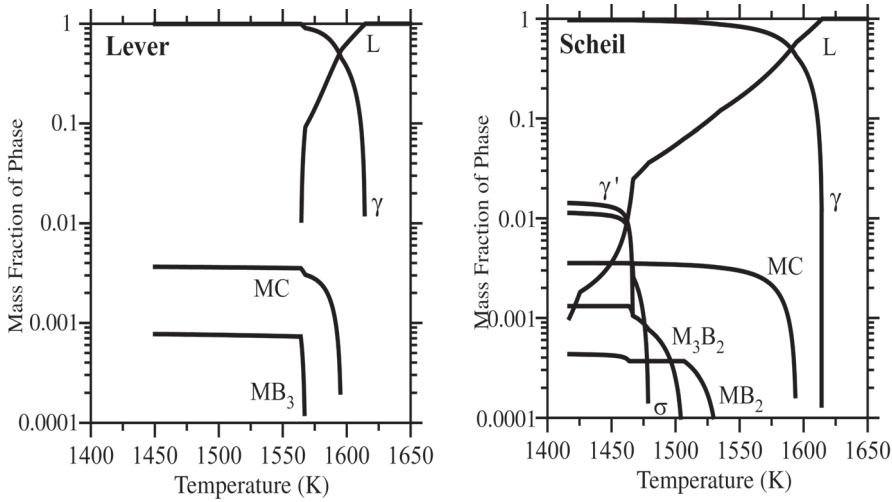

Figure G4. *Phase fraction vs. temperature computed using Ni alloy thermodynamic database [96Sau2] for lever and Scheil conditions for Udimet 700 alloy.*

G.2 - Udimet 700

A second example is the Ni alloy, Udimet 700, with mass composition of 15 % Cr, 18.5 % Co, 5 % Mo, 3.5 % Ti, 4.4 % Al, 0.07 % C, and 0.025 % B. The thermodynamic parameters were taken from [96Sau2]. The phase formation sequences are given in Table G2, the phase fractions in Figure G4 and dH_S / dT_S and the DTA signals in Figure G5. To be noted here is the very large difference between the sizes of the freezing ranges of the two cases. The particular peaks and their sizes for real DTA signals for this alloy would be difficult to predict given the large difference between the diffusion rates of the interstitials B and C and the substitutional elements in the FCC phase.

Table G2 - Sequence of phase formation during lever and Scheil freezing of Udimet 700

Lever	Scheil
L	L→FCC
L→FCC	L→FCC+MC
L→FCC+MC	L→FCC+MC+MB_2
L→FCC+MC+MB_2	L→FCC+MC+MB_2+M_3B_2
	L→FCC+MC+MB_2+M_3B_2+σ
	L→FCC+MC+MB_2+M_3B_2+σ+γ
	L→FCC+MC+σ+γ+MB_2

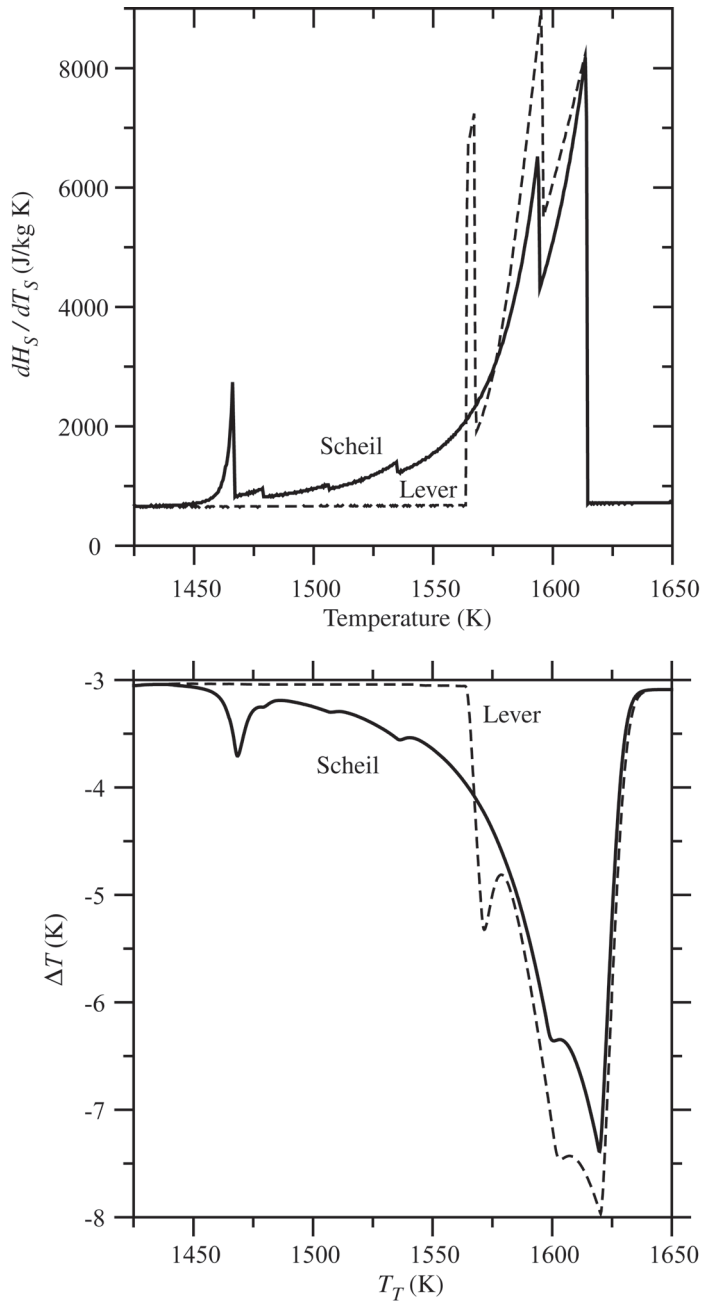

Figure G5. *Top) dH_S / dT_S obtained from the enthalpy-temperature predictions for Udimet 700 alloy computed using thermodynamic database [96Sau2] for lever and Scheil conditions for Udimet 700 alloy. Bottom) Corresponding DTA plots for melting of 180 mg sample at 15 K/min.*

References

49Vol M. J. Vold, Analyt. Chem. 21 (1949) 683-688.

56Rhi F.N Rhines., Phase Diagrams in Metallurgy, McGraw-Hill Book Comp., 1956.

60Mas Massing G and Rodgers BA, Ternary Systems, Dover Publications. NY 1960 p 49.

65Gar P.D.Garn, Thermoanalytical Methods of Investigation, Academic Press, New York, 1965, Chapter 4 and 5.

66Pri A. Prince, Alloy Phase Equilibria, Elsevier Amsterdam (1966), pp. 211.

66Tsa N.F. Tsang, Handbook of Differential Thermal Analysis, Eds. W.J. Smothers and Y. Chiang, Chem. Publ. Comp., New York, NY, 1966, pp. 91-123.

68Gra A.P. Gray, Analytical Calorimetry, Vol.1, Eds. R.S. Porter and J.F. Johnson, Plenum Press, New York, NY, 1968, pp. 209-218.

69Bar C.R. Barber, Metrologia 5, 35-44 (1969).

70Cun A.D. Cunningham and F.W. Wilburn, Differential Thermal Analysis, Vol.1, Ed. R.C. Mackenzie, Academic Press, London, UK, 1970, pp. 31-62.

74Fle M.C. Flemings, Solidification Processing, McGraw Hill, New York, 1974, pp. 177-183.

75McN J.L. McNaughton and C.T. Mortimer, in Thermochemistry and Thermodynamics, edited by Henry Alistair Skinner, International Review of Science: Physical Chemistry. Series Two. Vol. 10, Butterworths, London, 1975, pp. 1-44.

78Bar E.M. Barral and R.J. Gritter, in Systematic Materials Science, Volume IV, edited by J.H. Richardson and R.V. Peterson, 1978, Academic Press, New York, Chapter 39.

79Fre H. Fredriksson and B. Rogberg, Metal Science 13 (1979) 685-690.

82Wes D.R.F. West, Ternary Equilibrium Diagrams, 2nd Edition. Chapman-Hall, London UK 1982.

84Per J.H. Perepezko, Mat. Sci. and Eng. 65 (1984) 125-135.

86Hay F. H. Hayes, H. L. Lukas, G. Effenberg and G. Petzow, Z. Metallkunde 77(1986) 749-754.

86Hey W. Heyroth, J. Thermal Analysis 31 (1986) 61-72.

86Ohn I. Ohnaka, Transactions of the Iron And Steel Institute of Japan 26 (1986) 1045-1051.

88Fly J.H. Flynn, J. Thermal Analysis 34 (1988) 367-381.

88Fre H. Fredriksson, ASM Metals Handbook (1988) 9th Edition Volume 15 "Casting", ASM International, Materials Park, OH, pp. 182-185.

88Bro M. E. Brown, Introduction to Thermal Analysis; Techniques and Applications, Chapter 4: Differential thermal analysis (DTA) and differential scanning calorimetry (DSC), Chapman & Hall, 1988, New York.

88Met Principles of Solidification, in Volume 15: Casting, Metals Handbook 9th. Edition., (ASM, Metals Park, OH 1988)

90Pre H. Preston-Thomas, Metrologia, 27, 3-10 (1990).

90Höh G.W.H. Höhne, H.K. Cammenga, W. Eysel, E. Gmelin and W. Hemminger, Thermochim. Acta 180, 1-12 (1990).

91Cao W.D. Cao, R.L. Kennedy & M.P. Willis, in Superalloys 718,625 and Various Derivatives, Ed. E. A. Loria, TMS, Warrendale, PA, 1991, pp. 147-160.

91Höh G.W.H. Höhne, J. Thermal Analysis 37, 1987-2000 (1991).

92Shu R.D. Shull, Thermal Analysis in Metallurgy, Eds. R.D. Shull and A. Joshi, TMS, Warrendale, PA, 1992, pp. 95-119.

92Feu Y. Feutelais, G. Morgant, J. R. Didry and J. Schnitter, CALPHAD 16, 1992, pp. 111-119.

94Spe R. F. Speyer, Thermal Analysis of Materials, Marcel Dekker, Inc. (1994) New York, NY.

95Ban D. K. Banerjee, W. J. Boettinger, R. J. Schaefer, M. E. Williams, Modeling of Casting, Welding and Advanced Solidification Processes, VII, Eds. M. Cross and J. Campbell, TMS, Warrendale, PA, 1995, pp. 491.

96Bed R.E. Bedford, G. Bonnier, H. Maas and F. Pavese, Metrologia, 33, 133-154 (1996).

96Kat U.R. Kattner, W.J.Boettinger, S.R. Coriell, Z. Metallkunde 87 (1996) 522-528.

96Sau1 N. Saunders, Mater. Sci. Forum, 217-222, 1996, pp. 667.

96Sau2 N. Saunders, Superalloys 1996, Eds. R. Kissinger et al. TMS, Warrendale, PA, (1996) pp. 101.

96Bil H. Biloni and W. J. Boettinger, Physical Metallurgy, 4th edition, Eds. P. Haasen and R. W. Cahn, 1996, North Holland, Amsterdam, pp. 669-842.

98Boe W.J. Boettinger, U.R. Kattner and D.K. Banerjee, Modeling of Casting, Welding and Advanced Solidification Processes, VIII, Eds. B.G. Thomas and C. Beckermann, TMS, Warrendale PA, 1998, pp 159-170.

00Wu R.I. Wu and J.H. Perepezko, Metall. and Matls. Trans. A 31A (2000) 497.

00Opf J. Opfermann, ThermoKinetics: A Software Module for the Kinetic Analysis of Thermal Measurements using Multivariate Linear Regression Software, Netzsch-Gerätebau GmbH, Selb, Germany, (2000).

00Moo K.-W. Moon, W.J. Boettinger, U.R. Kattner, F.S. Biancaniello and C.A. Handwerker, J. Electronic Materials, 29 (2000), pp. 1122 - 1136.

01Göd T. Gödecke, Z. Metallkd. 92(2001) 966 [in German].

02Boe W.J. Boettinger and U.R. Kattner, Metall. and Matls. Transactions, 33A (2002), 1179.

02Wes D.R.F. West and N. Saunders, Ternary Phase Diagrams in Materials Science, Maney-Institute of Materials, London UK 2002.

03Don H.B. Dong, M.R.M. Shin, E.C. Kurum, H.Cama, J.D. Hunt, Metallurgical and Materials Transactions A34 (2003) 441-447.

03Fer R. Ferro, G. Cacciamani and G. Borzone, Intermetallics 11(2003) 1081-1094.

03 Liu H.S. Liu, C.L. Liu, K. Ishida and Z.P. Jin, J. Electron. Mater. 32 (2003) 1290-1296.

03Rab A. Rabinkin, Solidus-Liquidus, Brazing Course Lecture Notes, ASM/AWS "International Brazing and Soldering Conference 2003."

04Sta M.J. Starink, Internbational Materials Rev. 49(2004) 191-226

05Don H.B. Dong and J.D. Hunt, Matls Sci and Eng A 413-414 (2005) 470-473.